Computer Modeling of Liquid Crystals

Muataz S. Al-Barwani

H. H. Wills Physics Laboratory

University of Bristol

A thesis submitted to the University of Bristol

in accordance with the requirements for the degree of

Doctor of Philosophy

in the Faculty of Science

1999

Abstract

In this thesis, we investigate several aspects of the behaviour of liquid crystal molecules near interfaces using computer simulation. We briefly discuss experiment, theoretical and computer simulation studies of some of the liquid crystal interfaces. We then describe three essentially independent research topics.

The first of these concerns extensive simulations of a liquid crystal formed by long flexible molecules. We examined the bulk behaviour of the model and its structure. Studies of a film of smectic liquid crystal surrounded by vapour were also carried out. Extensive simulations were also done for a long-molecule/short-molecule mixture, studies were then carried out to investigate the liquid-vapour interface of the mixture.

Next, we report the results of large scale simulations of soft-spherocylinders of two different lengths. We examined the bulk coexistence of the nematic and isotropic phases of the model. Once the bulk coexistence behaviour was known, properties of the nematic-isotropic interface were investigated. This was done by fitting order parameter and density profiles to appropriate mathematical functions and calculating the biaxial order parameter. We briefly discuss the ordering at the interfaces and make attempts to calculate the surface tension.

Finally, in our third project, we study the effects of different surface topographies on creating bistable nematic liquid crystal devices. This was carried out using a model based on the discretisation of the free energy on a lattice. We use simulation to find the lowest energy states and investigate if they are degenerate in energy. We also test our model by studying the Frederiks transition and comparing with analytical and other simulation results.

Acknowledgements

I would like to thank my advisor, professor Mike Allen, for his insights, teaching, guidance, encouragement and most of all patience.

I wish to acknowledge support from Sultan Qaboos University for the Ph.D. studentship. This research is supported by the EPSRC by providing computer time on the Cray T3E in Edinburgh through the High Performance Computing Initiative and by the Joint Research Equipment Initiative towards the purchase of the SGI Origin 2000.

I would like to thank Mark R. Wilson, Alexey V. Lyulin and Nicholas K. Allsopp for developing the generalized parallel code `GBMOL` and for helpful discussions. I would like to thank Mark Warren and Bill Smith for developing the parallel code `GBMEGA`. I would also like to thank Guido Germano and Kenji Takeda for porting to the Cray T3E. I would like to thank Timothy P. Spiller and Chris J. Newton at Hewlett-Packard Laboratories, Bristol, for collaboration and discussions related to the lattice model.

On a more personal level, I would like to thank past and present members of our group - Alexey, Denis, Guido, Hector, Jeroen, Mark, Matthew and Philip - and members of the theory group - Bob, James, Andy, Duncan, Jason, Kevin, Marjolein, Paul, Rene and Jon. I would also like to thank Dan Lewis my Karate instructor and all the other members of the Combat Karate club in Bristol for making me as hard as nails and giving me a way to channel my aggressions.

Finally, I thank my wife Suhaila and daughter Eithaar and the rest of my family for their love and support.

بِسـمِ اللّٰهِ الرَحمٰنِ الرَحِيمِ

Author's Declaration

I declare that no part of this thesis has been submitted for a higher degree in this, or any other, university. The research reported herein is the result of my own investigation except where reference is made to the work of others. All research was carried out under the supervision of Professor M.P. Allen at the University of Bristol, between October 1996 and December 1999.

Muataz S. Al-Barwani

December 1999

Contents

List of Figures

List of Tables

Chapter 1

Introduction

1.1 Liquid Crystals

1.1.1 What are liquid crystals?

The liquid crystalline phase is an intermediate phase between the solid and liquid phases. Liquid crystals have properties of both solids and liquids. A liquid crystal can flow like an ordinary liquid, however other properties, such as birefringence are reminiscent of the crystalline phase. This combination explains the name Liquid crystal. Other names in use are mesophase (meaning intermediate phase) and mesomorphic phase [1].

At the molecular level, liquid crystal molecules are non-spherical and elongated (rod-like or disk-like), these molecules could be either rigid or flexible. An essential characteristic is the presence of orientational order, with the positional order of the centre of mass either absent or reduced. Roughly speaking, two classes of liquid crystals can be distinguished: thermotropic and lyotropic liquid crystalline phases. Single component systems that show mesomorphic behaviour in a definite temperature range are called thermotropic. Lyotropic liquid crystalline phases on the other hand show mesomorphic behaviour when the concentration is varied. In this thesis, we mainly address thermotropic liquid crystals. A liquid with no orientational or

positional ordering is known as an isotropic liquid. If it has orientational ordering but no positional ordering, i.e. the centres of mass of the molecules have three translational degrees of freedom, it is known as a nematic liquid crystal as shown in Figure 1.1(a). The smectic phases are characterised in addition by a positional order in at least one dimension. The centres of the molecules are, on average, arranged in equidistant planes forming a layer structure as shown in Figure 1.1(b). There are many types of smectic phases. These differ in the orientation of the preferred direction of the molecules with respect to the layer normal (orthogonal and tilted smectic phases). They also differ in the organisation of the centres of mass of the molecules within the layers (e.g. cubic, hexagonal) [2]. If the molecules constituting these phases are chiral, then the nematic and some of the smectic phases do not occur. Instead, they are replaced by chiral versions of these phases with different physical structures. For example, in a chiral nematic phase (also known as a cholesteric phase)[3] the director rotates along a direction perpendicular to the direction of the helical twist as shown in Figure 1.1(c). Chiral phases are not studied in this thesis.

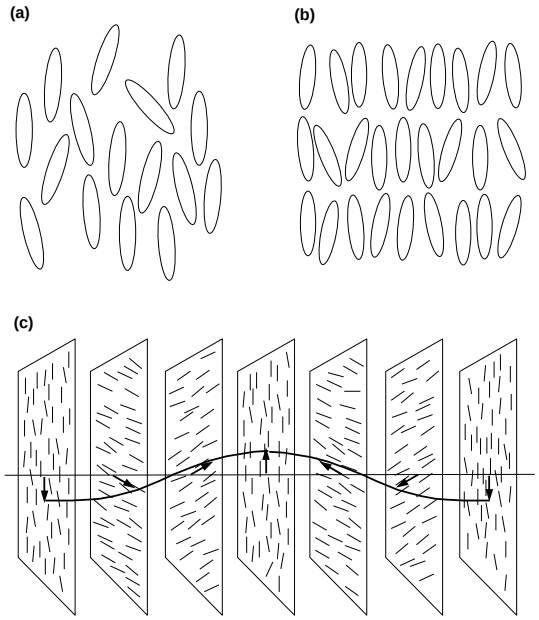

Figure 1.1: a) Nematic, b) Smectic and c) Cholesteric liquid crystals

1.1.2 Order in liquid crystals

The average alignment of the molecules with their long axes parallel to each other leads to a preferred direction in space. One usually describes this local direction of alignment by a unit vector **n**, called the director. Hence, the director gives the direction of the preferred axis at each point in a sample. The states described by **n** and **-n** are indistinguishable. To characterise the orientational order, two aspects have to be taken into account: the local preferred direction $\mathbf{n}(\mathbf{r})$ and the amount of ordering, i.e. the distribution of the long molecular axes around **n**.

The uniaxial nematic phase possesses a quadrupole-type symmetry and is characterised by the order parameter $Q_{\alpha\beta}$ which is a symmetric traceless second-rank tensor

$$Q_{\alpha\beta} = \frac{1}{N}\sum_{ij}\left(\frac{3}{2}\hat{\mathbf{u}}_{i\alpha}\hat{\mathbf{u}}_{j\beta} - \frac{1}{2}\delta_{\alpha\beta}\right) = S(\frac{3}{2}n_\alpha n_\beta - \frac{1}{2}\delta_{\alpha\beta}). \tag{1.1}$$

The unit vectors **u** ares the orientational vectors of the molecules and $\delta_{\alpha\beta}$ is the Kronecker delta function. The unit vector **n** is the director that specifies the preferred orientation of the primary molecular axes. The quantity S is the scalar order parameter that characterises the degree of nematic ordering.

Smectic ordering in liquid crystals is usually characterised by the complex order parameter $\rho_\alpha e^{i\psi}$. Here $\rho_\alpha = \langle\cos(\mathbf{k}\cdot\mathbf{r})\rangle$ is the amplitude of the wave density. ψ is the phase and **k** is the wave vector. This order parameter appears naturally in the Fourier expansion of the one-particle density $\rho(\mathbf{r})$.

1.1.3 Frank free energy

By considering the symmetry requirements of the nematic liquid crystal, Frank derived the elastic free energy density [4]:

$$f_{\text{el}} = \frac{1}{2}\left[K_1(\nabla\cdot\mathbf{n})^2 + K_2(\mathbf{n}\cdot(\nabla\times\mathbf{n}))^2 + K_3(\mathbf{n}\times(\nabla\times\mathbf{n}))^2\right] \tag{1.2}$$

where K_1, K_2 and K_3 are the Frank elastic coefficients [1, 4]. The three basic deformations associated with the Frank elastic coefficients are shown in Figure 1.2. The

elastic constants have values of the order of 10^{-11} Newtons and are measured from experiments involving the competing effects of field alignment and wall alignment on a sample.

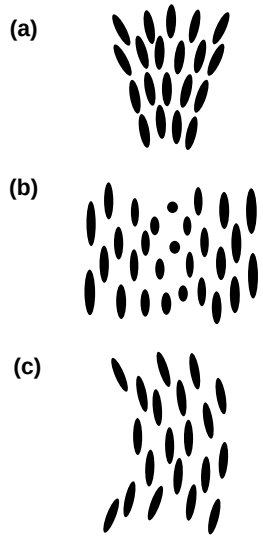

Figure 1.2: a) Splay:K_1, b) Twist:K_2 and c) Bend:K_3

1.2 Models

1.2.1 Introduction

Realistic intermolecular interaction potentials for mesogenic molecules can be very complex and are generally unknown. At the same time molecular theories are often based on simple model potentials. This is justified when the theory is used to describe some general properties of liquid crystal phases that are not sensitive to the details of the interaction. Model potentials are constructed in order to represent only the qualitative mathematical form of the actual interaction energy in the simplest possible way. Most of the popular model potentials correspond to the first few terms of the full potential energy expansion. These generally are the two-body and three-body interaction terms [5]. There also exist some special model potentials that

combine an attraction at large separation and repulsion at short distances. The most popular potential of this kind is the Lennard-Jones potential and its generalisation for anisotropic particles, the Gay-Berne potential [6]. Another class of models is the lattice models, the most famous being the Lebwohl-Lasher model [7]. This class of model is appropriate for studying the N-I transition when viewed as a rotational order-disorder transition in an effective crystalline solid with all fluctuations ignored [8].

Below we give a brief description of the different type of model potentials used in this thesis.

1.2.2 Non-bonded Potentials

The first of the non-bonded site to site potentials is the Lennard-Jones (LJ) potential. The famous 12-6 potential of Lennard-Jones provides a fair description of the interaction between pairs of rare-gas atoms and also quasi-spherical molecules such as CH_4. The LJ potential is given by

$$U_{ij}^{LJ} = 4\epsilon_{ij}^{LJ}\left[\left(\frac{\sigma_{ij}^{LJ}}{r_{ij}}\right)^{12} - \left(\frac{\sigma_{ij}^{LJ}}{r_{ij}}\right)^{6}\right] \tag{1.3}$$

where σ is the separation of the particles when $U_{ij} = 0$, also known as the collision diameter. ϵ is the depth of the potential well at the minimum in U_{ij} [9].

Another non-bonded potential based on the Gaussian overlap model is the Gay-Berne potential (GB). The GB potential was modeled to give the best fit to the pair potential for a molecule consisting of a linear array of four equidistant LJ centres. The Gay-Berne potential is a phenomenological model that includes both attractive and repulsive forces. The molecules in the GB system have translational and orientational degrees of freedom. The GB potential is given by

$$U_{ij}^{GB} = 4\epsilon_0\left[\epsilon(\hat{\mathbf{u}}_i, \hat{\mathbf{u}}_j)\right]^{\nu}\left[\epsilon'(\hat{\mathbf{u}}_i, \hat{\mathbf{u}}_j, \hat{\mathbf{r}}_{ij})\right]^{\mu}$$

$$\times \quad \left[\left(\frac{\sigma_0}{r_{ij} - \sigma(\hat{\mathbf{u}}_i, \hat{\mathbf{u}}_j, \hat{\mathbf{r}}_{ij}) + \sigma_0} \right)^{12} \right.$$
$$- \quad \left. \left(\frac{\sigma_0}{r_{ij} - \sigma(\hat{\mathbf{u}}_i, \hat{\mathbf{u}}_j, \hat{\mathbf{r}}_{ij}) + \sigma_0} \right)^{6} \right] \tag{1.4}$$

where σ is the intermolecular separation at which the attractive and repulsive terms cancel and is given as

$$\sigma(\hat{\mathbf{u}}_i, \hat{\mathbf{u}}_j, \hat{\mathbf{r}}_{ij}) = \sigma_0 \left[1 - \frac{\chi}{2} \left\{ \frac{(\hat{\mathbf{r}} \cdot \hat{\mathbf{u}}_i + \hat{\mathbf{r}} \cdot \hat{\mathbf{u}}_j)^2}{1 + \chi(\hat{\mathbf{u}}_i \cdot \hat{\mathbf{u}}_j)} + \frac{(\hat{\mathbf{r}} \cdot \hat{\mathbf{u}}_i - \hat{\mathbf{r}} \cdot \hat{\mathbf{u}}_j)^2}{1 - \chi(\hat{\mathbf{u}}_i \cdot \hat{\mathbf{u}}_j)} \right\} \right]^{-\frac{1}{2}}. \tag{1.5}$$

The shape anisotropy parameter χ is

$$\chi = \frac{\kappa^2 - 1}{\kappa^2 + 1} \tag{1.6}$$

where $\kappa = \sigma_{ee}/\sigma_{ss}$ and σ_{ee} is the separation when the molecules are end-to-end and σ_{ss} that when they are side-by-side.

The depth of the well is expressed as

$$\epsilon(\hat{\mathbf{u}}_j, \hat{\mathbf{u}}_j, \hat{\mathbf{r}}_{ij}) = \epsilon_0 \epsilon^{\nu}(\hat{\mathbf{u}}_i, \hat{\mathbf{u}}_j) \epsilon'^{\mu}(\hat{\mathbf{u}}_i, \hat{\mathbf{u}}_j, \hat{\mathbf{r}}) \tag{1.7}$$

where

$$\epsilon(\hat{\mathbf{u}}_i, \hat{\mathbf{u}}_j) = (1 - \chi^2(\hat{\mathbf{u}}_i \cdot \hat{\mathbf{u}}_j)^2)^{-\frac{1}{2}} \tag{1.8}$$

and

$$\epsilon'(\hat{\mathbf{u}}_i, \hat{\mathbf{u}}_j, \hat{\mathbf{r}}_{ij}) = 1 - \frac{\chi'}{2} \left\{ \frac{(\hat{\mathbf{r}} \cdot \hat{\mathbf{u}}_i + \hat{\mathbf{r}} \cdot \hat{\mathbf{u}}_j)^2}{1 + \chi'(\hat{\mathbf{u}}_i \cdot \hat{\mathbf{u}}_j)} + \frac{(\hat{\mathbf{r}} \cdot \hat{\mathbf{u}}_i - \hat{\mathbf{r}} \cdot \hat{\mathbf{u}}_j)^2}{1 - \chi'(\hat{\mathbf{u}}_i \cdot \hat{\mathbf{u}}_j)} \right\} \tag{1.9}$$

where the parameter χ' is related to the anisotropy in the well depth via

$$\chi' = \frac{1 - \kappa'^{\frac{1}{\mu}}}{1 + (\epsilon_{ee}/\epsilon_{ss})^{\frac{1}{\mu}}} \tag{1.10}$$

where $\kappa' = \epsilon_{ss}/\epsilon_{ee}$ is the ratio of well-depths for end-to-end and side-by-side.

In the above equations $\hat{\mathbf{u}}_i$ and $\hat{\mathbf{u}}_j$ are the orientation vectors of two molecules, $\mathbf{r}_{ij}$ is the vector joining the two centres and $\hat{\mathbf{r}}_{ij}$ is the unit vector $\frac{\mathbf{r}_{ij}}{r}$. ϵ_0 and σ_0 are scaling parameters [10, 11]. Figure 1.3 shows the GB potential for two GB units at different orientations with respect to each other.

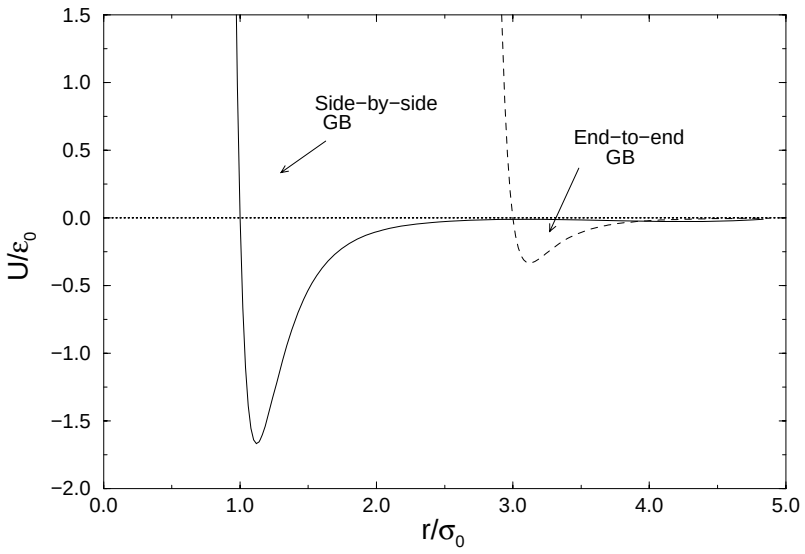

Figure 1.3: GB-GB interactions: side by side and end to end using the GB parameters $\kappa = 3$ and $\kappa' = 5$.

The Kihara potential for spherocylinders is another non-bonded potential based on the LJ potential. A spherocylinder can be thought of as the set of points that are within a distance R from a line segment of length L. A sphere of radius R can be drawn around every point on this line segment. The sphere contains all points that are within a distance R. Hence, a spherocylinder can be considered as the volume that is swept out by a sphere of radius R that is moved along a line segment of length L.

Following the method of Allen *et al* [12] of calculating the distance of closest approach of convex bodies, the interaction between two spherocylinders was calculated. Since a sphere can be drawn around each point on the line segments which maps out the spherocylinder, these spheres can be used to calculate the interaction between the two points of closest approach.

To calculate this interaction the repulsive form of the Lennard-Jones potential was used

$$U_{ij} = \begin{cases} 4\epsilon_0 \left[\left(\frac{\sigma}{S_{ij}} \right)^{12} - \left(\frac{\sigma}{S_{ij}} \right)^{6} \right] + \epsilon_0 & S_{ij} \leq 2^{\frac{1}{6}}\sigma \\ 0 & S_{ij} > 2^{\frac{1}{6}}\sigma \end{cases} \tag{1.11}$$

where S_{ij} is the distance of closest approach, ϵ_0 is the potential well depth and σ is the radius R of the sphere or spherocylinder [13]. Figure 1.4 show the behaviour of the repulsive LJ potential.

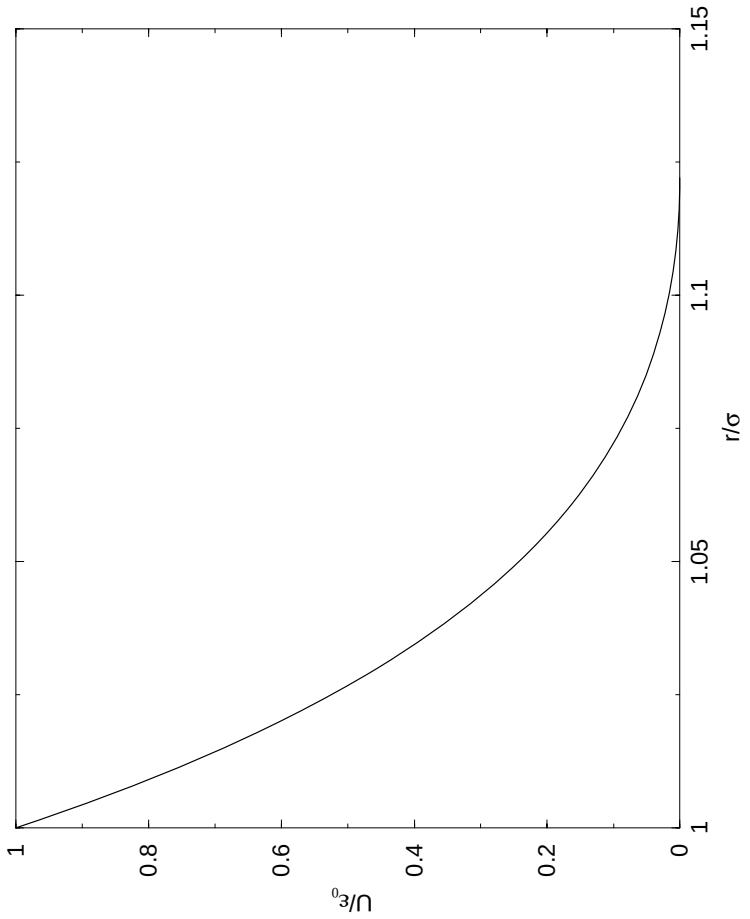

Figure 1.4: Repulsive Lennard-Jones Potential

1.2.3 Bonded potentials

Bonded potentials are used to model more realistic molecules by adding elastic bonds and flexibility to the molecules. These properties are modeled by adding two, three

and four body interactions. The most common two-body interactions are the FENE (the finitely extendable non-linear elastic) potential and the Harmonic potential. The FENE potential has the following form

$$U^{FENE}(r) = \begin{cases} 0.5R_0^2 k \ln[1 - (\frac{r}{R_0})^2] & r \leq R_0 \\ \infty & r > R_0 \end{cases} \tag{1.12}$$

were $k > 0$ is the force constant and R_0 is the maximum possible separation.

The force law of this spring is linear for small extensions, but will get stiffer and stiffer as the spring is extended; furthermore the spring cannot be extended beyond a separation R_0 [14]. The FENE potential is normally combined with a repulsive Lennard-Jones potential. This combination gives the behaviour of the harmonic potential, since the force calculation for the FENE does not require taking a square root, it is cheaper computationally than the harmonic potential.

The other most common two-body interaction potential is the harmonic potential. The harmonic potential has the following form

$$U^{Harmonic}(r) = \frac{1}{2}K(r - R_0)^2 \tag{1.13}$$

where were $K > 0$ is the force constant and R_0 is the equilibrium separation [15].

A three-body interaction or the bending potential is the potential for change in bond angle, this allows bending of the molecules to occur. Changes in the bond angle are modeled using the harmonic potential suggested by van der Ploeg and Berendsen [16, 17] as follows

$$U_i^{bend}(\theta_i) = \frac{k_i}{2}(\theta_i - \theta_i^0)^2 \tag{1.14}$$

where θ_i is the instantaneous C-C-C bond angle, θ_i^0 is the equilibrium bond angle and k_i the force constant [18, 17].

Finally, the four-body interaction is modeled using a torsional potential. The torsional (or dihedral) potential, initially proposed by Ryckaert and Bellemans [19] has the following functional form

c_0/k_BK	c_1/k_BK	c_2/k_BK	c_3/k_BK	c_4/k_BK	c_5/k_BK
1116	1462	-1578	-368	3156	-3788

Table 1.1: Torsional potential parameters where k_B is the Boltzmann constant.

$$U_i^{torsional}(\phi) = \sum_{n=0}^{n=5} c_n(\cos\phi_i)^n \tag{1.15}$$

where the coefficients are given in Table 1.1 and ϕ_i is the dihedral angle [17]. Figure 1.5 shows the behaviour of the Ryckaert torsional potential with respect to the dihedral angle.

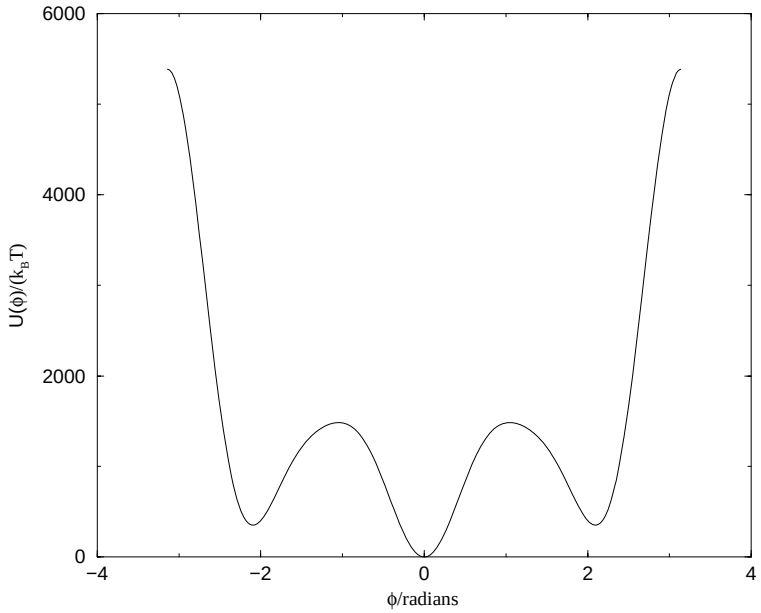

Figure 1.5: Ryckaert torsional potential for the coefficients shown in Table 1.1.

1.2.4 Lattice models

The most famous of the lattice models is the Lebwohl-Lasher model. The Lebwohl-Lasher model is the lattice version of the Maier-Saupe model of a nematic. The

Hamiltonian of the model is defined as

$$H = -J \sum_{<i,j>} P_2(\hat{s}_i \cdot \hat{s}_j). \tag{1.16}$$

P_2 is the second Legendre polynomial, $\hat{s}_i$ is a unit vector parallel to the long axis of the moleculer at site i and J is the strength of the nematic coupling. Because the molecules are fixed on the sites of a lattice, translational motion is absent. Nevertheless the model has been useful in studying the I-N transition and has been intensively investigated using Monte Carlo techniques [8].

Another type of lattice model, is due to Gruhn and Hess [20] and is described later in this thesis.

1.3 Molecular Dynamics

1.3.1 Introduction

Molecular dynamics (MD) is a technique used to solve the classical equations of motion for a system of N molecules/particles interacting via a potential U. This potential is generally approximated by a pairwise interaction of the form $U = \sum_i \sum_{j>i} \nu_2(r_{ij})$ The approximation gives a remarkably good description of liquid properties.

The most fundamental equation of motion is the Lagrangian equation of motion

$$\frac{d}{dt}\left(\frac{\partial \mathcal{L}}{\partial \dot{r}_i}\right) - \left(\frac{\partial \mathcal{L}}{\partial r_i}\right) = 0. \tag{1.17}$$

The use of the Lagrangian function $\mathcal{L}(\mathbf{r}, \dot{\mathbf{r}}) = \mathcal{K} - U$ in the equation above gives $m_i \ddot{r}_i = f_i$ which is Newton's equation of motion obtained by using $\mathcal{K} = \sum_i \frac{1}{2} m_i \dot{r}_i^2$ the kinetic energy and $f_i = -\nabla_{r_i} \mathcal{L} = -\nabla_{r_i} U$ the force [21]. The Hamiltonian is $\mathcal{H}(\mathbf{r}, \mathbf{p}) = \sum_i \dot{r}_i p_i - \mathcal{L}(\mathbf{r}, \dot{\mathbf{r}})$. Here p_i is the generalised momentum defined as $p_i = \frac{\partial \mathcal{L}}{\partial \dot{r}_i}$. Hamilton's equations become

$$\dot{r}_i = \frac{p_i}{m_i}$$

and

$$\dot{p}_i = -\nabla_{r_i} U = f_i.$$

Computing the centre of mass trajectories involves solving a system of $6N$ first order differential equations. Several algorithms exist that solve these equations of motion. This thesis uses two of these algorithms: the Leapfrog algorithm and the Velocity Verlet algorithm.

In the Leapfrog method, the stored quantities are the current positions $\mathbf{r}(t)$ and the current accelerations $\mathbf{a}(t)$ together with the mid-step velocities $\mathbf{v}(t - \frac{1}{2}\delta t)$. The velocity equation $\mathbf{v}(t + \frac{1}{2}\delta t) = \mathbf{v}(t - \frac{1}{2}\delta t) + \delta t \mathbf{a}(t)$ is implemented first so the velocities leap over the coordinates. The current velocities can be calculated using $\mathbf{v}(t) = \frac{1}{2}[\mathbf{v}(t + \delta t) + \mathbf{v}(t - \delta t)]$ which is necessary to calculate the energy at time t. The next move then is to advance the positions ahead of the velocities using $\mathbf{r}(t + \delta t) = \mathbf{r}(t) + \delta t \mathbf{v}(t + \frac{1}{2}\delta t)$. Now the new accelerations can be calculated for the new step [5]. This method is used in both the `GBMEGA` [22] and `GBMOL` [23] codes. The code `GBMEGA` is a large-scale parallel code used to simulate a large number of single type particles interacting through a pairwise potential at a constant temperature and volume. The interacting potential is commonly the Gay-Berne potential. The code `GBMOL` is a large-scale parallel code used to simulate hybrid atomistic model built from combining Gay-Berne units with Lennard-Jones units.

The velocity Verlet algorithm is split up into two stages with a force evaluation in between. The stored quantities are the current positions, velocities and accelerations. Firstly, the new positions at time $t + \delta t$ are calculated using $\mathbf{r}(t + \delta t) = \mathbf{r}(t) + \delta t \mathbf{v}(t) + \frac{1}{2}\delta t^2 \mathbf{a}(t)$ then the velocities at mid-step are computed using $\mathbf{v}(t + \frac{1}{2}\delta t) = \mathbf{v}(t) + \frac{1}{2}\delta t \mathbf{a}(t)$. The forces and accelerations are calculated at time $t + \delta t$. Then, the velocity move is completed using $\mathbf{v}(t + \delta t) = \mathbf{v}(t + \frac{1}{2}\delta t) + \frac{1}{2}\delta t \mathbf{a}(t + \delta t)$. At this point, the kinetic energy at time $t + \delta t$ is available and so is the potential energy which was evaluated in the force loop [5].

1.3.2 Special techniques

Constraint dynamics

Special techniques have been developed to handle the dynamics of a molecular system in which certain arbitrarily selected degrees of freedom i.e. bond lengths, are constrained, while others remain free to evolve under the influence of intermolecular and intra-molecular forces. This approach in effect uses a set of undetermined multipliers to represent the magnitudes of forces directed along the bonds. These are required to keep the bond lengths constant. The technique is to solve the equations of motion for one time step in the absence of constraint forces, then, subsequently determine their magnitudes and correct the atomic positions. There are several algorithms that perform this task; the one used in this thesis is called SHAKE. The SHAKE algorithm goes through the constraints one by one, cyclically, adjusting the coordinates so as to satisfy each constraint in turn. The procedure is iterated until all constraints are satisfied within a given tolerance [24]. The SHAKE algorithm is used in the code `GBMOL`.

Constant temperature: Ad hoc rescaling

Ad hoc methods of temperature control involve amending the conventional molecular dynamics algorithm, usually by rescaling the velocities at some stage, in an attempt to constrain the total kinetic energy [25]. It has been shown that when rescaling is performed at every time step, the method becomes equivalent to an algorithm for solving the equation of Hoover, Ladd and Moran [26] and Evans [27].

The rescaling factor is usually of the form

$$\lambda = \left(1 + \frac{\delta t}{t_T}\left(\frac{T}{\tau} - 1\right)\right)^{\frac{1}{2}} \tag{1.18}$$

where τ is the current kinetic temperature, T is the desired temperature, δt is the time step and t_T is a pre-set time constant. This will force the system towards the desired temperature at a rate determined by t_T, while slightly perturbing the forces

on each molecule [28]. This thermostat is used in the code `GBMEGA` when performing a simulation in the constant-NVT ensemble. In the code, t_T is set equal to the time step δt. This gives a scaling factor of $\lambda = \left(\frac{T}{\tau}\right)^{\frac{1}{2}}$.

Constant temperature: Andersen's thermostat [29]

In this method, atoms are selected randomly in each step, and their velocities are replaced by values chosen randomly from a Maxwell-Boltzmann distribution corresponding to a collision with an imaginary heat bath at the desired temperature. The times between collision for an atom conform to a Poisson distribution, with a collision rate that may be fixed [25]. Denote this rate by ν. The probability that a particle undergoes a stochastic collision in a time step δt is $\nu \delta t$ [30].

Alternatively, the velocities of all the particles could be replaced at the same time from values chosen randomly from the Maxwell-Boltzmann distribution. The times of these interventions are equally spaced along the trajectory. This has the advantage that normal Newtonian dynamics exist between the stochastic collisions [25]. This is the thermostat used in the code `GBMOL` and is used in simulating a fluid in the constant-NPT and constant-NVT ensembles.

Constant pressure: Stochastic method

The stochastic constant pressure molecular dynamics method incorporates MC-like box-size moves.

In constant pressure MD, the volume of a system of N particles fluctuates to maintain the pressure at a constant. To describe such fluctuations, the volume of the system can be thought of as a dynamical variable. We assume the system is in a cubic box of length $L = V^{\frac{1}{3}}$. The coordinates are now scaled by $\mathbf{s}_i = L^{-1}\mathbf{r}_i$, for $i = 1, 2, \ldots, N$. Using the Metropolis scheme, a new state n can be generated from the old state o by making a random change in volume from V_o to V_n. Once the new

state has been produced the quantity δH is calculated,

$$\delta H_{no} = \delta U_{no} + P(V_n - V_o) - N\beta^{-1} \ln\left(\frac{V_n}{V_o}\right) \tag{1.19}$$

δH_{no} is closely related to the enthalpy change in moving from state o to state n [28]. Moves are accepted with a probability equal to min(1,exp($-\beta H_{no}$)). If the moves are accepted, the coordinates are rescaled using the new volume. It has been shown that it is more convenient in terms of computation to make random changes in $\ln V$ rather than in V itself [28].

1.3.3 Parallelisation

Replicated data

The replicated data method is the most popular technique for parallel molecular dynamics. This is due to the inherent simplicity of the method; often only minor changes are required to convert a serial program into a parallel form. The essence of the method is that each computer node runs the same MD program, undertaking the same operations - with the exception of reading and writing to disk - up to the point where a task can be carried out in parallel. At this point each node takes part of the parallel task, and at the end of this task any data required by all nodes must be passed and received in a communication step. In MD programs, the parallelisation is mostly used in the evaluation of forces in the force loops [31]. A method is required to allow the independent nodes to exchange data when needed. This is done by a set of communication routines that are called from within the program to carry out message passing tasks. The two most common set of routines are MPI (Message Passing Interface) and PVM (Parallel Virtual Machine) both can be called from FORTRAN or C code [31].

The code `GBMOL` [23] described and used in this work is a parallel replicated data MD code that uses both MPI and PVM; the former was used on an SGI Origin 2000 and the latter on a Cray T3E.

Domain Decomposition

Unlike replicated data methods, where all the data is copied to all the nodes, domain decomposition methods involve distributing the data among the nodes. This is done by partitioning the system into spatial domains. Each domain is assigned to a node. In the case of MD, the simulation box is divided into cuboidal domains. The positions and velocities of the particles in each domain are assigned to a node. Only neighbouring nodes need to exchange data. This exchange of data is accomplished by six communication steps, which transfer information in the $\pm x, y$, and z directions. Each node updates data in its own domain and exports any particles that have moved outside its domain to neighbouring nodes [32].

The code `GBMEGA` [22] used in this work is a domain decomposition parallel MD code that uses both MPI and PVM and runs on the Cray T3E.

1.4 Monte Carlo

1.4.1 Introduction

The Monte Carlo method (MC), is an efficient technique for sampling from a multi-dimensional probability distribution; it has applications in many fields. Here we give a brief summary of this method in its simplest form applied to statistical mechanics. The aim is to calculate ensemble averages such as

$$\langle A \rangle_{NVT} = \frac{\int d\mathbf{r} A(\mathbf{r}) \exp(-\beta U(\mathbf{r}))}{\int d\mathbf{r} \exp(-\beta U(\mathbf{r}))} \approx \frac{1}{N_{obs}} \sum_{obs} A_(obs) \tag{1.20}$$

N_{obs} is increased until the ensemble average is estimated to the desired accuracy. At realistic liquid densities this can be solved using a sample mean integration where the random coordinates are chosen from a non-uniform distribution. This method is called importance sampling. Importance sampling techniques choose random numbers from a distribution which allows the function evaluation to be concentrated in the regions of space that make important contributions to the integral [5]. A

method is needed to generate a sequence of random states such that by the end of the simulation each state has occurred with the appropriate probability. This can be done by setting up what is known as a Markov chain. A Markov chain is a sequence of trials that satisfy two conditions:

(a) The outcome of each trial belongs to a finite set of outcomes called phase space.

(b) The outcome of each trial depends only on the outcome of the trial that immediately preceeds it.

Since the simulations are of finite length, it is essential that the Markov chain samples a representative portion of phase space in a reasonable number of moves. One method that gives a quicker convergence of the Markov chain is the Metropolis method. The Metropolis method starts an MC move by picking an atom at random and giving it a uniform random displacement along each of the coordinate directions. The maximum displacement is an adjustable parameter that controls the convergence of the Markov chain. The next MC move is to determine the difference in energy δU between the old state and the new state. If the move is downhill in energy ($\delta U \leq 0$) then the probability of the new state is greater than the old state and the new state is accepted. If the move is uphill in energy ($\delta U > 0$) then the move is accepted with a probability equal to the ratio of the two distributions. This can be expressed as the Boltzmann factor of the energy difference $\exp(-\beta\delta U)$. To accept a move with a probability of $\exp(-\beta\delta U)$, a random number is generated uniformly between 0 and 1. The random number is compared with the Boltzmann factor. If it is less then $\exp(-\beta\delta U)$ the move is accepted. If the move is rejected, the system remains in the old state, and the old configuration is recounted as a new state in the chain [5, 30].

A common practice in MC simulation is to select the particles to move sequentially rather than randomly. This cuts down on the amount of random number generation and is an equally valid method. This is the approach taken in this work.

1.4.2 Gibbs Ensemble Monte Carlo

Gibbs Ensemble Monte Carlo (GEMC) is a direct method to simulate a fluid at phase equilibrium. Panagiotopoulos introduced the Gibbs ensemble as a combination of NVT, NPT and μPT ensembles [33]. The method uses two basic simulation boxes that are within two coexisting phases. The boxes are surrounded by the normal periodic images and there is no attempt to simulate the interface between the phases [5]. The technique uses three types of moves; one of these is the independent particle displacements in each box which are made using the normal Metropolis algorithm. There is a combined attempted volume move in which the volume of one box changes by ΔV while the volume of the other box changes by $-\Delta V$. The pressure in the two boxes is equal but its precise value is not required in the algorithm. Only the difference in pressure between the two phases is fixed (namely, $\Delta P = 0$). Finally, there is a combined attempted creation/destruction move, where a randomly chosen particle is extracted from one box and placed at random in the other. The chemical potential in the two boxes is equal but its precise value is not required. Only the difference between the two phases is fixed (namely, $\Delta \mu = 0$). The total number of particles and the total volume of the two boxes remain constant; that is the total system is at constant NVT. It can be shown that - in the thermodynamic limit - the Gibbs ensemble is equivalent to the canonical ensemble [30].

1.4.3 Simulated annealing

Simulated annealing is a stochastic optimisation procedure which is widely applicable and has often been applied in conjunction with the Metropolis algorithm [34, 28]. The trick is to statistically model the evolution of the physical system at a series of temperatures that allow it to anneal into a state of high order and very low energy. The process consists of first melting the system being optimised at a high effective temperature, then lowering the temperature in slow stages until the system freezes and no further changes occur. At each temperature the simulation must proceed long

enough for the system to reach a steady state. Annealing, as implemented by the Metropolis procedure differs from the iterative improvement in that the procedure need not get stuck in local minima. The temperature in the iterative improvement method always decreases while in simulated annealing, there is a probability that the temperature would go up. Hence for simulated annealing, transitions out of a local minimum are always possible at nonzero temperatures [35, 36].

1.5 Scope of this thesis

In this thesis, we investigate the behaviour of liquid crystals near interfaces using various models. We concentrate on three types of interfaces, namely, nematic-vapour, nematic-isotropic and the effects of different solid surfaces on a nematic liquid crystal. In Chapter 2 we describe the different physical properties of these interfaces and some of the work done in this area. The remainder of the thesis describes our work and scientific results, and is structured as follows:

- Chapter 3 concerns extensive simulations of a Gay-Berne/Lennard-Jones model of the form C7GBC7 in pure bulk and mixed with C7GB fluids. Thin films are also studied for the pure and mixed fluids.

- In Chapter 4 we report simulations of a nematic-isotropic film of a spherocylinder fluid. We measure density and order parameter profiles of the nematic-isotropic interface for molecules oriented normal and parallel to the interface.

- Chapter 5 covers the effects of different shapes of solid surfaces in contact with a nematic fluid, here a lattice model is used. We investigate bistability in systems in contact with triangular and bigrated surfaces.

Finally, conclusions are drawn in Chapter 6.

Chapter 2

Interfaces

2.1 Introduction

Dietrich [37] defines an interface as a structure that emerges when two phases of condensed matter are brought into spatial contact. This interface interpolates smoothly between the bulk properties of the adjacent phases [37].

Liquid crystals - as described in Chapter 1 - are characterised by long ranged orientational ordering and short ranged positional order (e.g. nematic liquid crystals). Liquid crystalline interfaces are formed when a liquid crystal comes in contact with a solid surface and liquid crystal molecules are anchored to the surface. Interfaces may also occur when the liquid crystal forms a film surrounded by vapour or when an ordered phase (nematic or smectic) comes into contact with an unordered phase (isotropic). When the translational symmetry is broken by a surface, or spontaneously by an interface, the free energy of the system will depend on the direction of the director. The molecules will adopt the orientation that minimises the free energy, in particular, minimising the surface tension of the interface. This is known as anchoring. The main focus in anchoring discussions is on the identification of an anchoring angle. The anchoring angle is defined as the nematic director orientation at the surface or interface relative to the surface normal, or to some other

direction defined by the surface geometry, for example an 'easy axis'. An anchoring angle normal to the surface is known as homeotropic anchoring while planar anchoring describes anchoring in the plane of the surface or interface. All intermediate anchoring orientations are classed as oblique [38], conic or tilted. A study of the interface can therefore yield information on molecular interactions that are averaged out in the bulk [39].

Other interesting phenomena include wetting and wetting transitions. Wetting in liquid crystals is concerned with enhanced (or diminished) order near an interface. Order in a liquid crystal depends on direction as well, but in wetting transitions it is the magnitude of the surface order that undergoes a transition. Conversely in surface orientational transitions, changes in magnitude of the surface order are frequently ignored and all the concentration is on the major qualitative feature: the direction of the surface order [40]. Two types of wetting can occur. The first is complete wetting which occurs when the contact angle $\theta = 0$, as shown in Figure 2.1(a). Here the solid substrate γ is fully wet by the fluid β. This complete wetting corresponds to a film with a thickness that is much larger than microscopic lengths. The second type of wetting is partial or incomplete wetting which occurs when the contact angle is larger than zero [41], as shown in Figure 2.1(b). Here the $\alpha - \gamma$ interface is partially wet by the fluid β. In both cases the two phases β and γ are in coexistence with a third fluid α, with γ being either a solid substrate - as in the figure - or another fluid. Detailed reviews of wetting are presented by Sullivan and Telo da Gama [42] and references within.

A lot of progress was made in the last decade on the studies of surfaces and interfacial properties. Here three types of interfaces that are relevant to the work presented in this thesis are reviewed. These are the nematic-vapour (N-V) interface, the isotropic-nematic (I-N) interface and the nematic-solid surface interface. Section 2.2 will review experimental, theoretical and simulation studies of the N-V interface. The section after that, will review experimental, theoretical and simulation studies of the I-N interface. Finally, Section 2.4 will briefly review some of the

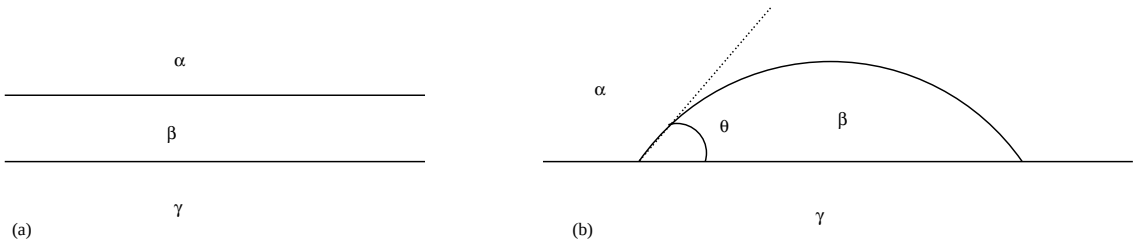

Figure 2.1: Relationship between wetting behaviour and contact angle. (a) Complete wetting by phase β, $\theta = 0$, (b) Partial wetting by phase β and $\theta \neq 0$

work done in investigating the nematic-solid interface and especially the effect of the shape and topography of the surface on the bulk.

2.2 Nematic-Vapour Interfaces

2.2.1 Introduction

The nematic-vapour interface has been extensively studied both experimentally and theoretically and more recently through simulation. The anchoring angle, also known as the tilt angle - which is the preferred direction of the nematic molecules relative to the interface - seems to vary with the nematogen and in general it is different from the tilt angle of the I-N interface for the same system. Additionally, these interfaces may exhibit structural changes including tilt angle (anchoring) transitions and orientational disordering (wetting) transitions [39].

2.2.2 Experiments

Experimental studies of the nematic-vapour interface show a wealth of physical behaviour. The results of these studies show that the anchoring alignment at the nematic vapour interface can be either planar as found in PAA, homeotropic as for cyano-biphenyls nCB (n=5,6,7,8) or oblique (i.e. at an angle between the two) as observed in MBBA and EBBA. Oblique to homeotropic anchoring transitions were

also observed experimentally for the liquid crystals MBBA and EBBA.

Bouchiat and Langevin-Cruchon in 1971 [43] were the first to measure the anchoring angle. They did light reflection measurements on the nematic liquid crystals PAA and MBBA. They found that PAA molecules lie in the plane of the free surface. In 1972, Langevin [44] measured the surface tension of the nematic free surface of PAA and MBBA. She used a high resolution spectrum analysis of the scattered light from the free surface. She found the surface tension of PAA to be $\gamma = 38 \pm 4$ dynes cm^{-1}. Chiarelli, Faetti and Fronzoni [45] also measured the anchoring angle θ between the director and the vertical axis at the free surface of the nematic liquid crystal PAA. To achieve better accuracy in their measurement Chiarelli *et al* made certain improvements to the techniques of Bouchiat and Langevin-Cruchon. They confirmed earlier results that PAA molecules lie parallel to the free surface i.e. planar anchoring ($\theta = 90^o$).

Bouchiat and Langevin-Cruchon [43] applied the same techniques on the liquid crystal MBBA and found that the anchoring angle of MBBA is tilted at an average angle $\theta \approx 75^o$ from the surface. The actual angle varied slightly from $\theta \approx 68^o$ to $\theta \approx 79^o$ as the temperature increased towards the critical temperature T_c. This tilt was also observed by Gannon and Faber [46] for MBBA. The surface tension of MBBA was later found by Langevin [44] to be $\gamma \approx 38$ dynes cm^{-1}. These results were confirmed by Chiarelli, Faetti and Fronzoni [47] for MBBA. They also obtained similar results for the liquid crystal EBBA. They found that a structural transition occurs in MBBA and EBBA when the temperature reaches a critical point T_o close to the clearing temperature T_c of the nematic liquid crystal. Below T_o they showed that the angle θ tends to zero as $\theta = C(T_o - T)^\beta$ where $\beta \simeq 0.5$ and C is a constant. They compared their results with the results of theoretical models of the free surface done by Parsons [48] and found good agreement.

Homeotropic anchoring was first observed experimentally in 1978 by Gannon and Faber [46] who measured the surface tension of two cyanobiphenyls (5CB and 8CB) at temperatures near the nematic-isotropic transition temperature, using the

Liquid Crystal Molecule	Anchoring	Surface Tension γ (dynes cm^{-1})
PAA	Planar [43, 45]	38 ± 4 [44]
MBBA	Oblique [43, 46, 47]	38 [44]
EBBA	Oblique [43, 47]	–
5CB	Homeotropic [46, 49]	28.1 ± 0.3 [46]
6CB	Homeotropic [49]	–
7CB	Homeotropic [49]	–
8CB	Homeotropic [46, 49]	26.2 ± 0.3 [46]

Table 2.1: Summary of experimental results for different liquid crystals at the nematic-vapour interface

Wilhelmy plate method. They found the surface tension of 5CB to be $\gamma = 28.1 \pm 0.3$ dyne cm^{-1} and $\gamma = 26.2 \pm 0.3$ dyne cm^{-1} for 8CB. Observing thin films of 5CB and 8CB microscopically, Gannon and Faber observed a preferred orientation of the director adjacent to the free surface that was normal to the surface. Recently, Kasten and Strobl [49] confirmed Gannon and Faber results when they studied the free surface of a homologous series of low molecular weight liquid crystals (nCB, n=5,6,7,8) by reflection ellipsometry. They found that the isotropic phase was completely wet by a homeotropically aligned nematic film for n=6,7,8 and partially wet for n=5. They also found strong evidence of a thin surface layer possessing enhanced order on top of the homeotropically aligned nematic bulk. For n=6,7,8 the layer was seen to grow as the temperature approaches the nematic-isotropic transition temperature. This was not the case for n=5, where no surface effects were observed.

2.2.3 Theory

Theoretically, all three anchoring orientations were predicted, as were orientational and wetting transitions. In order to study these various anchoring angles and

physical phenomena, different theoretical models and approaches were used. Planar anchoring was first predicted theoretically in the early studies of Parsons in 1976. Parsons [48] calculated the surface tension at the free surface of a nematic liquid crystal. Parsons used the Fowler-Kirkwood-Buff approximation to estimate the surface tension and a mean field approximation to the molecular pair distribution function. He found that for a model of molecules interacting with the van der Waals interaction, the surface tension was at a minimum when the anchoring was planar. Parsons then looked at the effects of the molecules having permanent dipoles on the interface. He assumed that the dipoles were oriented along the long axis of the molecules. From this, he observed that the dipole-dipole interaction enhanced planar anchoring. Parsons indicated that if the permanent dipoles were off axis, then the competing forces between the Van der Waals forces and the dipole-dipole interaction might lead to oblique anchoring. Since the two order parameters associated with the two interactions have different temperature dependence, the tilt angle should change with temperature.

More recently, Osipov and Hess [50] also predicted planar anchoring. They derived general expressions for the free energy of the nematic liquid crystal in the interfacial region using a density functional approach. They expressed the anisotropic part of the surface tension and the coefficients of the Landau-de Gennes theory for the nematic free surfaces in terms of the direct correlation functions. Osipov and Hess found a preferred alignment parallel to the interface. They attributed this to the contribution from the short ranged intermolecular interactions.

Homeotropic anchoring was first predicted by Telo da Gama and co-workers. Telo da Gama [51] developed a mean field theory for interfacial properties of nematics. The model consists of spherical hard-core particles interacting via a long-range attractive potential of the Maier-Saupe type. The model exhibits nematic, isotropic and vapour phases; these phases coexist in pairs and coexist simultaneously at a low temperature triple point. Telo da Gama obtained explicit phase diagrams of the model which were found to be in good agreement with the experimental results.

She also calculated order parameter and density profiles for both the nematic-vapour and the nematic-isotropic interfaces. These were done for different anisotropic ratios of the Maier-Saupe potential and for different temperatures. Telo da Gama calculated the interfacial N-I surface tension and concluded that the model grossly overestimated it. A missing feature of this model is a preferred orientation at the interfaces. This is perhaps due to the lack of coupling between the orientational and translational degrees of freedom in the potential. Thurtell, Telo da Gama and Gubbins [52] corrected the problem by adding a coupling between the orientational and the translational dependence of the potential. They found that, the preferred orientation depended on the strength of this coupling, which in turn was governed by a constant. This constant could be either positive which represents a prolate molecule with an predicted planar anchoring, or it is negative which corresponds to an oblate shaped molecule with a homeotropic anchoring at the interface. When the constant is zero, the earlier results [51] are obtained where no preferred alignment was observed. A drawback of this theory is that oblique anchoring cannot be explained.

Kimura and Nakano [53] calculated the surface tension in the mean field approximation for a system of rod-like molecules interacting via an attractive as well as repulsive hard core potential. They concluded that hard-core repulsions favour the normal alignment of molecules at the free surface while the attractive interaction favours planar anchoring. They attribute the temperature dependence of oblique anchoring to the counterbalance between the effects of repulsion and attraction.

Tjipto-Margo and Sullivan [54] have used molecular perturbation methods to derive an approximate free energy functional for nonuniform nematic liquids interacting via the Gay-Berne potential. They simplified the free energy to a Landau-de Gennes form and applied it to orientational alignment and nematic wetting at the free isotropic liquid-vapour interface. Tjipto-Margo and Sullivan predicted a preferred nematic alignment that was perpendicular to the interface. They also found that the wetting by the nematic phase changed from complete to incomplete

as the molecular elongation increased. This contradicts the findings of Kasten and Strobl [49] whose experiments on the nCB series found partial wetting for 5CB and full wetting for 6CB, 7CB and 8CB. Tjipto-Margo, Sen, Mederos and Sullivan [55] extended and refined the earlier studies of Telo da Gama *et al* [51, 52]. By using improved numerical techniques, they found that the theory does exhibit nematic wetting, a feature that was absent from the earlier findings of Telo da Gama *et al*. They managed to show that the observed non-monotonic variation of the liquid-vapour surface tension with temperature - as observed experimentally by Gannon and Faber [46] - was a direct consequence of the approach to complete nematic wetting. More recently, Martín del Rio, Telo da Gama, de Miguel and Rull [56] applied the generalised van der Waals theory to a model of liquid crystal that includes all of the second-order terms in the spherical harmonic expansion of the anisotropic intermolecular potential. They investigated the orientational order induced by each term as well as the order resulting from the competition between the various terms included in the potential. For appropriate choices of the relative strengths of the spherical harmonic coefficients they showed that the theory could account for all the orientational effects observed at nematic interfaces. They also managed to describe qualitatively the molecular orientation at the interfaces of certain nematogens. They found that a single set of coefficients can describe correctly the anchoring alignment of the nCB series at both the N-V and the N-I interfaces. They obtained similar results that described the alignment of molecules at the interfaces of the liquid crystal MBBA. They also observed biaxial behaviour at the interface when the anchoring is planar at the N-I interface. Additionally, they have shown that temperature driven orientational transitions, such as a first order transition from tilted to homeotropic alignment, may occur in systems that are characterised by such interactions. This is in contrast to experimental findings that show that this transition is second order [47]. Martín del Rio *et al* found an orientational transition which they related to a wetting transition at the nematic-vapour interface [57]. Their theory accounts for the growth of the surface ordered layer that develops at the nematic-vapour inter-

face as the temperature increases towards the triple point. This is in agreement with experimental results obtained by Kasten and Strobl for 8CB [49].

Finally, Braun, Sluckin, Velasco and Mederos [38] predicted oblique anchoring theoretically. They generalised earlier density functional theories of nematic interfaces by adding an electrostatic quadrupole term to the orientationally coupled hard-core Lennard-Jones potential. They applied the Fowler approximation to the interface: this involves constraining the interfacial structure to a step function, thus neglecting interfacial width and structure. Braun *et al* predicted oblique anchoring at the nematic-vapour interface in agreement with experimental results of MBBA [43]. They also predicted a second-order oblique to homeotropic anchoring transition which was observed in the experiments of Chiarelli *et al* [47].

2.2.4 Simulation

There are a large number of studies of the liquid-vapour interface using simulation of the Lennard-Jones model and numerous attempts have been made to calculate the surface tension of argon (see for example Holcomb, Clancy and Zollweg [58] and references therein). Later on, these attempts were extended to the Gay-Berne model to simulate the isotropic-liquid-vapour interface and finally the nematic-vapour interface using the corresponding parametrization of the well known phase diagram of the Gay-Berne model [59, 60].

This work was initially done by de Miguel, Rull, Chalam and Gubbins [61] using Gibbs-ensemble Monte Carlo simulation to predict the liquid-vapour coexistence of a Gay-Berne fluid. They used a molecular elongation of $\kappa = 3$ and well-depth ratio $\kappa' = 5$. They also presented evidence of the existence of the vapour-isotropic-solid triple point, but they were unable to see the vapour-isotropic-nematic triple point predicted by Somoza and Tarazona [62] using the local density-functional approximation. de Miguel *et al* did not simulate the actual interface or measure any of the isotropic-nematic interfacial properties. A few years later Martín del Rio,

de Miguel and Rull [63] simulated the liquid-vapour interface using the Gay-Berne model with the above GB parameters. They used molecular dynamics (MD) in the constant-NVT ensemble to study the system at different temperatures. For each temperature; the density, orientation, energy and pressure tensor profiles were obtained. Their density profiles fitted well to the hyperbolic tangent function and their order parameter profiles show a perpendicular preferred orientation at the interface at low temperature. Lowering the temperature even further showed the formation of a smectic phase at one of the interfaces with a preferred orientation parallel to the interface. Martín del Rio *et al* indicated that the system may not have reached equilibrium. Finally, they measured the surface tension and surface thickness and observed an increase in the value of the surface tension as the system approaches the vapour-isotropic-smectic triple point. Martín del Rio and de Miguel [64] simulated the liquid-vapour interface of the Gay-Berne model for a range of temperatures above and below the vapour-isotropic-nematic triple point. They used a molecular elongation $\kappa = 3$ and two values of the energy anisotropy parameter ($\kappa' = 1$ and $\kappa' = 1.25$). Martín del Rio and de Miguel found that molecules in the nematic phase oriented themselves parallel to the interface.

Emerson, Faetti and Zannoni [65] simulated the nematic-vapour interface for a Gay-Berne (GB) liquid crystal using Monte Carlo. They used an energy anisotropy parameter $\kappa' = 1.25$ to obtain a stable nematic film. This parameterization is known to show evidence of nematic-vapour coexistence [63]. This was used instead of the original GB parameterisation of $\kappa' = 5$. They left the other parameters unchanged. Emerson *et al* observed a preferred orientational ordering that was planar to the interface. They found no nematic wetting of the film in the isotropic phase. Mills, Care, Neal and Cleaver [66] used molecular dynamics to simulate an unconfined Gay-Berne film in equilibrium with its vapour. They used the parameterisation $\kappa = 2.0, \kappa' = 5.0, \mu = 1.0$ and $\nu = 2.0$. This is a much shorter molecule with stronger exponents. Mills *et al* found stable nematic-vapour coexistence using Gibbs ensemble Monte Carlo. They then simulated a nematic thin film sandwiched between

two nematic-vapour interfaces. From the simulation, they observed a preferred molecular alignment in the nematic film perpendicular to the interface. At slightly higher temperatures, they observed a wetting of the nematic phase by the isotropic phase. Finally, they evaluated the surface tension and compared it successfully with theoretical predictions. As liquid crystal molecules are characterised by their length anisotropy, models with short elongations (i.e. $\kappa = 2$) seem unrealistic. This indicated that there maybe another factor behind homeotropic anchoring at the nematic-vapour interface observed by experiments.

2.2.5 Summary

Experimental results show that the anchoring alignment at the nematic-vapour interface can be either planar as is the case for PAA[43, 45], homeotropic as for cyanobiphenyls nCB (n=5,6,7,8)[46, 49] or oblique (i.e. at an angle between the two) as observed in MBBA and EBBA [43, 46]. A second-order oblique to homeotropic transition was observed for MBBA and EBBA [47]. Theoretically, planar anchoring [48, 50], homeotropic anchoring [52, 53, 54] and oblique anchoring [38] have been predicted. A second-order transition between oblique anchoring and homeotropic anchoring was also predicted theoretically [38]. A few theories attempted to explain all types of anchoring for most of the different liquid crystal interfaces [53, 52] . All simulations of the nematic vapour interface were done using the Gay-Berne model. The original parameters $\kappa = 3$ and $\kappa' = 5$ did not give an N-V interface, since the nematic phase is only stable for temperatures above the critical point[63]. The changing of the energy anisotropy parameter κ' to $\kappa' = 1$ and $\kappa' = 1.25$ gave planar anchoring [64, 65]. Homeotropic anchoring was observed for GB parameters $\kappa = 2.0, \kappa' = 5.0, \mu = 1.0$ and $\nu = 2.0$ [66]; this is a very short and unrealistic molecule. However, the potential is strongly attractive, which may be the cause of homeotropic anchoring.

Oblique anchoring as observed in the nematic-vapour interface of MBBA and

EBBA might be caused by quadrupole interactions [67, 38]. Other theoretical studies have suggested that it might be the competition between hard-core repulsive forces and attractive forces [53, 52] that are the drive behind oblique anchoring. To the author's knowledge, no studies of oblique anchoring using computer simulations have been attempted. What drives the molecules to orient normal to the interface rather than parallel is still not quite understood. Most of the theoretical and simulation models of liquid crystals model the molecule as a rigid uniaxial particle. None of the models take into account the flexible nature of liquid crystal molecules. This is one of the objectives of this work: to investigate the effect of molecular flexibility on the alignment of molecules at the nematic-vapour interface. This is described in detail in Chapter 3.

2.3 Isotropic-Nematic Interfaces

2.3.1 Introduction

The isotropic-nematic interface is the simplest interface of nematogens, since for all practical purposes the isotropic and nematic liquids are incompressible, so the pressure is not an experimental parameter. Further more, due to the small difference between the isotropic and nematic densities at the transition, the density is not believed to play an important role at the I-N interface [39]. An understanding of the interfacial alignment in this simple inhomogeneous system presents some fundamental questions about which molecular features, if any, are necessary to produce a certain type of anchoring.

2.3.2 Experiments

There is a lack of experimental data for non-polar mesogens. This makes it difficult to separate the roles of the steric and electrostatic interactions. For example Langevin and Bouchiat [68] did light reflectivity measurements and found a tilt an-

Liquid Crystal Molecule	Anchoring Angle	Surface Tension γ (dynes cm^{-1})
MBBA	Planar [68]	$2.3 \pm 0.4 \times 10^{-2}$ [68]
nCB	Oblique [69]	–
Lyotropic	Planar [70]	2.4×10^{-2} [70]

Table 2.2: Summary of experimental results for different liquid crystals at the isotropic-nematic interface

gle of $\pi/2$, i.e. planar anchoring, for the liquid crystal MBBA. They also measured a surface tension of $\gamma = (2.3 \pm 0.4) \times 10^{-2}$dyne cm^{-1}. Faetti and Palleschi [69] studied the properties of the isotropic-nematic interface of some members of the nCB series using optical reflectometry. They found tilt angles that range between $\theta = 48.5^o$ to $\theta = 64.5^o$ and interfacial thicknesses of the order of 400-700Å. More recently, Chen, Sato and Teramoto [70] measured the interfacial tension between coexisting isotropic and nematic phases of a lyotropic polymer liquid crystal. A polarising microscope observation revealed that the nematic in the vicinity of the interface is aligned parallel to the interface. The measured value of the surface tension was $\gamma = 0.024$ dyne cm^{-1}.

2.3.3 Theory

The work of Onsager [71] in 1949 was one of the earliest theoretical studies investigating isotropic-nematic phase transitions. Onsager developed a theory now known by his name based on the minimisation of the free energy of the fluid. Onsager showed that a system of rigid rodlike molecules interacting with each other through steric, excluded-volume interactions can undergo a first-order phase transition from the isotropic phase to the nematic phase and that the two phases can coexist. Twenty-two years later, de Gennes [72] developed a theory based on the Landau expansion of the free energy as a function of the order parameter tensor. Expressing the surface

tension at the isotropic-nematic interface in terms of the free energy and calculating its minimum, de Gennes predicted that the tilt angle at the interface can only have two orientations: normal to the interface or at a planar orientation. More recently, Telo da Gama [51] used a model consisting of a spherical hard core particle interacting via a long-range attractive potential of the Maier-Saupe type. This model does not exhibit any preferred orientation at the nematic-isotropic interface. This is due to the lack of coupling between the orientational and translational degrees of freedom in the potential. Telo da Gama calculated order parameter and density profiles and surface tension of the isotropic-nematic interface for different anisotropy ratios. These calculations give poor surface tension estimates. The reader is directed to Section 2.2 for a more detailed description.

As with experiments, different anchoring orientations were theoretically predicted. Planar anchoring was first predicted theoretically by Doi and Kuzuu [73]. They derived a theoretical estimate of the surface tension of the isotropic-nematic interface of a hard rod solution using an approach that treated the interfacial thickness on a macroscopic length scale. Using Onsager's theory they found an interfacial thickness of $0.638L$ gave a minimum in the surface tension and the surface tension had a minimum of $\gamma = 0.257\ k_BT/(DL)$, where k_B is the Boltzmann constant, T is the temperature, L is the molecular length and D the molecular diameter. Kimura and Nakano [74] calculated the surface tension of the isotropic-nematic interface in a mean field approximation for a system of rod-like molecules interacting via an attractive and hard-core repulsion. They found that the hard-core repulsion favors the planar orientation at the I-N interface. They made no attempts to calculate the values of the surface tension. In two separate studies McMullen [75, 76] did calculations on hard spherocylinders at the isotropic-nematic interface using phenomenological methods. McMullen predicted tilt angles that were either parallel or normal to the interface. Moore and McMullen later [77] investigated the isotropic-nematic interface of hard spherocylinders in the square-gradient approximation. They found that for spherocylinders of $L/D > 10$ the anchoring at the interface was planar, but

predicted oblique anchoring for $L/D < 10$. The truncation of the theory at the level of two-body interactions is only accurate in the limit $L/D \to \infty$, hence the tilt may be an artefact of the approximation.

Chen and Noolandi [78] numerically solved the interfacial profile of the isotropic-nematic interface of a rigid-rod system using a generalised Onsager model. They found that the preferred tilt angle between the nematic director and the normal to the interface was $\theta = \pi/2$, i.e. planar anchoring. They also found that the interfacial widths and positions on the density profiles were different from those of the order parameter profiles. They found an offset between the two profiles to be $\sim 0.5L$ and the interfacial thickness to be approximately $1.5L$ for the planar orientation. They deduced an interfacial tension of $\gamma = (0.183 \pm 0.002)\ k_B T/(DL)$. Chen [79] later did biaxiality calculations using the same approach. By defining the biaxial order parameter as $\alpha(z) = \frac{3}{2}\langle \sin^2\theta(\cos^2\phi - \sin^2\phi)\rangle_z$, where θ and ϕ are the usual spherical-polar angles. Chen saw a weak biaxial effect near the isotropic side of the interface where the nematic ordering is relatively small. The width of the effect was roughly $2L$. Chen only examined two possible solutions for the tilt angle, one planar ($\theta = \pi/2$) for which the surface tension was minimum, and the other homeotropic ($\theta = 0$) for which the surface tension was maximum.

Cui, Akcakir and Chen [80] investigated the behaviour of liquid crystalline polymers in the interfacial region between the isotropic and nematic phases. They have used a mean-field approximation on a system of semi-flexible polymers interacting via an Onsager-type repulsive interaction. The density distribution of polymers crossing the interface was computed using a spherical-harmonics expansion. The interfacial tension was also calculated which was found to be consistent with the results of a scaling argument. Cui *et al* found a preferred planar orientation of the nematic at the interface with a surface tension of $(0.221 \pm 0.002)\ k_B T/(Da)$, where $2a$ is the persistence length. They also found a significant biaxiality effect in the interfacial region and a depletion in the density profile near the isotropic side of the interface. More recently, Koch and Harlen [81] obtained density and order parame-

ter profiles across the interface by minimising the free energy in the inhomogeneous fluid using an approach that generalises Onsager's classical theory to spatially inhomogeneous hard rod solutions. They found a planar alignment at the interface and an interfacial thickness of $0.431L$. Their order parameter profile grows monotonically from $S = 0$ in the isotropic phase to $S = 0.847$ in the nematic phase. The rod concentration exhibits a non-monotonic behaviour: it has a minimum that is smaller than the concentration in the isotropic phase. Koch and Harlen also calculated the surface tension which they found to be $\gamma = 0.316\ k_BT/(DL)$. They found that the biaxial nature of the rods' orientation distribution had a significant effect on the interface. Using a biaxial trial function reduced the surface tension by 19% compared to that of a uniaxial trial function. None of the experimental studies on the isotropic-nematic interface showed evidence of a non-monotonic behaviour of the density.

Finally, Hołyst and Poniewierski [82] who studied a fluid of hard spherocylinders using the Onsager model adapted to a nonuniform system observed oblique anchoring. They added quadrupolar interactions to the potential and found a tilt of the director at the interface of $\pi/3$ and that there was no dependence of this tilt on the length-to-width ratio L/D of the spherocylinder.

2.3.4 Simulation

To the author's knowledge, there have been very few computer simulation studies done to investigate the I-N interface. One such study, are the molecular dynamics simulations of Bates and Zannoni [83]. They used the Gay-Berne model with length to breadth ratio $\kappa = 3$, well depth anisotropy ratio $\kappa' = 5$ and energy exponents $\mu = 1$ and $\nu = 3$. The method they used to maintain the two bulk phases was to have a temperature inhomogeneity between the two phases in the same box. That is the nematic bulk phase is at a temperature slightly lower than the isotropic bulk phase. As a consequence this system is not at equilibrium as there will be a constant

heat flow from the high temperature region (isotropic) to the low temperature region (nematic). Their system consisted of 12960 molecules in a box of dimensions $30 \times 30 \times 48$ at $T_N^* = 3.45$ and $T_I^* = 3.60$ and density $\rho^* = 0.3$. They found that the molecules tend to align parallel to the interface. They calculated the density and order parameter profiles and found an offset between the profiles of $0.6L$ and an interfacial thickness of $3.46L$. No attempt was made to calculate the surface tension or biaxiality effects.

Recently, Allen [84] investigated the nematic isotropic interface for hard ellipsoids of revolution with molecular length $a/b = 15$ in the slab geometry, using Monte Carlo simulations for various anchoring conditions at parallel confining walls. He compared the results of the simulations with theoretical calculations using Onsager's density functional theory. Allen found a planar orientation at the interface. He found evidence of biaxiality in the theory but this was barely detectable in the simulation results. Allen found no sign of a minimum in the number density predicted by Koch and Harlen [81] from the Onsager theory or from the simulations.

For completeness, we mention the simulation study of the isotropic-smectic A (I-Sm A) interface done by Bates [85]. Bates repeated the earlier studies, using a temperature inhomogeneity, on the isotropic-nematic interface [83] and extended it to study the I-Sm A interface. This system was made of 14256 molecules in a box of $30 \times 30 \times 96$ at $T_{SmA}^* = 1.15$ and $T_I^* = 1.20$ and density $\rho^* = 0.162$. He also found a planar orientation of the director at the interface. A narrow layer of nematic structure was observed between the smectic-A and isotropic phase.

2.3.5 Summary

As with the nematic-vapour interface, the isotropic-nematic interface shows different anchoring alignment for different types of liquid crystals. Experiments show that MBBA prefers planar anchoring [68] while some members of the nCB series prefer oblique anchoring [69]. This seems to indicate that long range electrostatic

interactions might be the drive behind oblique anchoring at the isotropic-nematic interface since the nCB series have strong dipoles. No homeotropic anchoring was observed in experimental studies of the isotropic-nematic interface. Theoretically, earlier calculations of the surface tension showed that a minimum in the surface tension occurred when the anchoring was either planar or homeotropic [72, 75, 76] without any preference for one or the other. Most of the other theoretical studies predicted planar anchoring [73, 74, 78, 80, 81] which is in agreement with experimental results for MBBA. The exception is the work of Hołyst and Poniewierski [82] which shows oblique anchoring in agreement with the experimental results for the nCB series. Both simulation studies found planar anchoring at the isotropic-nematic interface [84]. No studies using simulation were done to investigate oblique anchoring at the isotropic-nematic interface. There is some doubt that the temperature inhomogeneity method [83] achieves thermodynamic equilibrium. Hence, an investigation using molecular dynamics simulation of an isotropic-nematic interface at equilibrium is needed. Such an investigation is attempted in this thesis using soft spherocylinders as described in Chapter 4.

2.4 Solid Surface Effects

2.4.1 Introduction

When a liquid crystal fluid comes into contact with a solid substrate, several regions can be identified. Far from the substrate, there is the bulk liquid crystal, with all the molecules having the same mean orientation. Right at the surface, liquid crystal molecules are in direct interaction with the substrate and have their orientational distribution determined by this interaction. In between, there is a transition region in which the molecular order evolves from that in the substrate to that in the bulk. Just outside this region, the director has a given orientation which depends on the structure of the interfacial region; this orientation is the anchoring direction of the

liquid crystal at the surface [86, 87].

For a detailed review of the different aligning mechanisms and surface effects in liquid crystals the reader is directed to read the review of B. Jérôme [88].

A particular type of aligning mechanism that is of interest to this work is the case of substrates having grooved surfaces. Shen *et al* [89, 90, 91] among others have investigated the nematic-substrate interface using optical second harmonic generation. The method used yields detailed information about the orientation of the molecules: mean tilt with respect to the surface normal and distribution of azimuthal orientation in the plane of the surface. They found that on rubbed glass and some chemically coated glass, the first monolayer of nematic molecules has an isotropic distribution of azimuthal orientations. This means that the molecule-substrate interactions are not responsible for the orientation of nematic liquid crystals parallel to the rubbing direction. On such substrates, the orientation of the nematic phase might come from the fact that this configuration minimises the elastic free energy distortion of the nematic orientation induced by the presence of grooves created by rubbing. With any other orientations, the molecules have to follow the topography of the grooves and this creates distortion and requires some energy as found by Berreman [92, 93] and Wolff [94] using the elastic distortion model.

2.4.2 Simulation

A few studies using off-lattice simulations of liquid crystal fluids constrained between walls have been done to date. All of these studies looked at the substrate-liquid crystal interaction and the effect of a particular type of potential on the bulk liquid crystal. One of the first of these studies was the work of Chalam, Gubbins, de Miguel and Rull. Chalam *et al* [95] studied a GB fluid confined between walls using constant-NVT MD. They found that the wall forces oriented the molecules normal to the wall. The molecule-substrate interaction used was separable - i.e. there was no coupling between the orientational part and the spatial part of the interaction.

Zhang, Chakrabarti, Mouritsen and Zuckermann [96] studied the GB model of liquid crystals in the presence of a substrate surface using the hybrid Monte Carlo method. They proposed a simple non-mean-field substrate-molecule potential to describe the effects of rubbed polymer-coated substrates. This potential takes into account the effects of the geometric shape of the GB molecules. Zhang *et al* showed that the bulk pretilt angle is controlled by the surface through the orientation of the adsorbed liquid crystal monolayer.

Stelzer, Galatola, Barbero and Longa [97] did MD simulations for liquid crystal near solid surfaces. The bulk liquid crystal was modelled using the GB interaction. The substrate-molecule interaction used was separable into a spatial part and an orientation part. The spatial part, took the form of a Lennard-Jones potential with a surface sinusoidally, modulated to give the effect of roughness. The orientational part of the surface potential used was of the Rapini-Papoular type. The initial configuration of Stelzer *et al* was set up by adding the two surfaces to an equilibrated bulk nematic. They observed smectic-C ordering near the two rough surfaces. They also observed a depletion in density at the smectic-nematic interface.

Wall and Cleaver [98] studied confined liquid crystal films using MD simulation. Their model was a GB fluid confined between two substrates in a slab geometry. The molecule-substrate interaction potential used is non-separable i.e. the angular and spatial parts of the interaction are coupled. Wall and Cleaver investigated the temperature dependence of the system and the effects of weak and moderate molecule-substrate coupling strengths. They found that for both coupling strengths, a well defined tilted molecular layer formed at each wall. The also found that the surface layers appear to be the major influence on the onset of orientational order in the central region of the bulk.

Allen [99] recently did molecular simulations of liquid crystal surface anchoring. The liquid crystal was confined in the slab geometry with homeotropic anchoring. The molecules were modelled as hard ellipsoids of revolution of elongation $e = a/b = 15$, where a is the length of the semi-major axis and b is the length of the two equal

semi-minor axes. Monte Carlo simulations were carried out in the constant-NPT ensemble. Allen obtained good agreement between simulation and calculations done using Onsager theory for different anchoring angles.

There are even fewer studies of surface effects using lattice models. One such model, is the model of Gruhn and Hess [20]. Gruhn and Hess used Monte Carlo simulations to generate an equilibrium director field of a nematic liquid crystal in two dimensions. They did not use any surface-liquid crystal interactions, but assumed a strong anchoring and fixed the molecules near the flat surfaces to have homeotropic or planar alignment. The model of Gruhn and Hess is discussed in further detail in Chapter 5 of this thesis.

Newton and Spiller [100, 101] used the Gruhn and Hess two dimensional model with different surface shapes to study the effects of the surfaces in producing bistability in a nematic liquid crystal device. The surfaces they used were triangular gratings of different triangular heights and symmetry, and surfaces obtained from real scanning electron micrograph profiles. The initial configurational distributions used were not random vectors on the surface of a sphere [5] as used by Gruhn and Hess and the work presented in this thesis, but rather a random distribution on a sector. This gave a number of possible initial configurations. Newton and Spiller used four: a vertical sector and a horizontal sector each being positive (to the right of the axis) and negative (to the left of the axis) these were designated: $v, v-, h, h-$. For the symmetric triangular grating they found that the equilibrium state obtained from the initial states v and $v-$ were degenerate as were the ones obtained from the states h and $h-$. They also found that the two sets were degenerate in energy at a certain groove depth. This signified a bistable state. The asymmetric triangular grating also showed degeneracy in energy, but in this case there were four separate states. The states v bistable and h were degenerate for a particular groove depth as were $v-$ and $h-$ for a higher groove depth. Newton and Spiller applied the same technique to real grating profiles. They observed 3 stable states which they designated: vertical v, horizontal h and π. The states differed slightly in energy with the

v state being the lowest and the h being the highest with the π state being at an energy level that is between the two. This system is obviously not a true tri-stable state as the three states are not degenerate in energy.

2.4.3 Summary

Various studies of liquid crystals near solid surfaces, both on- and off-lattice have been carried out. Almost all studies of the substrate-liquid crystal using off-lattice simulation were of flat surfaces. The only exception was the work of Stelzer *et al* [97]: the solid surface in this case was sinusoidally modulated along the x and y direction. They did not observe any bistable states.

Lattice models of nematics near triangular gratings and real grating profiles show evidence of bistability [100, 101] in two dimensions. As actual display devices are three dimensional, it is of great interest to investigate stable states generated by three dimensional surfaces and attempt to observe bistability in different surface topographies. This has been attempted in this thesis as described in Chapter 5.

Chapter 3

Studies using a Flexible Model

3.1 Introduction

One main feature of real liquid crystal molecules - which is often neglected in computer simulation studies of nematic-vapour interfaces - is molecular flexibility. Flexible alkyl chains are known to play a key role in determining mesophase stability [102] and may even be the drive behind homeotropic alignment at the nematic-vapour interface. Atomistic simulations include flexibility as they use potentials that follow the exact structure of real molecules [102]. To the author's knowledge no simulation studies using an atomistic model have been used to study the nematic-vapour interface. This is perhaps because of the extensive computational time and power required to perform these studies [103]. To overcome this problem, a pseudo atomistic model is considered. This model should maintain molecular flexibility but not all of the details of an atomistic model. The study presented in this thesis uses such a model. A second reason for the absence of such studies is the great difficulty in finding intermolecular potentials for which the bulk nematic phase is stable at sufficiently low pressure and temperature to coexist with a vapour phase[64, 66]. More frequently [61, 104, 59, 60] it transforms into a smectic or solid at temperatures below the critical temperature T_c.

The model presented is a hybrid atomistic model consisting of a mesogenic core linked to two flexible tails. The mesogenic core is represented by a Gay-Berne (GB) site and each flexible tail is represented by an array of seven Lennard-Jones (LJ) sites. This model is a variant of the model presented in an earlier study by Wilson [102]. He used a hybrid atomistic model to investigate the phase behaviour of liquid crystal dimers. His model consisted of two GB mesogens linked by a flexible chain. This approach is similar to that employed by La Penna, Catalano and Veracini [105] who simulated a single GB unit linked to a single alkyl chain. They studied the effects of varying the chain length on the static and dynamic properties of that system. La Penna *et al* found that qualitatively the model successfully reproduced the static properties of real mesogenic molecules. Lyulin *et al* [106] used this approach to analyse the structure and dynamics of a series of liquid crystalline main chain polymers. The polymer model was composed of a series of GB mesogens connected with each other through flexible alkyl spacers. The physical properties of such a model were measured for different spacer lengths. Recently, McBride and Wilson [107] used a model similar to the one presented in this thesis. Their model consisted of a GB core mesogen with two alkyl chains of different lengths. They studied the phase behaviour and bulk properties of their model and compared the results with real liquid crystals.

Other possible applications of this kind of model based on a GB/LJ combination is in forming banana and zigzag shaped molecules. These give rise to interesting effects, such as tilted smectics, and under the influence of electric fields, flexoelectric effects can occur.

The objective of this study is to investigate whether or not such a model forms a nematic-vapour interface, and if so, to investigate the structure of the interface. In particular, it would be of interest to discover how the nematic director is oriented relative to the surface.

3.2 The Model

3.2.1 Introduction

Molecules of the form shown in Figure 3.1 are known to form liquid crystals [108]. These two compounds provide impressive proof of the strong mesogenic character of cyclohexane derivatives. The cyclohexane ring is one of the most important moieties [109]. It differs from benzene by being more bulky in shape, having some flexibility and being non-aromatic in character. This non-aromaticity causes a strong decrease of intermolecular attraction relative to benzene derivatives, leading to materials with a much lower packing fraction [109]. Experimental results show that the cyclohexane and benzene derivatives of the form shown in Figure 3.1 form smectic phases [110, 111].

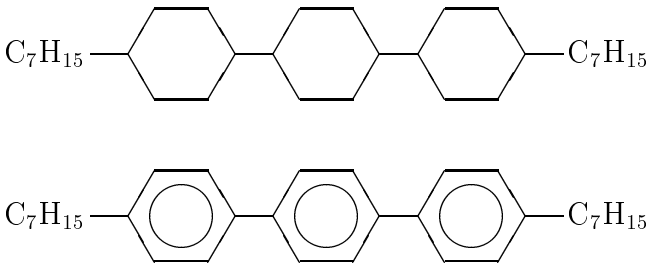

Figure 3.1: Cyclohexane and Benzene Derivatives

3.2.2 Model Details

To model liquid crystalline molecules of the form shown in Figure 3.1, a hybrid atomistic model is constructed. This molecule consists of a Gay-Berne (GB) core, which mimics the set of cyclohexane rings and is connected to two arrays of Lennard-Jones (LJ) sites of equal lengths that represent the alkyl chains. A schematic diagram of this model is shown in Figure 3.2. The bond lengths are fixed between the centres of adjacent sites and the angles between the different parts of the tails are allowed to

fluctuate around an equilibrium value. Figure 3.2 also shows a schematic diagram of the single-tailed molecule which was used together with the longer molecule to form a mixture. This type of liquid crystal molecule is widespread [108]. Compounds such as nCB, nOCB and nOFBA are of this type [105]. The model studied by La Penna *et al* [105] is also of this form. Mixtures of liquid crystal molecules are frequently used in devices, because the range of stability of the nematic phase against crystallization or smectic phase formation is extended relative to the stability range of the individual components.

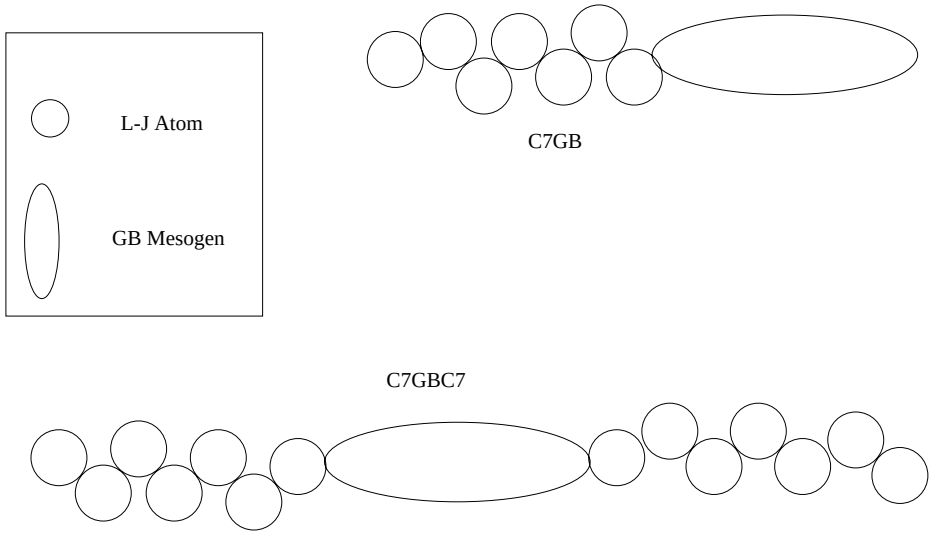

Figure 3.2: A schematic diagram of the C7-GB-C7 / C7-GB Model

Potential Details

The total potential energy of the system of the form

$$\begin{aligned} E &= \sum_{i=1}^{N_{angles}} U_i^{bend} + \sum_{i=1}^{N_{dihedrals}} U_i^{torsional} \\ &+ \sum_{i=1}^{N_{LJ}} \sum_{j>i}^{N_{LJ}} U_{ij}^{LJ} + \sum_{i=1}^{N_{GB}} \sum_{j>i}^{N_{GB}} U_{ij}^{GB} + \sum_{i=1}^{N_{LJ}} \sum_{j=1}^{N_{GB}} U_{ij}^{LJ/GB} \end{aligned} \tag{3.1}$$

was used to model the intra-molecular and the intermolecular contributions to the interaction energy. N_{angles}, $N_{dihedrals}$, N_{LJ} and N_{GB} are the number of angles, number of dihedral angles, number of Lennard-Jones sites and number of Gay-Berne sites in the system respectively [102], U_i^{bend} is a bend interaction of the harmonic type, this term also includes additional GB angle terms that prevent free rotaions of the GB sites about their centres. $U_i^{torsional}$ is a torsional interaction of the Ryckaert-Bellemans form [19], U_{ij}^{LJ} is the LJ-LJ interaction and U_{ij}^{GB} is the GB-GB interaction. All of these interactions were described in Chapter 1 of this thesis. The exception is the LJ-GB interaction $U_{ij}^{LJ/GB}$ which is based on the work of Cleaver *et al* [112], who derived a generalised potential for two unlike GB particles.

Accordingly, for a rod-sphere interaction, the potential can be written as

$$\begin{aligned} U_{ij}^{LJ/GB} &= 4\epsilon_0^{LJ/GB}\left[\epsilon^{LJ/GB}(\hat{\mathbf{u}}_j,\hat{\mathbf{r}}_{ij})\right]^{\mu} \\ &\times \left[\left(\frac{\sigma_0^{LJ/GB}}{r_{ij}-\sigma^{LJ/GB}(\hat{\mathbf{u}}_j,\hat{\mathbf{r}}_{ij})+\sigma_0^{LJ/GB}}\right)^{12}\right. \\ &- \left.\left(\frac{\sigma_0^{LJ/GB}}{r_{ij}-\sigma^{LJ/GB}(\hat{\mathbf{u}}_j,\hat{\mathbf{r}}_{ij})+\sigma_0^{LJ/GB}}\right)^{6}\right]. \end{aligned} \tag{3.2}$$

The Gay-Berne potential variant used by de Miguel *et al* [113] was employed. The values of the parameters are shown in Table 3.1. Here μ and ν are the potential exponents, κ is the length to breadth ratio and κ' is the well depth ratio. Table 3.2 shows the values used for the particle diameters, well depths and spherical potential cut-offs for the three pairwise interactions. The expansion coefficients for the Ryckaert-Bellemans potential [19] are given in Table 1.1. The above parameter values are the ones originally used by Wilson [102] to model dimers and recently by McBride and Wilson [107] for the C7GBC3 model.

κ	κ'	μ	ν
3	5	2	1

Table 3.1: Potential Parameters I: Ratios and exponents.

Parameter	GB-GB	GB-LJ	LJ-LJ
σ (Å)	4.721	4.117	3.93
$\epsilon/k_B(K)$	406.51	171.08	47.0
r_{cut} (Å)	18.884	16.4679	9.8075

Table 3.2: Potential Parameters II: Diameters, well depths and potential cut-offs.

3.3 Simulations

3.3.1 Introduction

All simulations used the parallel molecular dynamics (MD) simulation code `GBMOL`[23]. The bulk phases were studied in the isobaric-isothermal (NPT) ensemble using the Andersen thermostat [29, 102] and implementing a Monte Carlo procedure to alter the volume as described in Chapter 1. A zero pressure was maintained for all the runs. This is because we are seeking phases which coexist with the vapour; for the liquid branch, the coexistence pressure will be effectively very close to zero. Due to the attractive intermolecular forces, such zero-pressure states are indefinitely metastable in periodic boundary conditions. The SHAKE procedure was used to fix the bond length [114, 102, 107]. During the simulations, orientational and translational ordering of the Gay-Berne sites were monitored. This was done respectively through the calculation of the orientational order parameter S, as described in Chapter 1, the radial distribution function

$$g(r) = \frac{V}{[N_{GB}]^2} \left\langle \sum_{i}^{N_{GB}} \sum_{j \neq i}^{N_{GB}} \delta(\mathbf{r} - \mathbf{r_{ij}}) \right\rangle, \tag{3.3}$$

and its components $g(r_{\parallel})$ and $g(r_{\perp})$, which were used to respectively monitor translational order parallel and perpendicular to the director [102]. To monitor smectic ordering, the smectic order parameter, as described in Chapter 1, which is essentially the structure factor

$$S(\mathbf{k}) = \langle |\rho(\mathbf{k})|^2 \rangle \tag{3.4}$$

$$\rho(\mathbf{k}) = \frac{1}{\sqrt{N_{GB}}} \sum_{i=1}^{N_{GB}} \exp(i\mathbf{k} \cdot \mathbf{r}_i) \tag{3.5}$$

was calculated.

The liquid crystal-vapour simulations were done in the constant-NVT ensemble. The temperature was maintained constant by using the same thermostat as before. At the end of the simulation run, density, order parameter, director and structure factor profiles are calculated.

Constant-NVE MD

To determine how well the parallel code `GBMOL`[23] conserved energy, and to determine the ideal time-step, constant-NVE molecular dynamics simulations were done. Figure 3.3 is a plot of energy fluctuations against time-step. The figure shows that a time step of 4 fs conserves energy well. It is not quite understood why the smallest time step produced a larger fluctuation, it is possible that the system had not reached proper equilibrium and that different degrees of freedom were at different temperatures. Similar constant-NVE runs were done to determine the ideal number of processors when the code was ported to the SGI Origin 2000. Figure 3.4 shows that four processors give a good speedup of 3.5 relative to the speed of a single processor for the C7GBC7 system with 512 molecules. The dashed line is the one-to-one ratio line. The closer the points are to the line, the better the speed-up is. For larger systems the number of processors used was increased to eight. Some of the simulations were done on a Cray T3E, where sixteen processors were used.

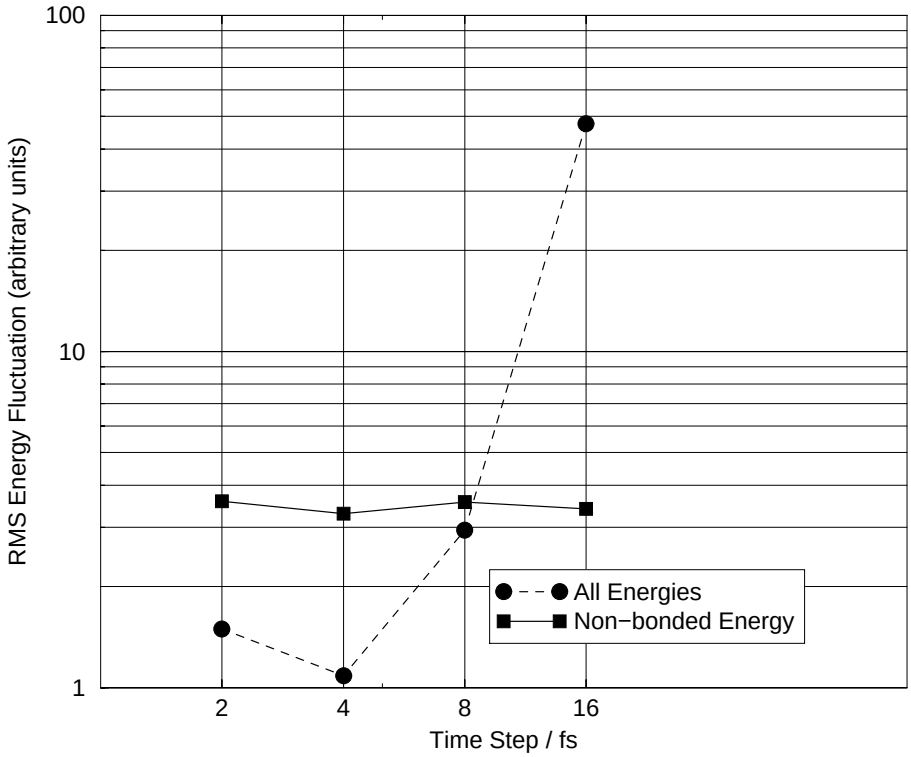

Figure 3.3: Energy fluctuation versus time step.

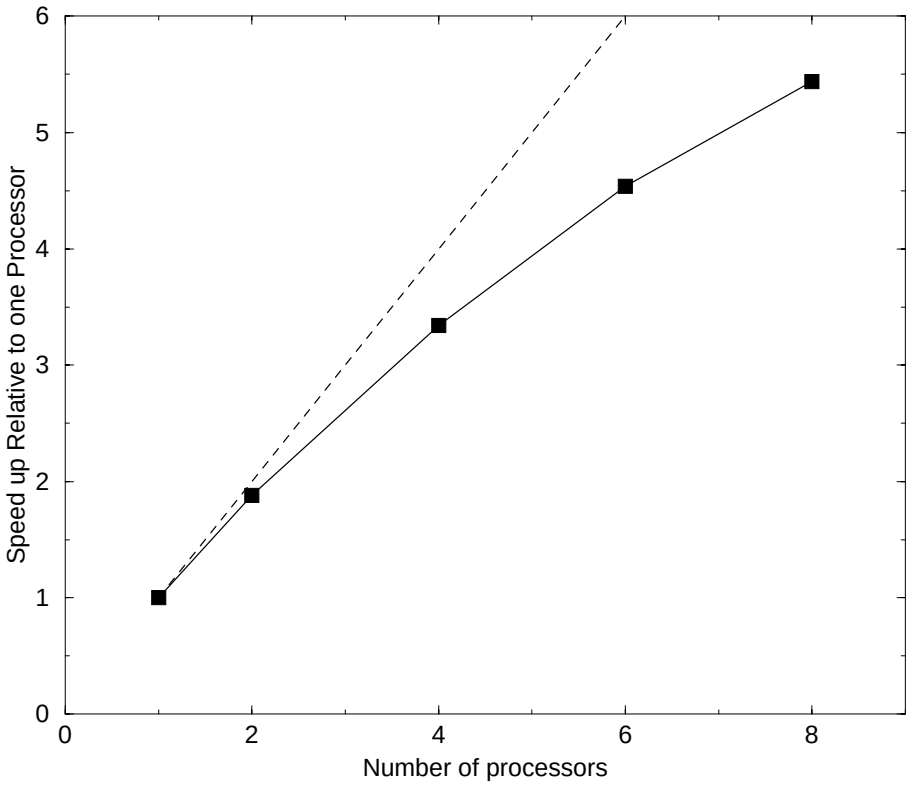

Figure 3.4: Speed up of the code `GBMOL` on the SGI Origin 2000.

3.3.2 Bulk C7GBC7

The bulk C7GBC7 system consisted of 512 molecules in a cubic box with periodic boundary conditions in the x-, y- and z-directions. Initial configurations were obtained from melting a lattice under high pressure and temperature. Once a suitable liquid had formed, the pressure was reduced to zero and the run was continued at that temperature to check the stability of the fluid at zero pressure. The bulk phase, at this stage, is a pseudo nematic phase. Once it was determined that a stable fluid was obtained, the temperature was varied and the respective systems were allowed to equilibrate.

This system showed an isotropic phase at high temperatures and a condensed phase at low temperatures. At intermediate temperatures, a liquid crystalline phase was observed. Figure 3.5 shows the progress of the nematic order parameter as a function of time. As the graph shows, some of these runs are extremely long ~ 50 ns. A spontaneous growth of an ordered phase occurred at T=300K starting from an isotropic phase as shown in Figure 3.5; at this temperature, the system turned out to be a solid. Starting from a highly ordered phase, the fluid rapidly became isotropic when the temperature was increased to T=385K. The progress of the order parameter at T=350K shows some interesting behaviour. This behaviour would perhaps not be observable in a shorter run. Looking at the director profile as a function of time, and at the snapshots of the configuration throughout the run, shows a director reorientation towards one of the diagonals of the simulation box. A snapshot of the configuration at a temperature of T=300K is shown in Figure 3.6. This figure also shows the orientation of the layer normal pointing along one of the diagonals of the box. A highly ordered phase also appeared at T=350K which turned out to be a very dense smectic. The value of $S(\mathbf{k}) = 0.587$ was found at the wave-vector $\mathbf{k} = (2, 1, 0)$. Figure 3.7 shows the full zero-pressure equation of state of the reduced density as a function of temperature and the order parameter as a function of temperature. The reduced density is defined as $\rho^* = \rho^*_{LJ} + \rho^*_{GB}$

where $\rho^*_{LJ} = \frac{N_{LJ}V_{LJ}}{V}$, $\rho^*_{GB} = \frac{N_{GB}V_{GB}}{V}$ and $V_{LJ} = \frac{\pi}{6}(\sigma_{LJ})^3$ and $V_{GB} = \frac{\pi}{6}\kappa(\sigma_{GB})^3$ are the approximate volume of a single LJ and a single GB unit respectively. These graphs show that as the temperature is reduced the density increases and the degree of ordering increases. They also show a phase transition occurring as temperature goes from T=385K to T=365K.

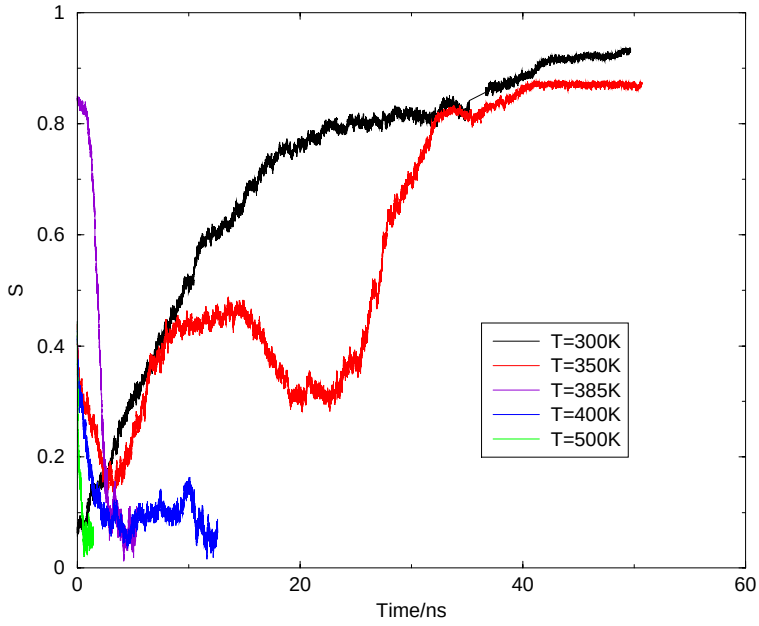

Figure 3.5: Order parameter versus time for bulk C7GBC7.

The system was then rotated such that the layer normal pointed along the z-direction of the box. This was to ensure that the smectic layers could relax. This was done by making multiple copies of the box then rotating the large system to desired directions. A box of about the same size as the original was placed around the centre and the excess molecules were removed. This generated a box containing 516 molecules with the layer normal pointing along the z-axis of the box. The temperature was then increased slightly to T=365K and T=375K. The system was equilibrated at each temperature for 6-8 ns allowing the box dimensions to vary independently. At T=375K the fluid became isotropic. Figure 3.8 shows the pair distribution function and its components parallel and perpendicular to the director

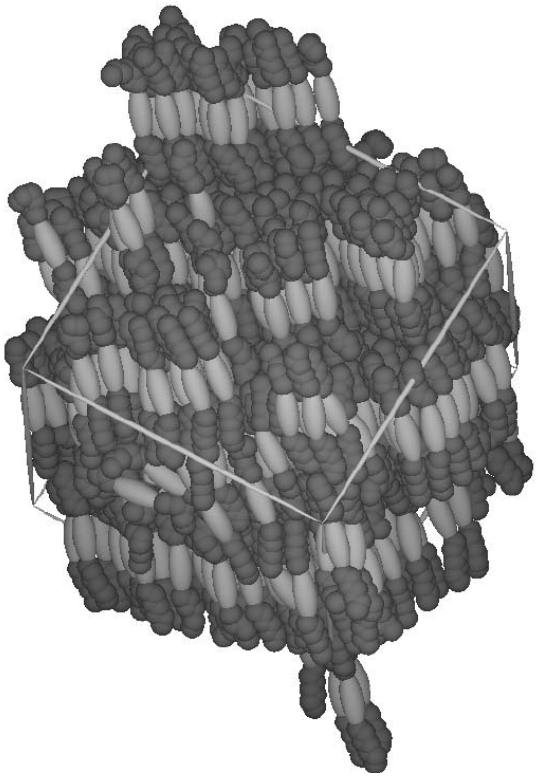

Figure 3.6: A snapshot of the unrotated configuration for bulk C7GBC7 at T=300K.

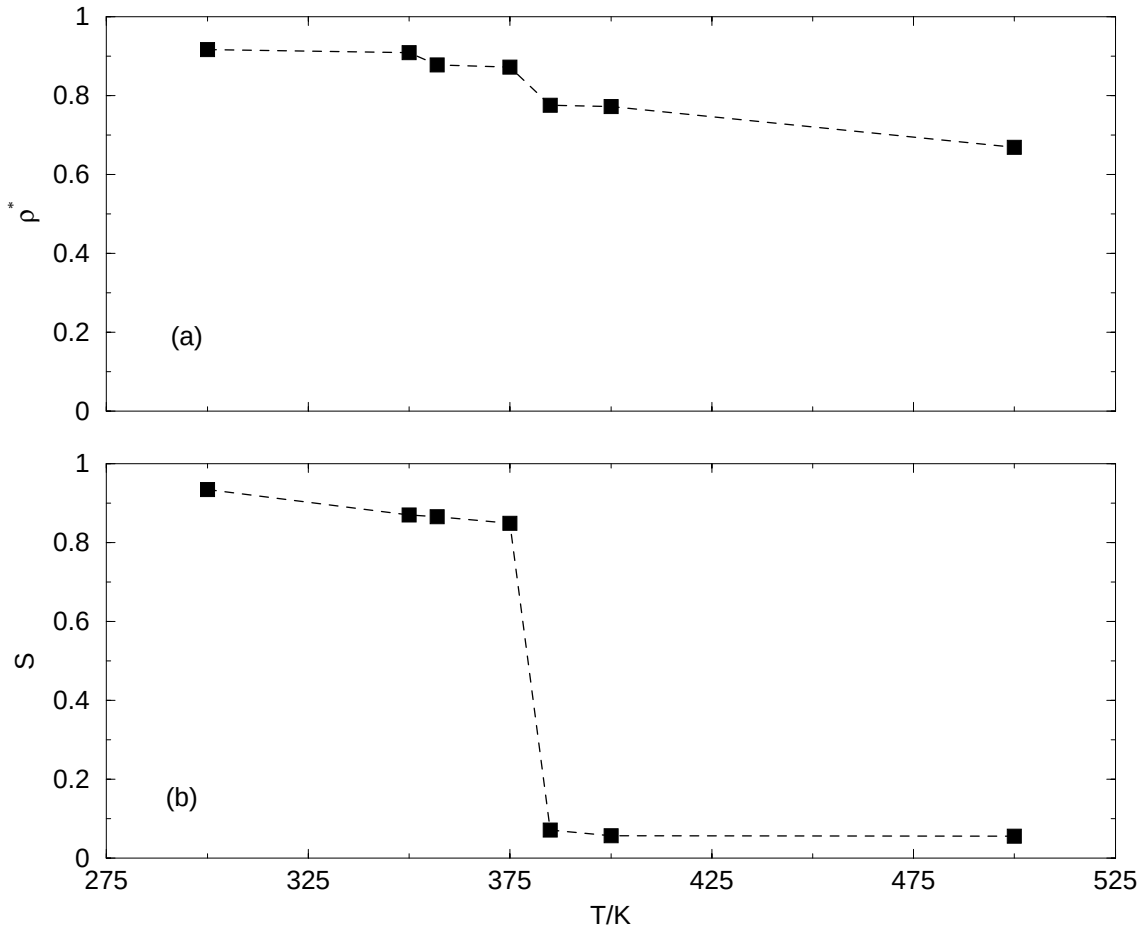

Figure 3.7: The zero-pressure equation of state for bulk C7GBC7: (a) Density versus temperature and (b) Order parameter versus temperature.

Compound	Phase Sequence
Cyclohexane derivative	Crystal 347K smectic-B 522K isotropic [110]
Triphenyl derivative	Crystal 454K smectic-B 480K isotropic [111]

Table 3.3: Transition temperatures of the benzene and cyclohexane derivatives.

for T=365K. The oscillations in $g_{\parallel}(r)$ indicate weak smectic ordering as the $g_{\parallel}(r)$ does not go to zero. The type of smectic phase case also be determined from the plot of $g_{\perp}(r)$ which shows the formation of a smectic-B phase at this temperature. This is characterised by the double peak in $g_{\perp}(r)$ caused by hexagonal packing within the layers [107]. To study this smectic phase further, the system size was doubled in the z-direction to a total of 1032 molecules. The system was then allowed to equilibrate for 6 ns. Figure 3.9 is a snapshot of the smectic system showing the fluid forming a smectic phase at T=365K, from this snapshot, the degree of ordering and the orientation of the director and the layer normal are apparent. The structure factor and smectic order parameter were calculated. The value of $S(\mathbf{k}) = 0.363$ was found at the wave-vector $\mathbf{k} = (0, 0, 4)$. This value of $S(\mathbf{k})$ shows a moderate degree of smectic order; the $\mathbf{k}$ vector indicates that the direction of the layer normal is along the z-axis and that there are 4 layers as shown in Figure 3.9, where the bottom-most layer is actually part of the topmost layer, since the system has periodic boundary conditions. A transition to a solid phase is also observed when the temperature is lowered further.

The C7GBC7 model forms a smectic-B phase in agreement with the experimental results of Billard *et al* [110] in their study of the phase behaviour of 1,4-bis(4′-heptyl-cyclohexyl)-cyclohexane. Comparing the transition temperatures of the C7GBC7 with experimental results shown in Table 3.3. It is observed that the isotropic to smectic-B transition occurs at a much lower temperature (between 365K and 385K) than the experimental finding which is much closer to 500K. The smectic-B to crystal transition (between 300K and 350K) is closer to the experimental findings of the cyclohexane derivatives.

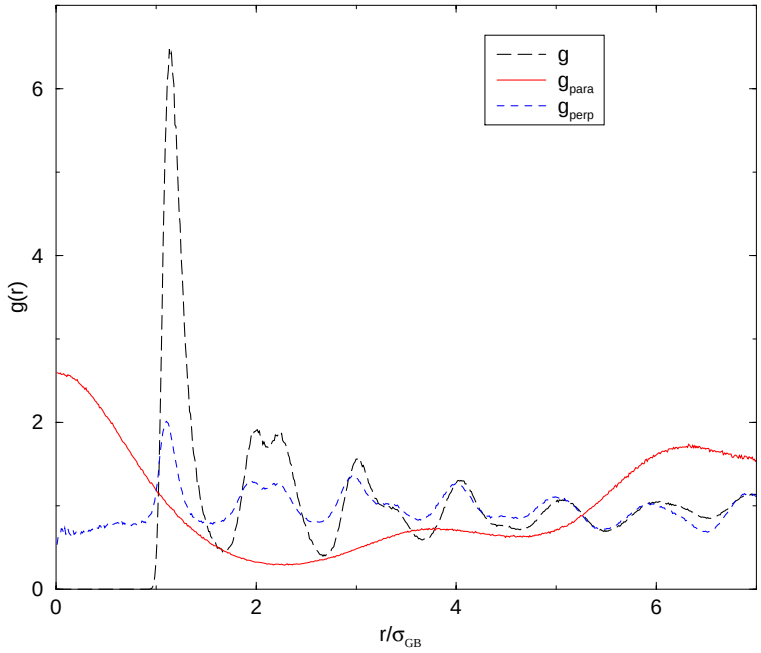

Figure 3.8: The pair distribution function for bulk C7GBC7 at T=365K.

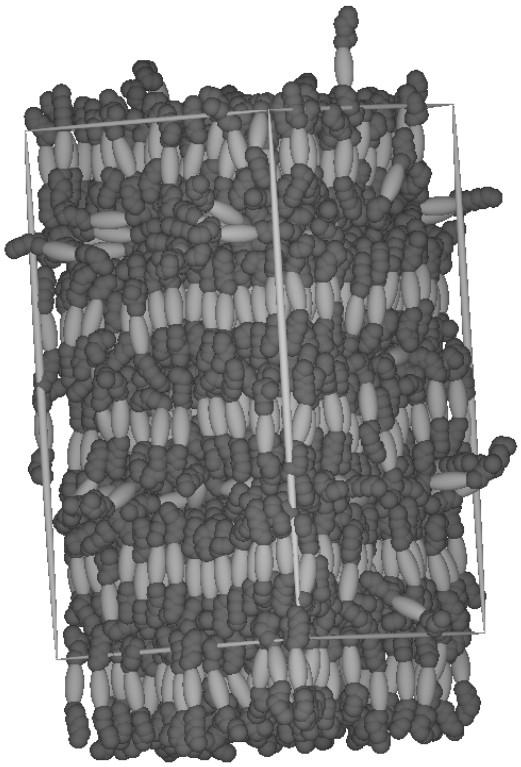

Figure 3.9: A snapshot of the configuration for bulk C7GBC7 at T=365K.

3.3.3 Liquid-vapour Film of C7GBC7

A film was set up by taking the large $N = 1032$-molecule, bulk smectic system at T=365K and adding two boxes of vapour at each end giving a box dimension of $1 \times 1 \times 4$ relative to the original cubic box. The new box contained 1048 molecules. MD simulations were done in the constant-NVT ensemble for a total of 4-7 ns at various temperatures. Setting the temperature at T=365K or higher caused the film to become isotropic. Signs of a stable film were seen at a temperature of T=350K. Density, order parameter and director profiles were calculated along the long axis of the box. Figure 3.10(a) shows the density profiles. The GB density profile shows three distinct peaks corresponding to three smectic layers. The LJ density profile - on the other hand - has four peaks. This is expected as the LJ chains are mostly in between the layers of the GB units. This behaviour can be easily seen in a snapshot of the configuration as shown in Figure 3.11. The order parameter profile - represented by the largest eigenvalue - is shown in Figure 3.10(b), the figure also shows the profiles of the other two eigenvalues. The high layer ordering is also visible here in the form of three peaks in the order whose positions coincide with the positions of the three peaks in the GB density profile. Figure 3.10(c) shows the director profile along the box. Here the profiles show that the molecules within the layers are oriented along the layer normal. The order parameter profiles indicate that the interlayer molecules are preferentially aligned in the xy-plane (the eigenvalue pattern has two 'high' values and one 'low' one); the small number of molecules between the layers makes it impossible to conclude whether there is a preferred direction within this plane. From the profiles and the snapshot of the configuration, the liquid-vapour interfacial region is totally disordered i.e. in the isotropic phase, so a kind of surface 'melting' of the smectic happens. This kind of disorder at the interface was also observed by Martín del Rio *et al* [115] who simulated the liquid-vapour interface of liquid crystals using the GB model. Their anisotropy parameters were $\kappa = 3$ and $\kappa' = 5$. These are the choice of parameters used in this study.

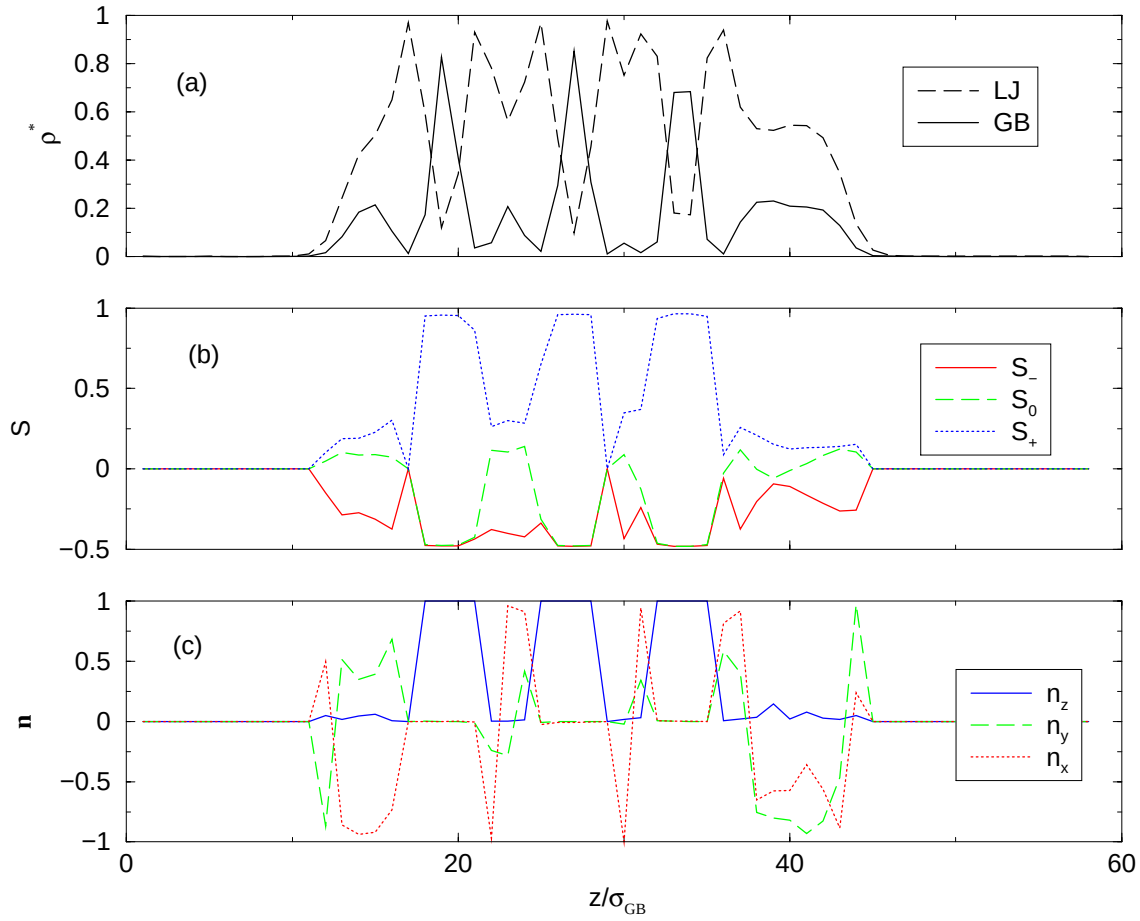

Figure 3.10: (a) The density profile, (b) the nematic order parameter profile (where S_+, S_0 and S_- are the largest, middle and lowest eigenvalues respectively) (c) The director profile (where $\mathbf{n}$ is the eigenvector corresponding to the largest eigenvalue) for a smectic film at T=350K.

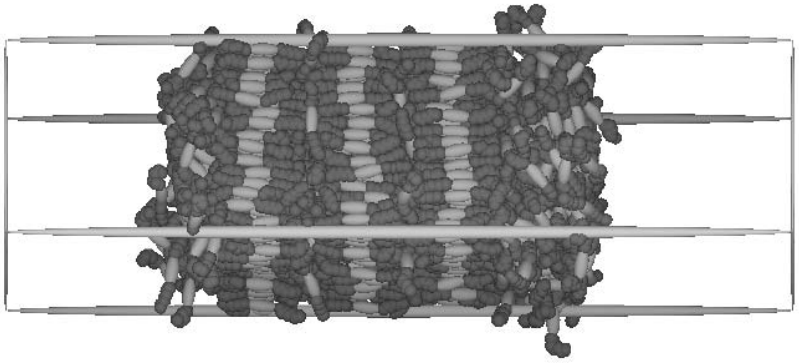

Figure 3.11: A snapshot of the configuration for the smectic film at T=350K.

3.3.4 Bulk C7GBC7/C7GB Mixture

In an attempt to achieve a nematic phase, a mixed system was created. This mixture consisted of two types of molecules: the original C7GBC7 molecule and a shorter, single-tailed molecule C7GB. The new molecule was created by removing one of the flexible tails of the original molecule. A molecule was chosen at random and one of its chains was removed. The process was repeated until 25% of the molecules were of the C7GB form. This was applied to the newly equilibrated smectic phase at T=365K consisting of 516 molecules.

The system was equilibrated at T=365K and an isotropic phase was observed. The temperature was then lowered further until a stable liquid crystalline phase was observed. Figure 3.12 shows the progress of the order parameter as a function of time from the initially ordered starting configuration for different temperatures. The figure shows that the system disordered very rapidly at temperatures of T=350K and above. High ordering was observed from the value of the nematic order parameter ($S \sim 0.78$) at T=325K. The equilibration for this system took $\sim$ 30 ns. Figure 3.13(a) shows the zero-pressure reduced density as a function of temperature and Figure 3.13(b) shows the order parameter versus temperature. As with the results for bulk C7GBC7, these show an increase in density and degree of ordering as the temperature is reduced. This also shows that a phase transition occurs when the

temperature goes from T=350K to T=325K. A plot of the pair distribution function and its components is shown in Figure 3.14 for T=325K. The oscillations in $g_{\|}(r)$ are very shallow. The smectic order parameter at this temperature was found to be $S(\mathbf{k}) = 0.085$, this value suggests that there is no smectic ordering and that a very highly ordered nematic had formed. Figure 3.15 shows a snapshot of the mixed system at a temperature of T=325K showing a highly ordered phase and Figure 3.16 is a snapshot of the same system at a higher temperature of T=350K. The latter snapshot shows the system in the isotropic phase. The GB units of the two species are colour coded to distinguish them from each other. The blue coloured molecules are C7GBC7 while the red coloured are C7GB. The dense phase at a temperature of T=300K is thought to be a solid.

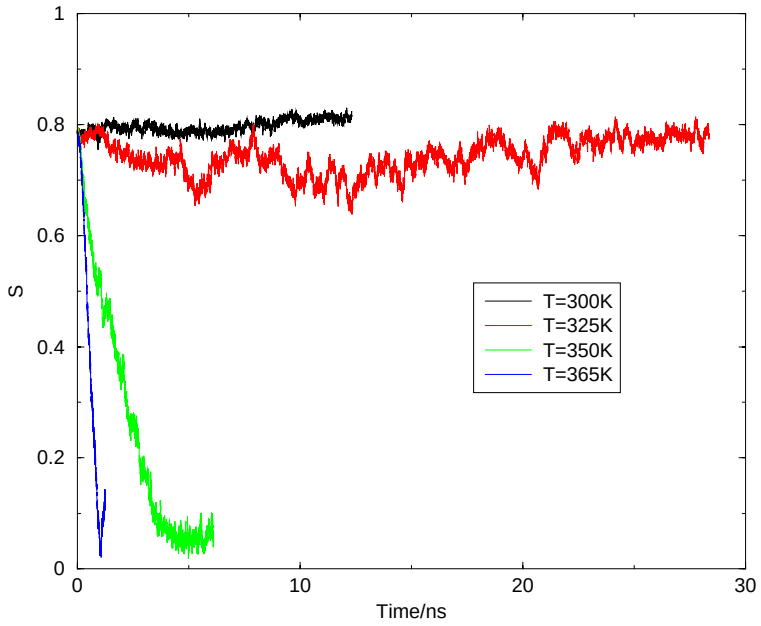

Figure 3.12: Order parameter versus time for the mixture.

3.3.5 Liquid-vapour film for the C7GBC7/C7GB mixture

To set up the liquid-vapour system, a simulation box of the C7GBC7/C7GB mixture containing 516 molecules was duplicated to form a $2 \times 1 \times 2$ film. Two boxes of

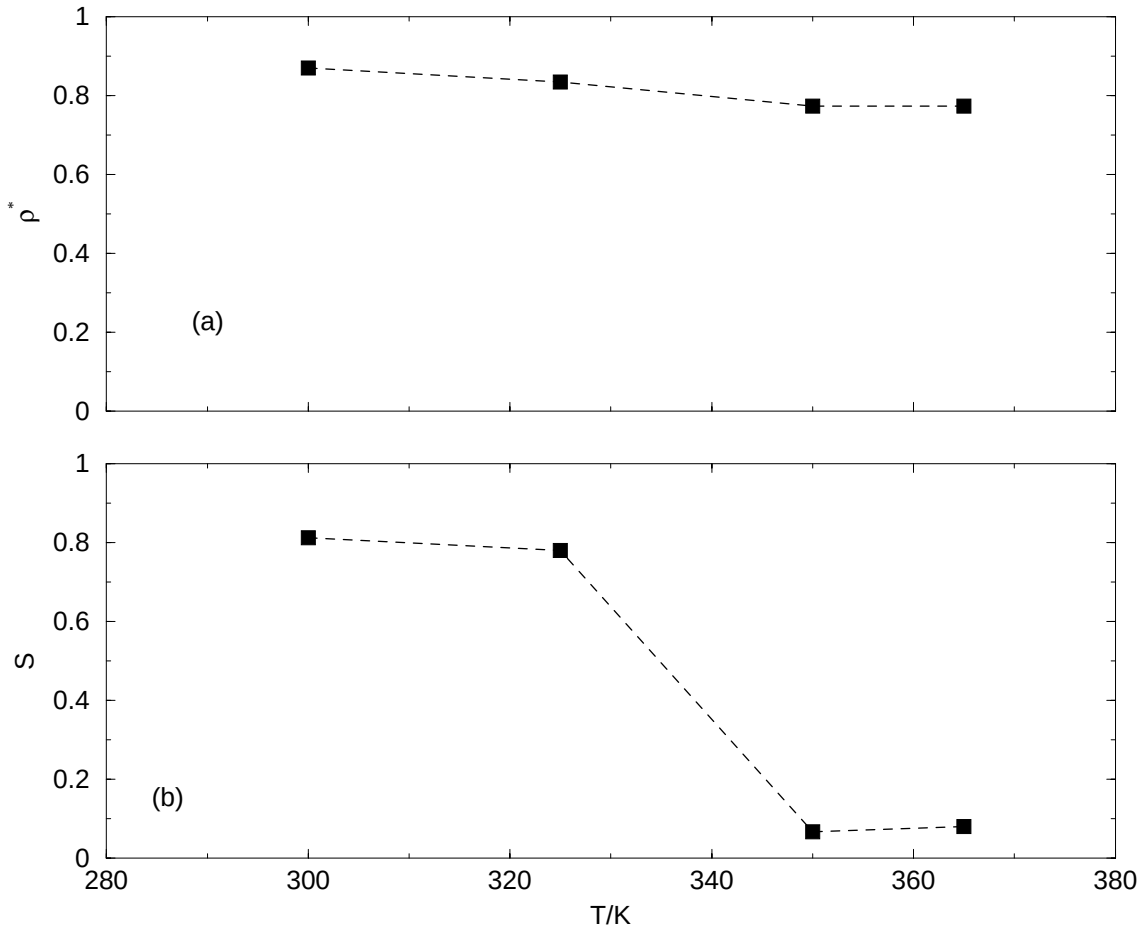

Figure 3.13: The zero-pressure equation of state for the mixture C7GBC7/C7GB: (a) Density versus temperature and (b) Order parameter versus temperature.

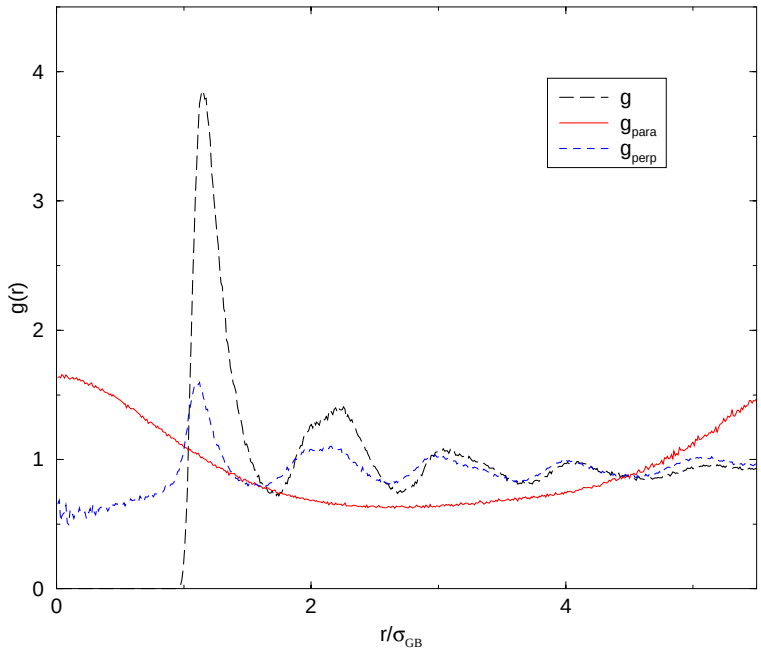

Figure 3.14: The pair distribution function for bulk C7GBC7/C7GB Mixture at T=325K.

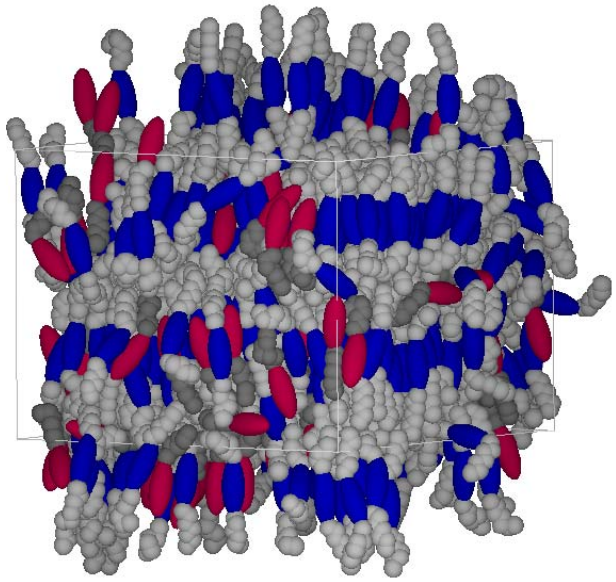

Figure 3.15: A snapshot of the configuration for the mixed bulk at T=325K.

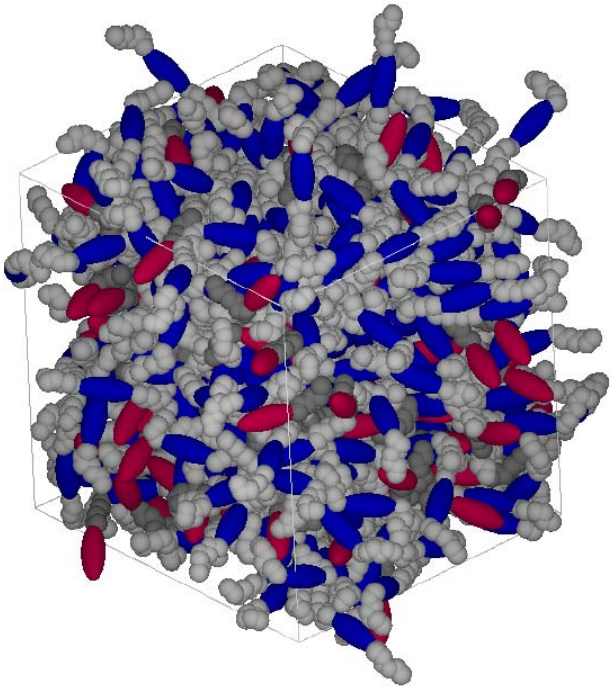

Figure 3.16: A snapshot of the configuration for the mixed bulk at T=350K.

vapour were added to the two ends to form a $2 \times 1 \times 4$ simulation box with a total of 2104 molecules. The box dimensions were, in units of σ_{GB}, $24.47 \times 16.20 \times 65.33$. Initially, the system was set such that the the director was aligned normal to the interface. In this case the molecules at the interface very rapidly reoriented to a direction planar to the interface and finally disordered. This is in contrast to the C7GBC7 system which maintained a normal orientation relative to the interface. A planar orientation of the molecules at the interface was then setup. After running for about 4 ns, the film rapidly became isotropic. It is thought that this occurred when the interfaces became disordered, this left a very thin layer of ordered phase in the centre that rapidly disordered. The disorder in this case occurred at a slower rate than that of the normal orientation at the interface. It was concluded that a planar orientation was more likely the preferred orientation.

To overcome this problem, the system size was increased to form a simulation box of $2 \times 1 \times 6$ of the original box, which is $24.47 \times 16.20 \times 98.00$ in units of σ_{GB}. A

planar orientation at the interface was maintained. The total number of molecules in this case was 4168 giving a total number of 55100 particles. Due to the size of the system, these simulations progressed very slowly. To give an idea of the time scale, the system took just over 100 days of continuous running on four parallel processors to do 370000 steps corresponding to a real time of 1.5 ns. The system was also restricted by the amount of computer memory available to the program: since `GBMOL` is a replicated data code, the memory requirement increases as the number of processors used is increased. For a system this size, using four processors required 1 GB of memory, which was the total amount available on the SGI Origin 2000. Using eight processors would require twice as much memory, and this proved to be impossible. Consequently, an exhaustive study of this system was judged to be beyond reach at present, and the results reported here are just indicative.

Molecular dynamics simulations in the constant-NVT ensemble were used to equilibrate the system at T=325K. The total lengths of the runs took 1.5 ns of which the last 0.8 ns were used to calculate the density, order parameter, director and structure factor profiles. Figure 3.17 shows the density profiles across the long axis of the box. Figure 3.17 (a) shows the overall density profile of the fluid and the profiles of the two types of molecules. The LJ units density profiles are shown in Figure 3.17 (b) and the GB units density profiles in Figure 3.17 (c). The density profiles show a sharp interface. The figure also shows an oscillation of the density profiles of the two molecules. These oscillations are out of phase with each other indicating a possible phase separation. However it turns out that the situation is complicated by the fact that the layer normal is perpendicular to the interfaces.

Figure 3.18(a) shows the order parameter profiles measured from the orientation of GB units. This figure also shows that there is a higher ordering of the C7GBC7 molecules over the C7GB molecules as expected. Similar effects have been seen by Bemrose *et al* [116] in their simulations of GB mixtures. Figure 3.18(b) shows the director profile across the box expressed through the two angles θ and ϕ. This shows that the director is pointing along the x-axis throughout the film, the exception

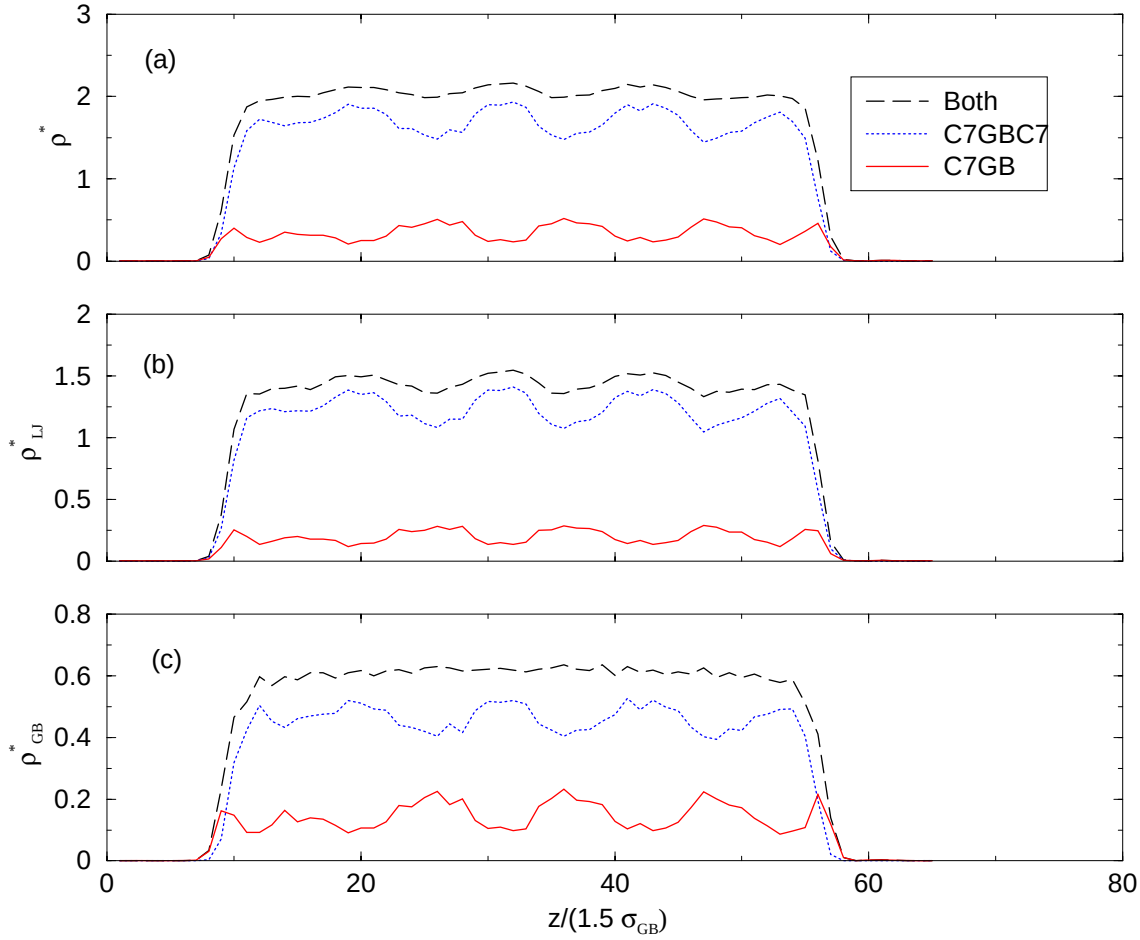

Figure 3.17: Density profiles: (a) Full densities for both types, (b) the density of the LJ units and (c) the density of the GB units.

being the interfacial region where the system is disordered - as shown from the order parameter profile. The structure factor profile is shown in Figure 3.18(c). These are the maximum values obtained by varying the wavevector $\mathbf{k}$. In this case $\mathbf{k}_{\max} = (4, 0, 0)$ throughout the system, away from the interfaces. The profile shows three distinct peaks away from the interfaces: these occur at the same position along the box axis as the three peaks in the order parameter. They also coincide with the positions of the three peaks in the density profile for the C7GBC7 molecules. This is a strong indication that this molecule is forming distinct smectic domains within the film. Looking at a snapshot of the system as depicted in Figure 3.19, the system does show some evidence of this. This is even clearer when looking at snapshots of the GB units of each type independently as in Figure 3.20. The top figure shows the C7GBC7 type of GB units coloured in blue. This figure clearly shows smectic ordering forming in the centre between the two interfaces. The bottom figure shows the C7GB kind of GB units coloured in red. The snapshot shows some demixing with the separation into areas of high and low density of molecules along the box. Three high-density regions can be seen which correspond to the three peaks clearly visible in the GB density profile. The longer molecules have a slight preference for the ordered smectic domains, while the shorter C7GB molecules slightly prefer the disordered regions in between the domains. The interfacial region is highly disordered. This is evident in the order parameter profile shown in Figure 3.18(a). Figure 3.18(c) shows two peaks at the interfaces, this is due to a few molecules at the surface layer.

3.4 Summary

The original aim was to locate a stable nematic phase at low pressure, using a flexible molecule model (C7GBC7), or a mixture of species of different lengths (C7GBC7/C7GB) in the eventual hope of studying the nematic-vapour interface. In the event, neither system showed evidence of a nematic phase at zero pressure

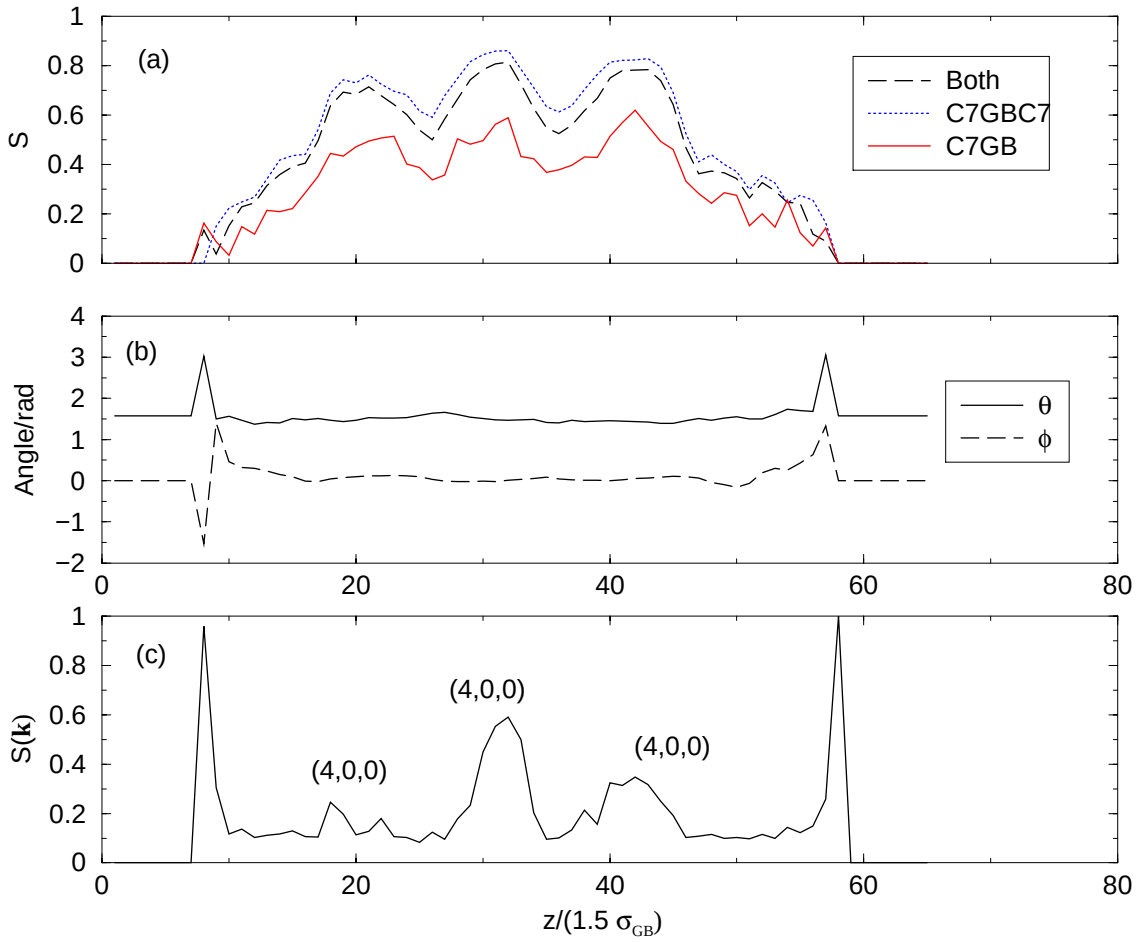

Figure 3.18: (a) Order parameter profiles, (b) Director profiles and (c) Structure factor profiles.

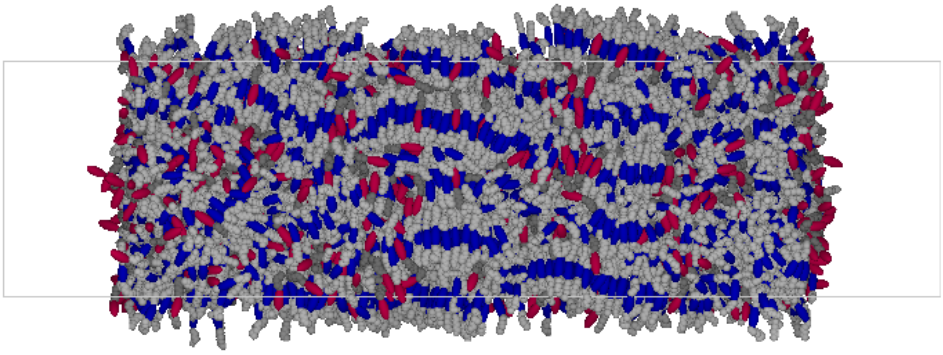

Figure 3.19: A snapshot of the configuration for the mixed film.

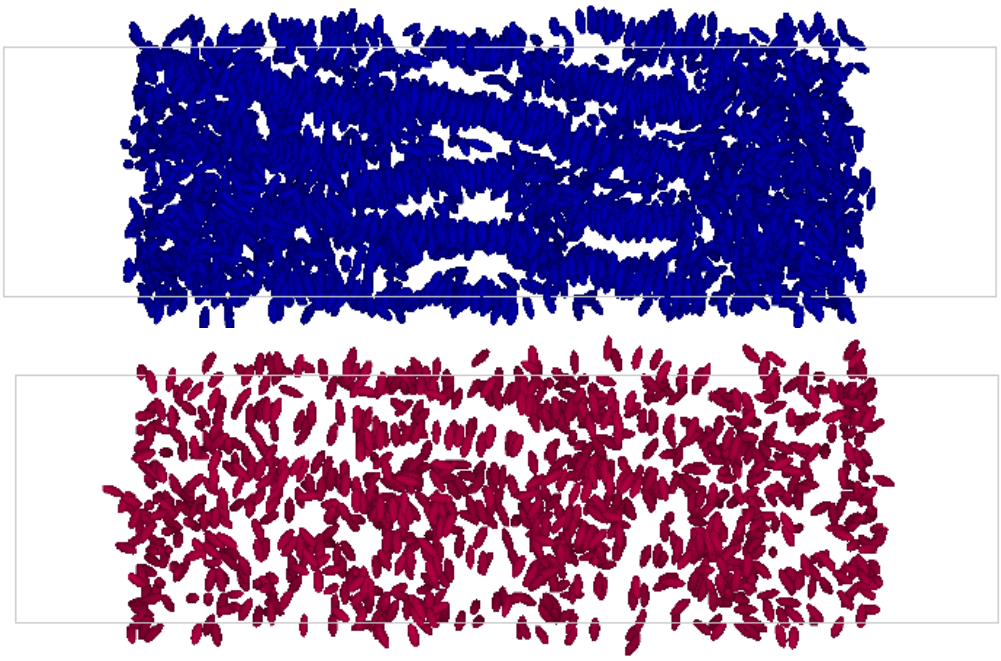

Figure 3.20: Two snapshots of the configuration for the mixed film showing the GB units of the two molecules separately. Blue: C7GBC7 and Red: C7GB.

(although the situation was not immediately clear for the mixture) and the study was restricted to examining the structure of smectic-vapour films. The interfacial region was found to be orientationally disordered in both cases. The disorder at the interfaces is similar to the findings of Martín del Rio *et al* [115] for the GB parameterisation used in this study. In the case of C7GBC7, smectic layers parallel to the interface seemed to be stable. In the case of the mixtures, the layers were rotated to become perpendicular to the interface, substantial disordered regions between smectic domains were observed. A small amount of segregation of the two species was seen in this case, the longer molecules preferring the ordered regions, the shorter molecules the disordered ones. Limitations of computer time restricted what could be achieved in this study, but further progress could be made using a domain decomposition version of the code currently under development [117].

Future work could include investigating various ways to obtain a stable nematic, these would include the use of shorter flexible tails as done by La Penna *et al* [105] or varying the energy anisotropy parameter as done by Martín del Rio *et al* [64].

Chapter 4

Isotropic-Nematic Interface

4.1 Introduction

In 1949, Onsager demonstrated that a system of long rigid rod-like molecules interacting with each other through steric excluded-volume interactions exhibits a first order isotropic to nematic phase transition at sufficiently high density [71]. When the nematic and isotropic phases coexist, the interface breaks both translational and orientational symmetry. Though the bulk free energy of the nematic phase is independent of the director $\hat{\mathbf{n}}$, the surface tension does depend on $\hat{\mathbf{n}}$. The system will adopt the orientation for which the surface tension is minimized [82].

There are very few investigations using simulations to try and understand the behavior of the isotropic-nematic (I-N) interface. This is because of the weak nature of the phase transition, and thus the dominant role of fluctuations on the interfacial properties has discouraged simulations of the I-N interface for models with dimensions appropriate to thermotropic liquid crystals.

The purpose of the current work is to study the isotropic-nematic interface and to make a quantitative comparison of both experiments and theory with computer simulation.

4.2 The Model

4.2.1 Model Details

The objective is to simulate a fluid of purely repulsive spherocylinders. This is a model that is similar to the hard spherocylinder model but more suitable for use with molecular dynamics simulation. The phase behavior of hard spherocylinders is well known theoretically - see for example the work of McGrother *et al* [118] - and through simulation and Gibbs-Duhem integration - see Bolhuis and Frenkel [119]. To achieve this objective, a soft spherocylinder model interacting via the Kihara potential was used. The Kihara potential is described in section 1.2.2.

The length to diameter ratios used in this work were $L/D = 20$ and $L/D = 50$ where L the length of the cylinder and D is the spherocylinder diameter set to 1.0. The segment-segment cutoff was $s_{cut} = 2^{1/6}$ and the center-center cutoff was $r_{cut} = L + s_{cut}$. The motivation for studying such elongated particles is that the Onsager theory makes certain predictions for the interfacial structure and properties that are expected to be valid in the limit $L/D \to \infty$.

4.2.2 Reduced units

The reduced temperature is given as $T^* = k_B T/\epsilon_0$, reduced energy as $U^* = U/\epsilon_0$ and pressure as $P^* = Pv_0/k_B T$, where v_0 is the volume of a spherocylinder. The positions and box dimension are scaled by the spherocylinder diameter: $z^* = z/D$. All densities are expressed as the reduced density $\rho^* = \rho/\rho_{cp}$ where $\rho = N/V$, the number density, and ρ_{cp} is the closed packed density of spherocylinders given as $\rho_{cp} = \frac{2}{\sqrt{2}+(L/D)\sqrt{3}}$ with L/D being the length to diameter ratio of the spherocylinder. All units will be expressed as reduced units unless otherwise stated. The spherocylinder can be thought of as a dumbbell which is a long massless rod with a point mass $m/2$ at each end. The moment of inertia of such an object is $I = 2(\frac{1}{2}m)(\frac{1}{2}L)^2 = \frac{1}{4}mL^2$. This distribution of the mass of the spherocylinder away from the center mimics a

more realistic slowly rotating spherocylinder than, for example, arbitrarily setting $I = mD^2$. Setting the mass of the spherocylinder as the unit of mass $m = 1$, the moment of inertia for a spherocylinder of length $L = 20$ will then be $I = 100$ and a spherocylinder of length $L = 50$ will have a moment of inertia of $I = 625$.

4.3 Simulation

4.3.1 Bulk Coexistence

To simulate isotropic-nematic bulk coexistence, GEMC simulations - as described in section 1.4.2 - were used. The initial configuration for the $L/D = 20$ system consisted of two, almost cubic ($\sim 50 \times 50 \times 50$), fully periodic boxes. One box contained a spherocylinder fluid in the isotropic phase, the other in the nematic phase. Each box contained ~ 1200 spherocylinders. For the $L/D = 50$ system, the initial configuration consisted of two, almost cubic ($\sim 103 \times 103 \times 103$), fully periodic boxes. Each box contained ~ 1800 spherocylinders. The overall combined densities of the two systems lie within their respective two-phase regions. As a guiding point for the initial densities, the coexisting densities observed by Bolhuis and Frenkel [119] for different length-to-breadth ratios of hard spherocylinders were used. Their results proved to be good starting points to find the coexisting densities for soft spherocylinders.

An equilibration period of $4.0 - 6 \times 10^4$ sweeps was carried out at a reduced temperature of $T^* = 1.0$. The number of particles exchanged between the two boxes was set to 10^4 particles attempted per sweep. Figure 4.1 shows the progress of the density and order parameter from an initial density $\rho^* = 0.16$. The figure shows a rapid separation of the densities to the coexistence densities of the two phases.

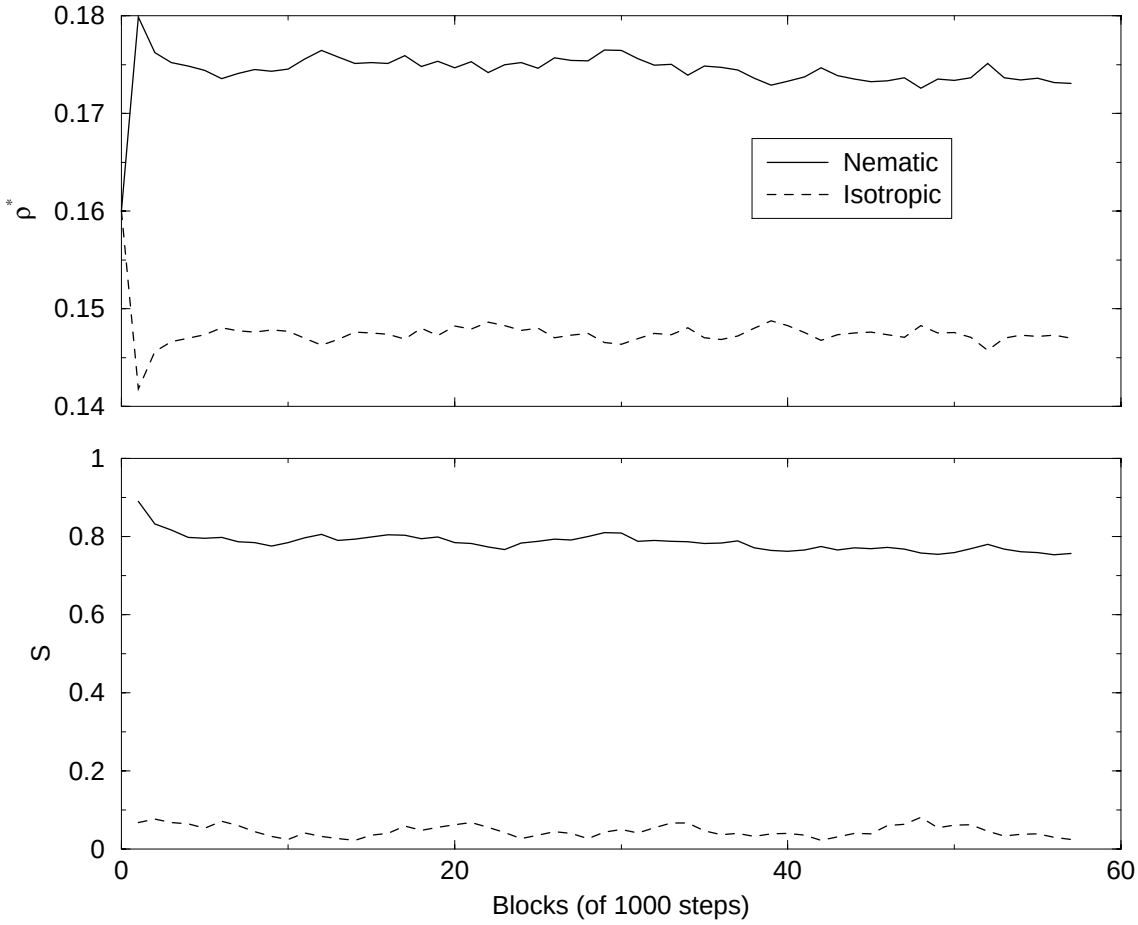

Figure 4.1: Density and order parameter as a function of MC sweeps for $L/D = 20$. Here ρ^* is the reduced density and S is the nematic order parameter for the nematic (solid line) and the isotropic (dashed line) phases.

ρ^*	0.130	0.145	0.150	0.155	0.160	0.164	0.167
Phase	I	I	I	N-I	N-I	N-I	N

Table 4.1: Observed Phases for different initial densities for $L/D = 20$.

ρ^*	0.065	0.067	0.069	0.071	0.073
Phase	I	N-I	N-I	N-I	N-I

Table 4.2: Observed Phases for different initial densities for $L/D = 50$.

Coexistence Results

Results show that soft-spherocylinders nematic and isotropic bulk phases coexist and are stable over a large period of time. Figure 4.2 shows the density and order parameter histograms. The histograms show the number of molecules at each density and order parameter. These distributions are quite narrow relative to their separation, reflecting the first-order character of the transition. Table 4.1 shows the observed phases for different starting overall densities of the two boxes for the $L/D = 20$ system and Table 4.2 shows the observed phases for the $L/D = 50$ system. An overall density $\rho^* = 0.16$ is well within the coexistence region for $L/D = 20$, and $\rho^* = 0.071$ similarly for $L/D = 50$.

Figure 4.3 shows the final configuration of the two coexisting bulk phases for $L/D = 20$. The molecules are colour coded according to orientation, such that all molecules aligned in the same direction have the same colour. The bulk on the left is in the nematic phase and the one on the right is in the isotropic phase. The nematic phase director is pointing towards the top of the page.

4.3.2 Overlaps in Interfacial Region

To model the isotropic-nematic interface the phases have to be in spatial contact with each other. This was done by combining the two boxes containing the bulk

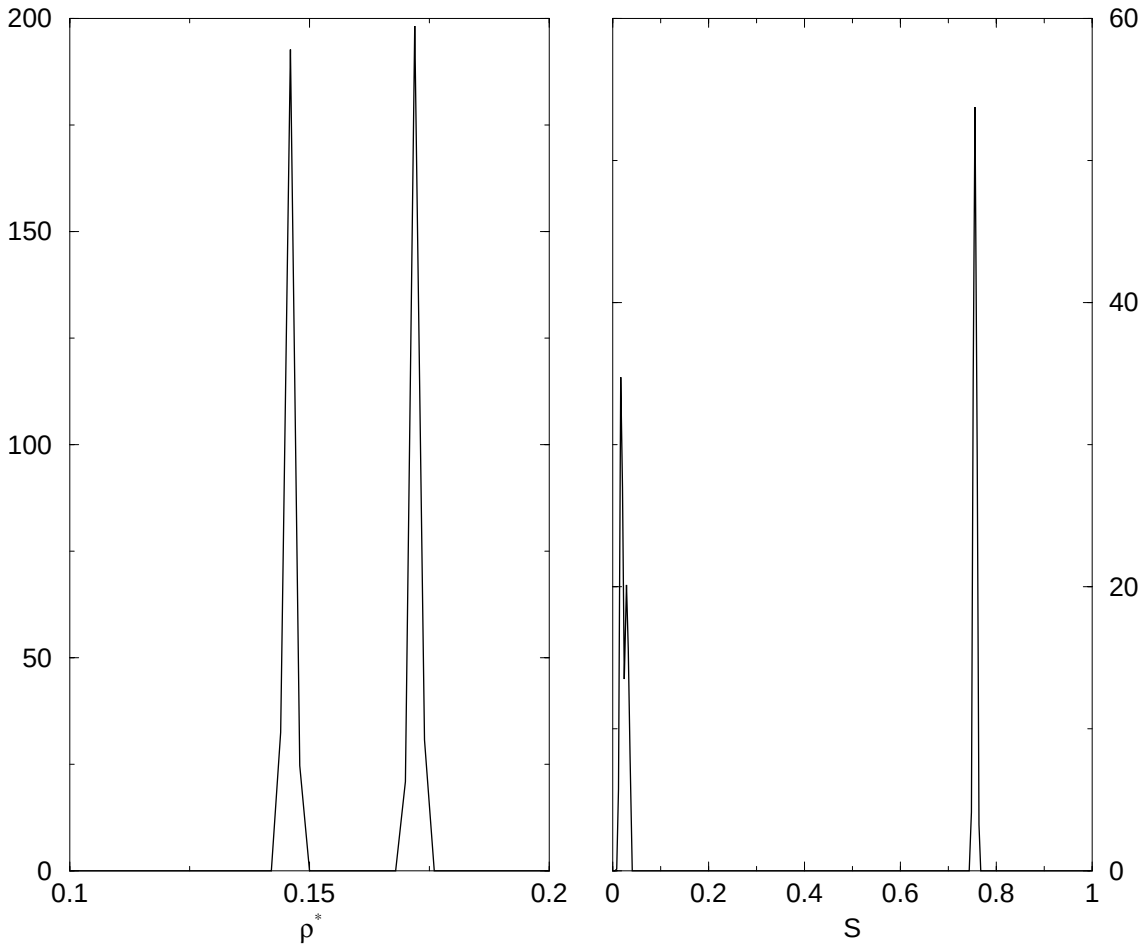

Figure 4.2: Coexistence density and order parameter probablity distributions for the $L/D = 20$ system with $\rho^* = 0.16$. ρ^* and S are the same as before. The vertical scales are such that the distributions are normalized.

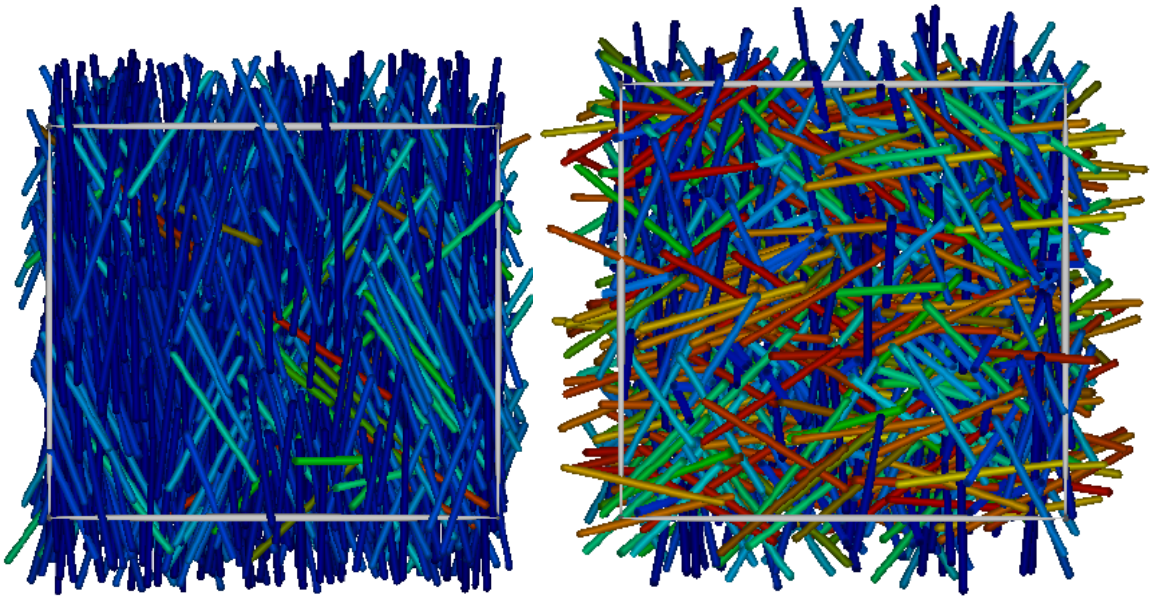

Figure 4.3: The nematic and the isotropic bulk phases of the $L/D = 20$ system.

nematic and bulk isotropic phases to form a nematic film surrounded by an isotropic fluid on both sides. Three 'copies' each of the two boxes were made. This gave a total of four boxes of each phase. The four nematic boxes were put together in the middle, while two isotropic boxes went on each end forming a $1 \times 1 \times 8$ simulation box relative to the original boxes. The new boxes are quite large, they are roughly of the order of $\sim 2 \times 2 \times 20$ molecular lengths for both the $L/D = 20$ and $L/D = 50$ systems. This is to ensure that there is enough of the fluid to maintain stable phases and to allow the interfaces to be well separated. For reasons of economy, in this study the transverse box dimensions were set close to the minimum required to avoid the possibility of a particle overlapping with two periodic images of a neighbour - ideally these dimensions should be larger. These new boxes are fully periodic and have a combined number of particles of $N = 9600$ and $N = 14400$ for the $L/D = 20$ and the $L/D = 50$ cases respectively. For the $L/D = 20$ system, two distinguishable anchoring orientations of the nematic director with respect to the interface were set up. The first had the nematic director parallel to the interface: planar anchoring. The second had the nematic director normal to the interface:

homeotropic anchoring. In the case of the $L/D = 50$ system, the anchoring was set up to be planar as it was already established from the results of the $L/D = 20$ that planar anchoring was the preferred anchoring orientation (without an applied constraint or field, the director would spontaneously rotate away from the normal direction, towards an in-plane direction).

When combining the two phases as just described, molecular overlaps occur at the interfaces. To get rid of these overlaps, Monte Carlo simulations in the constant-NVT ensemble were used. NVT-MC was discussed in section 1.4. Equilibration runs of $\sim 10^3$ MC sweeps were done at temperature $T^* = 1.0$ and constant volume to eliminate overlapping molecules at the interfaces. The total energy and pressure of each system was calculated at 10-sweep intervals throughout the run. Figure 4.4 shows the progress of energy and pressure as a function of MC sweeps for $L/D = 20$. The decrease in energy and pressure occurs as the overlaps are removed by translating molecules or by rotating them. This process was repeated until no overlaps existed.

4.3.3 Parallel Molecular Dynamics

To study the progress of the isotropic-nematic interface with time and to be able to compare with real experiments, Molecular Dynamics (MD) simulation was used. Due to the size of the system, time restrictions and available computer power, parallel MD methods were preferred. The parallel code `GBMEGA` [22] was modified to include the Kihara potential and the calculation of the corresponding forces. Constant energy molecular dynamics (Constant-NVE MD) runs were done to determine a time-step that would conserve energy to an acceptable error. A time-step of $\delta t = 0.01$ was found to give reasonable energy conservation with the fluctuation in the energy calculation being $\sim \mathcal{O}(10^{-3})$, this is an acceptable value. This time-step is in agreement with Grest and Kremer [15] for the bead-spring model that uses a similar type of repulsive Lennard-Jones potential as the Kihara potential.

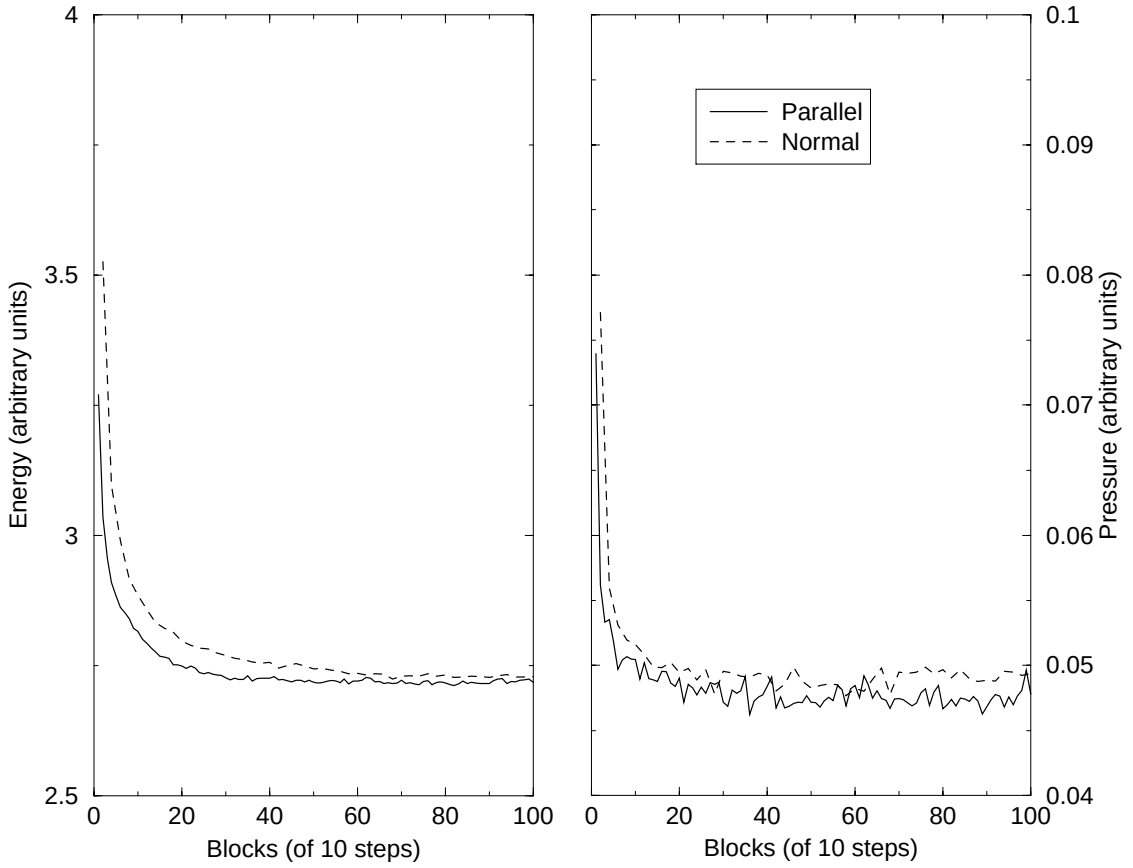

Figure 4.4: Progress of Energy and pressure during removal of overlaps for the two anchoring orientations for $L/D = 20$.

Equilibration and production runs were done at a constant temperature and constant volume (constant-NVT). The constant temperature was maintained using the ad hoc rescaling method described in section 1.3.2. The reduced temperature was set to $T^* = 1.0$ and the rescaling of the velocities was done at each time-step. For the $L/D = 20$ case, the system with the nematic director parallel to the interface, an equilibration period of 1.2×10^6 MD steps was done followed by a production period of 1.5×10^6 steps during which configurations were dumped every 500 time steps for later analysis of interfacial properties. The system with the director normal to the interface took 1.3×10^6 equilibration steps and 1.4×10^6 production steps. During the run, the system with the nematic director normal to the interface began to rotate towards a planar orientation. A director constraint method was applied to maintain the director normal to the interface. This constraint method was used by Allen *et al* [120] and is incorporated as part of the parallel code `GBMEGA`. For the $L/D = 50$ case, an equilibration period of 1.4×10^6 MD steps was done with a production period of 1.7×10^6 steps. Slightly longer equilibration and production times were needed for the longer spherocylinders which rotated much more slowly than their shorter counterparts, this was because of their larger moment of inertia. The code was run on a Cray T3E using $n_p = 32$ processors in the configuration of $2 \times 2 \times 8$. This was found to give reasonable speed-up times on the Cray T3E.

4.4 Results

Density profiles $\rho^*(z^*)$ taken along the z-axis of the box were calculated for the two systems. These profiles are averages over the whole production run of each system and director angle. Figure 4.5 shows the density and order parameter profiles for the $L/D = 20$ system with the nematic director parallel to the interface. Figure 4.6 shows the profiles when the nematic director is normal to the interface. These figures show well defined phases in both cases with very stable interfaces. The homeotropically oriented system has a much wider interface than the planar case

as expected. Figure 4.7 shows the profiles for the $L/D = 50$ system. The nematic director for this case is parallel to the interface. These profiles also show a stable and well defined interface.

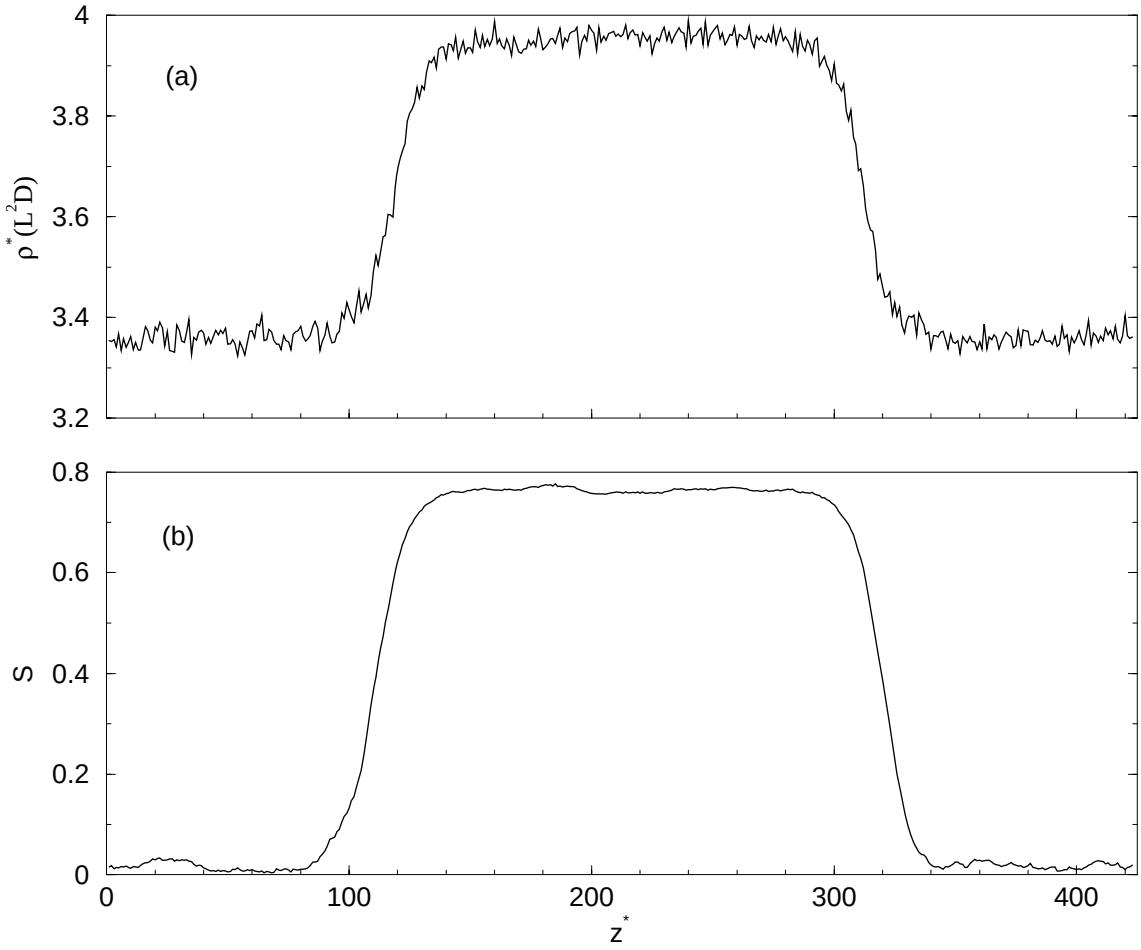

Figure 4.5: (a) Density profile and (b) Order parameter profile of the $L/D = 20$ system with nematic director parallel to the interface.

4.4.1 Surface Tension Calculations

The surface tension was calculated using the well-known expression:

$$\gamma = \int (P_N^*(z^*) - P_T^*(z^*))\, dz^* \tag{4.1}$$

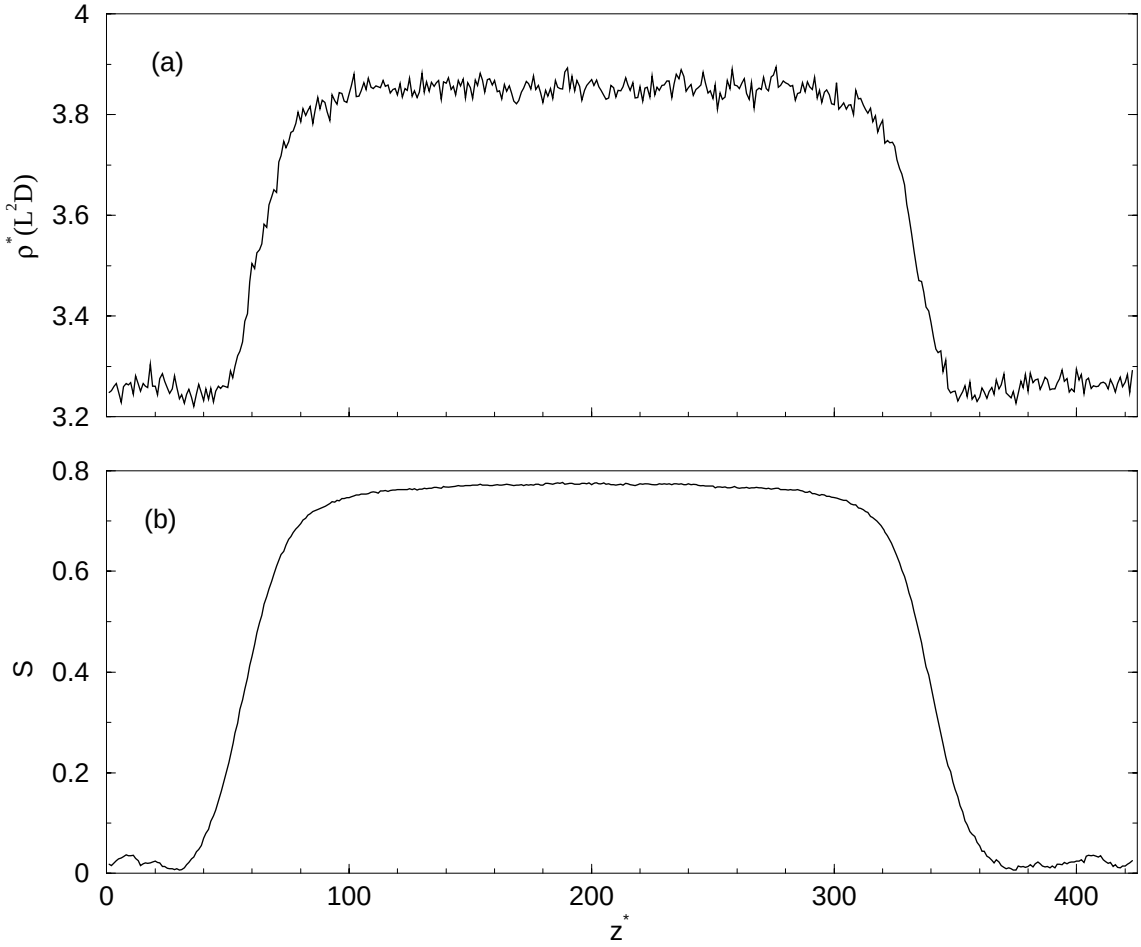

Figure 4.6: (a) Density profile and (b) Order parameter profile of the $L/D = 20$ system with nematic director normal to the interface.

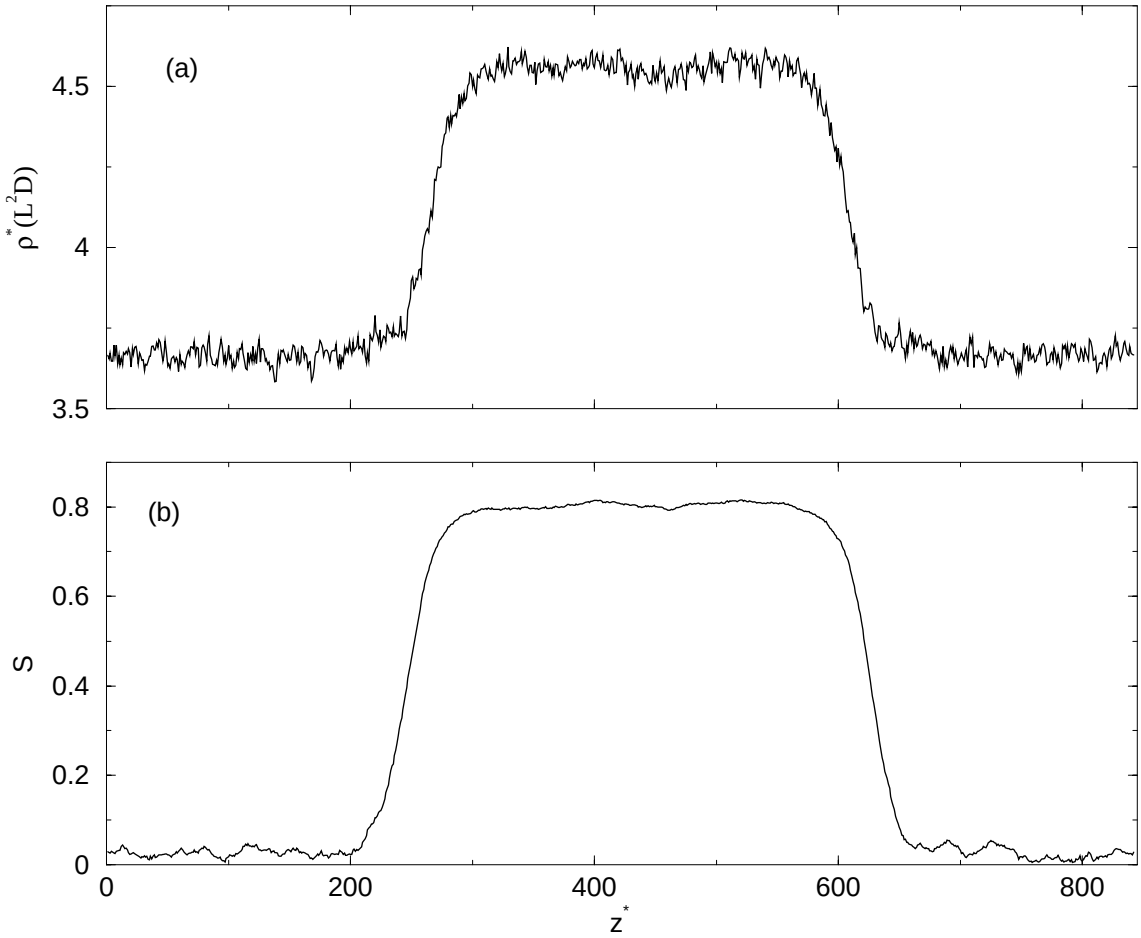

Figure 4.7: (a) Density profile and (b) Order parameter profile of the $L/D = 50$ system with nematic director parallel to the interface.

where $P_N^*(z^*)$ and $P_T^*(z^*)$ are the normal and transverse reduced pressure respectively with z^* being the axis normal to the interface [121]. The measured reduced surface tension for both spherocylinder lengths was of the order of $\mathcal{O}(10^{-4})$ while the error in our measurement was of the order of $\mathcal{O}(10^{-3})$. Due to the size of the error in the calculation of the surface tension in comparison to the measured value, it is concluded that no accurate estimation of the surface tension is possible for the current simulations.

Figure 4.8 and Figure 4.9 show the final configuration of the two $L/D = 20$ systems. These are colour coded such that all molecules aligned in the same direction have the same colour. Figure 4.10 shows the final configuration of the $L/D = 50$ system.

4.4.2 Fitting the Interface

To determine the position and width of each profile, the profiles were fitted to a hyperbolic tangent function of the following form:

$$S(z^*) = \frac{S_N + S_I}{2} + \left(\frac{S_N - S_I}{2}\right) \tanh\left(\frac{z^*}{\delta}\right) \tag{4.2}$$

where S_N and S_I are the nematic and isotropic second-rank order parameter respectively, δ is the thickness of the interface and z^* is the position in the simulation box in units of D the spherocylinder diameter.

Keeping in mind that the interface might move during the simulation, each entire run was split up into 10 sub-runs. Since the film had two interfaces, each interface was treated independently. Each sub-run was fitted independently to the hyperbolic tangent function and then shifted so that the center of the interface is at the origin. Finally, an average of all the sub-runs and sides was done. Figure 4.11 shows the fitting of the order parameter profiles of the two cases for $L/D = 20$ to a hyperbolic tangent. The density profiles were shifted by the same amount as their corresponding order parameter profiles. The order parameter profile for the $L/D = 50$ case was also fitted to a hyperbolic tangent function as is shown in Figure 4.12. The widths of

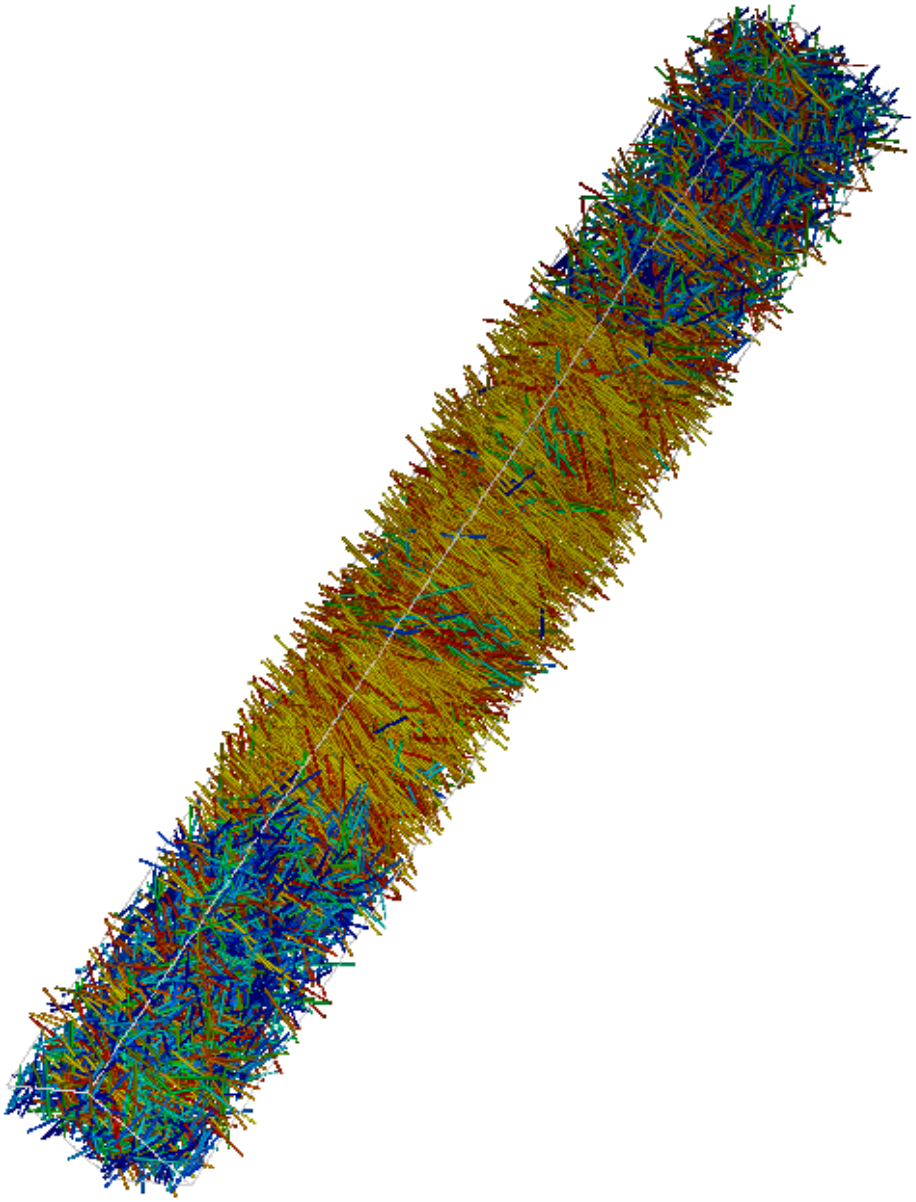

Figure 4.8: Snapshot of the configuration of the $L/D = 20$ system with the director parallel to the interfaces.

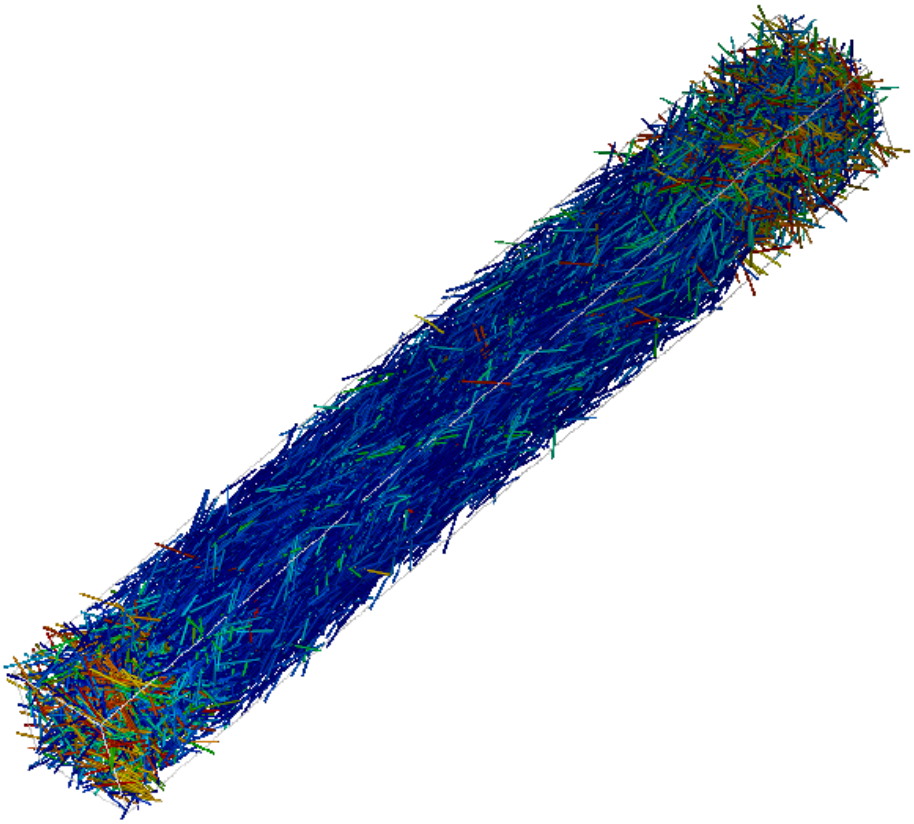

Figure 4.9: Snapshot of the configuration of the $L/D = 20$ system with the director normal to the interfaces.

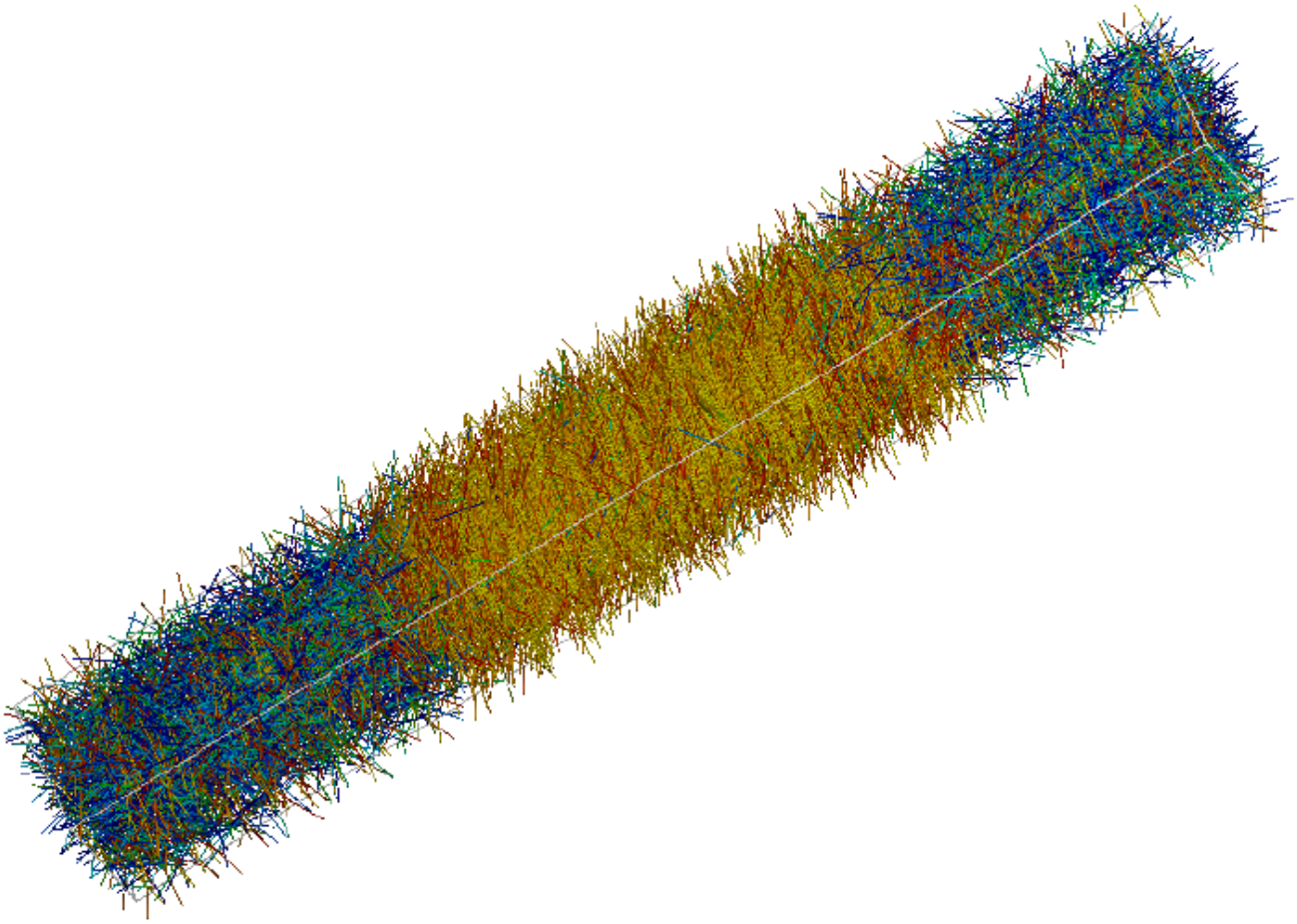

Figure 4.10: Snapshot of the configuration of the $L/D = 50$ system with the director parallel to the interfaces.

the interfaces were determined from the fitting and are presented in Table 4.3. The interfacial thickness δ of both profiles are of the order of half a spherocylinder length ($\delta \sim \frac{1}{2}L$) to within a certain error which arises from the fitting. This is in agreement with the work of Chen and Noolandi [78]. The width of the interface varies with the director angle in agreement with the findings of Allen [84] in his study of the isotropic-nematic interface of hard ellipsoids of revolution. The shift in position between the interfaces was found to be of the order of a third of spherocylinder length ($\Delta \sim \frac{1}{3}L$) also in agreement with the findings of Allen [84].

It is interesting to note that the coexisting nematic and isotropic densities for $L/D = 20$ are slightly higher for the case with the director in the interface plane than for the normal orientation. In the thermodynamic limit, we would expect these values to be the same. It is speculated that this small difference is a finite system size effect, which arises from the small transverse box direction: the free energy of the nematic phase may be different when the molecules mainly point across the box and this shifts the transition.

An interesting observation is that the density profile for all these cases was found to vary monotonically with z. This is in contrast to the Onsager theory predictions of Koch and Harlen [81], which were expected to be valid in the limit $L/D \to \infty$. It remains to be seen whether this effect will appear for even larger elongation than $L/D = 50$, or if there is some other explanation of the discrepancy.

4.4.3 Biaxiality Calculation

The biaxiality order parameter was calculated from the eigenvalues obtained from diagonalising the order tensor $\mathcal{Q}$ as written by Cui *et al* [80]:

$$\mathcal{U}\mathcal{Q}\mathcal{U}^{-1} = \begin{pmatrix} -\frac{1}{2}(\alpha + S) & 0 & \\ 0 & \frac{1}{2}(\alpha - S) & 0 \\ 0 & 0 & S \end{pmatrix} \tag{4.3}$$

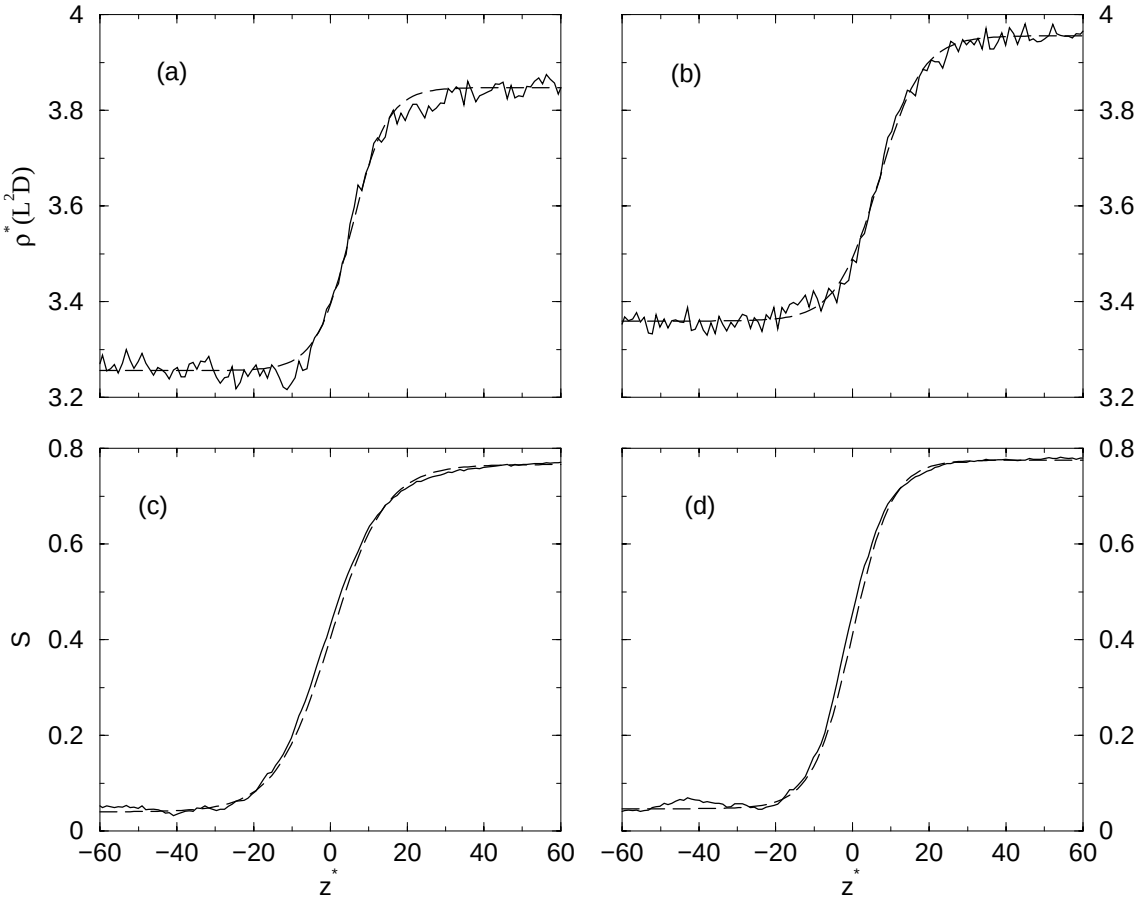

Figure 4.11: Fitting of the profiles to a tanh function for $L/D = 20$. Density profiles for: (a) Normal director and (b) In-plane director. Order parameter profiles for: (c) Normal director and (d) In-plane director. The solid lines are the actual profiles and the dashed lines are the fits.

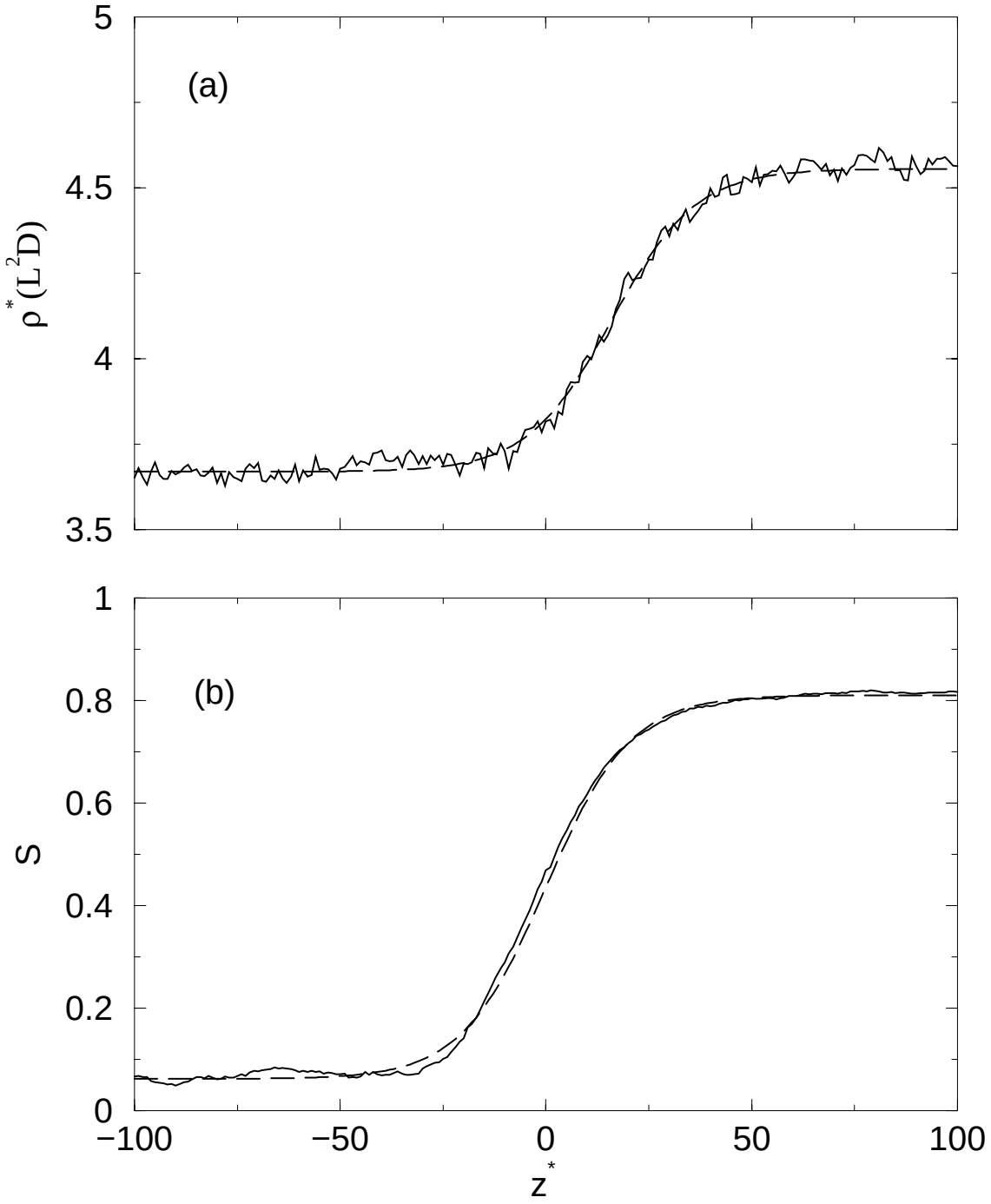

Figure 4.12: Fitting of the profiles to a tanh function for $L/D = 50$ with director in the interface plane. (a) Density profile and (b) Order parameter profile. The solid lines are the actual profiles and the dashed lines are the fits.

Director orientation	S_N	S_I	δ_S/D	
Planar($L/D = 20$)	0.78 ± 0.04	0.04 ± 0.04	10 ± 1	
Normal($L/D = 20$)	0.77 ± 0.04	0.04 ± 0.04	14 ± 2	
Planar($L/D = 50$)	0.81 ± 0.08	0.06 ± 0.08	20 ± 2	
Director orientation	$\rho_N/(L^2D)$	$\rho_I/(L^2D)$	δ_ρ/D	Δ/D
Planar($L/D = 20$)	4.0 ± 0.4	3.4 ± 0.4	11 ± 1	8
Normal($L/D = 20$)	3.8 ± 0.4	3.3 ± 0.4	9 ± 1	6
Planar($L/D = 50$)	4.6 ± 0.4	3.7 ± 0.4	20 ± 2	18

Table 4.3: Results of the fitting to a tanh function. Here S_N and S_I are the nematic and isotropic order parameters respectively, ρ_N and ρ_I are the nematic and isotropic densities respectively and δ_S and δ_ρ are the widths of the interface from the order parameter and density profiles respectively, and Δ is the shift in position between the two profiles.

where S is the nematic order parameter and α is the biaxiality order parameter defined in Chapter 2. The biaxiality order parameter profiles of both spherocylinder lengths were computed and the results are shown in Figure 4.13. This shows a significant effect for both planar anchoring cases in comparison to what was observed by Chen [79] and Cui *et al* [80]. However, the errors in these calculation are also quite significant. The nonzero value in the isotropic phase would disappear in the thermodynamic limit: it results from the finite number of molecules averaged over in each bin. Because the variation in α near the interface is no larger than this effect, we cannot conclude very much from the α profile.

4.5 Summary

A detailed simulation study of the isotropic-nematic coexistence and the interface region of a system of elongated soft spherocylinders was done. The coexisting densities

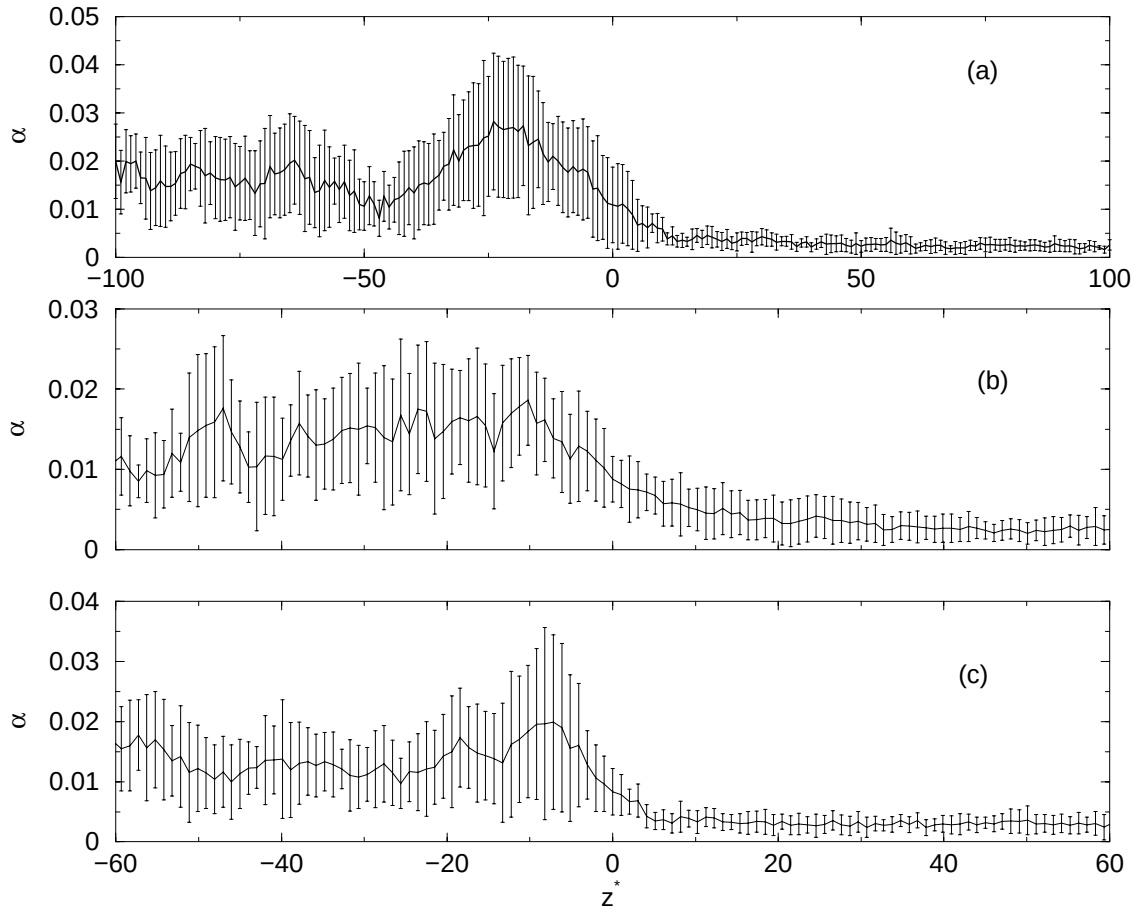

Figure 4.13: Biaxial order parameter profiles (a) $L/D = 50$ with director in interface plane, (b) $L/D = 20$ with director normal to interface and (c) $L/D = 20$ with director in interface plane.

of the two phases were found for spherocylinders of length-to-width ratio $L/D = 20$ and $L/D = 50$. The two phases were then combined to form a nematic film surrounded by isotropic liquid. Interfaces were allowed to form where the two phases came into contact. It was observed that the molecules preferred an orientation that was parallel to the interface -planar anchoring - in agreement with experimental results for MBBA [68]. This is also in agreement with theoretical results [78, 81] and other simulation results [83, 85, 84]. The interfacial profiles fitted well to a hyperbolic tangent function. The interface width was found to be of the order of $\frac{1}{2}L$. This is what was observed in the Onsager approach of Chen *et al* [78]. The interfacial width was found to vary with director orientation as found by Allen [84]. The positions of the orientational order interface and the density interface are shifted with respect to each other by about one third a molecular length, again as predicted by theory. No oscillations in the density profile as found by Koch and Harlen [81] for long hard spherocylinders were observed. A significant biaxiality effect was observed for the $L/D = 50$ case and is comparable to that found by Cui *et al* [80] for semiflexible polymers and by Chen [79] for rigid rods. A rather small biaxial effect was observed for the shorter spherocylinders in comparison to the theoretical findings, this was also observed by Allen [84] and for these rods the effect is comparable in magnitude to the artificial biaxiality seen in the isotropic phase. Surface tension measurements were done on both spherocylinder lengths, but due to the magnitude of the error, the measurements were found to be unreliable. Due to the size of the system, the thickness of the isotropic-nematic interface was of the order of the bulk correlation lengths. This prevented the observation of certain phenomena like capilary waves and wetting which are associated with larger length scales [37].

Chapter 5

Bistability in Nematics

5.1 Introduction

Bistable nematic liquid crystal devices offer obvious advantages for display addressing. An applied constant voltage would no longer be needed to maintain a single state. It would only be needed in switching between the two stable states. This would prolong the life of the liquid crystal display and conserve the power source needed to drive the display. Current experimental approaches for producing bistability in nematic systems include the use of fabricated gratings [100]. One well-known technique used to orient the nematic liquid crystal is based on SiO evaporation on glass substrates [122]. Another technique is based on constructing periodic micrometric surface structures (bigrating made with photosensitive materials) [123]. Gratings create bistability by imposing boundary conditions on the nematic which give rise to some bulk distortions. Simple elastic models proposed to connect such surface geometry with the anisotropic part of the anchoring energy are just an extension of the Berreman-de Gennes model [2, 92, 124] in which the nematic liquid crystal energy density reduces to the Frank elastic energy density. To be of use for a display, the director configurations for the bistable states must produce significantly different optical effects. To optimise both bistability and optical behaviour

as a function of grating shape and to better understand switching between bistable states under the influence of an applied field, a modelling scheme which can address practical gratings profiles and incorporate an electric and/or magnetic field interaction is desirable.

Studies concerning the bistability of nematic samples oriented by periodic sawtoothed surfaces - also known as triangular gratings - have been done [123]. The same model was used to measure the azimuthal anchoring energy on sinusoidal holographic unidimensional and bidimensional gratings [125]. Newton and Spiller [100, 101] have investigated bistability using the Gruhn and Hess two dimensional model. The surfaces they used were triangular gratings of different triangular heights and symmetry and they also used real scanning electron micrograph profiles. They observed bistability in both cases for the one-constant approximation, i.e. $K_1 = K_2 = K_3$ where K_1, K_2 and K_3 are the Frank elastic constants described in Section 1.1.

To study bistability of more realistic systems, the Gruhn and Hess model was extended to three dimensions and a bigrating (a sinusoidal grating in two directions) was imposed. Monte Carlo simulations were used with iterative annealing techniques to achieve an equilibrated low-energy state. We follow the Gruhn and Hess approach in this chapter. Details of the model are shown in Section 5.2. The details of the numerical technique are shown in Section 5.3. Section 5.4 presents and discusses the results of the simulation and Section 5.5 gives a summary of the results and a comparison with other related work.

5.2 The Model

5.2.1 Introduction

The model used here is a lattice model - see Section 1.2 of this thesis - due to Gruhn and Hess [20]. Like the Lebwohl-Lasher model [7], Gruhn and Hess have split up

the liquid crystal into cubic cells of size $\ell \times \ell \times \ell$. Each cell was assumed to have a local preferred orientation which was described by a local director at the centre of the cell. The whole system then formed a director field on a lattice. This form of coarse graining is shown in Figure 5.1. The equilibrium state of the orientation field is characterised by the minimum of the Frank free energy [4]. Gruhn and Hess [20] have used Monte Carlo simulations to generate an equilibrium director field of a nematic liquid crystal in two dimensions. They used a tensorial description of the director to properly describe the symmetry of the nematic where $\mathbf{n} \equiv -\mathbf{n}$. An advantage of this model over the Lebwohl-Lasher model is that it allows for the treatment of energy expressions with three elastic coefficients.

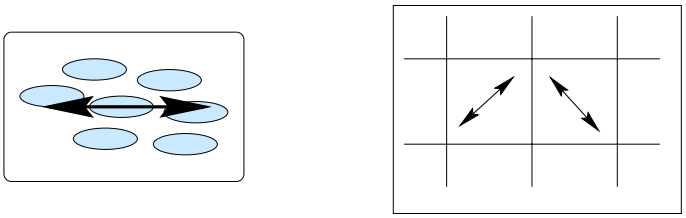

Figure 5.1: Coarse graining of a liquid crystal fluid to a lattice

Hobdell and Windle [126] have used a similar approach in modelling defects in nematic liquid crystals. They described the nematic director field as a vector where $\mathbf{n} \not\equiv -\mathbf{n}$. To overcome this shortcoming, they introduced a vector flipping method where a vector is flipped through 180^o if the angle between it and another vector is greater than 90^o. The approach gives a discontinuity in the gradient of the energy function whenever neighbours are at an angle normal to each other. They have accepted this as it will only happen at disclination cores where low angle elasticity is applicable [126]. This might not be the case near surfaces that are not flat.

5.2.2 Model details

In general, the orientation distribution of uniaxial molecules can be described by the second rank alignment tensor

$$a_{\mu\nu} = \sqrt{\frac{15}{2}} \langle \overleftrightarrow{u_\mu u_\nu} \rangle$$

where $\mathbf{u}$ is a unit vector parallel to the molecules' principal axis and the brackets $\langle\ \rangle$ indicate an average. The Greek subscripts refer to Cartesian components, for which the summation convention is used, and $\overleftrightarrow{\mathbf{b}}$ denotes the symmetric-traceless part of tensor $\mathbf{b}$. We assume a uniaxial orientation of the molecules distributed symmetrically around a director $\mathbf{n(r)}$. Hence, the alignment tensor becomes

$$a_{\mu\nu} = \sqrt{\frac{3}{2}} a\ \overleftrightarrow{n_\mu n_\nu}\ .$$

Here $a = \sqrt{5}S$, with $S = \langle P_2(u_\mu n_\mu) \rangle = \langle \frac{3}{2}\cos^2(\theta) - \frac{1}{2} \rangle$; the usual Maier-Saupe nematic order parameter. S characterizes the degree of alignment: in the isotropic phase, the distribution of the long molecular axis is random, hence $\langle \cos^2(\theta) \rangle = \frac{1}{3}$ and $S = 0$. In a perfectly aligned nematic phase, $S = 1$ since $\langle \cos^2(\theta) \rangle = 1$. Assuming S to be constant for the whole system, all that is needed to describe the orientation of the liquid crystal is $\overleftrightarrow{\mathbf{nn}}\ (\mathbf{r})$.

To describe the behaviour of the director field and the interaction between the director a discretized form of the Frank free energy was used. The Frank free energy equation is [4]:

$$f_{el} = \frac{1}{2}\left[K_1(\nabla \cdot \mathbf{n})^2 + K_2(\mathbf{n} \cdot (\nabla \times \mathbf{n}))^2 + K_3(\mathbf{n} \times (\nabla \times \mathbf{n}))^2\right]. \qquad (5.1)$$

This equation can be rewritten in a tensorial form. The various quantities in Equation (5.1) can be expressed as follows [1]:

$$\begin{aligned}
\nabla \cdot \mathbf{n} &= \nabla_\lambda n_\lambda \\
(\mathbf{n} \times (\nabla \times \mathbf{n}))^2 &= (\nabla \times \mathbf{n})^2 - (\mathbf{n} \cdot (\nabla \times \mathbf{n}))^2 \\
&= n_\lambda n_\mu (\nabla_\lambda n_\nu)(\nabla_\mu n_\nu) \\
(\nabla \cdot \mathbf{n})^2 + (\nabla \times \mathbf{n})^2 &= (\nabla \cdot \mathbf{n})^2 + (\mathbf{n} \cdot (\nabla \times \mathbf{n}))^2 + (\mathbf{n} \times (\nabla \times \mathbf{n}))^2 \\
&= (\nabla_\lambda n_\mu)(\nabla_\lambda n_\mu)
\end{aligned}$$

Inserting these expressions in Equation (5.1) gives

$$\begin{aligned} f_{\text{el}} &= \frac{1}{2}\Big[K_2(\nabla_\lambda n_\mu)^2 + (K_1 - K_2)((\nabla_\lambda n_\lambda)(\nabla_\mu n_\mu) \\ &\quad + (K_3 - K_2)(n_\lambda n_\mu)(\nabla_\lambda n_\nu)(\nabla_\mu n_\nu)\Big]. \end{aligned} \tag{5.2}$$

This is algebraically equivalent to Equation (5.1) with the exception of surface terms that have been disregarded.

In Equation (5.2) the director can be written in the form of a dyad **nn**, giving the following form:

$$\begin{aligned} f_{\text{el}} &= \frac{1}{2}\Big[\frac{1}{2}K_2(\nabla_\lambda n_\mu n_\nu)^2 \\ &\quad +(K_1 - K_2)(\nabla_\lambda n_\lambda n_\mu)(\nabla_\nu n_\nu n_\mu) \\ &\quad + \frac{1}{2}(K_3 - K_1)(n_\mu n_\nu)(\nabla_\mu n_\lambda n_\kappa)(\nabla_\nu n_\lambda n_\kappa)\Big]. \end{aligned} \tag{5.3}$$

Here $\nabla_\lambda n_\mu n_\nu \equiv \nabla_\lambda(n_\mu n_\nu)$. Equation (5.2) can be recovered by splitting the dyad.

The influence of an orienting external field is described by f_{field}. For a magnetic field **B** it is [1]:

$$f_{\text{field}} = -\frac{1}{2}\mu_0^{-1}\chi_a(n_\nu B_\nu)^2 \tag{5.4}$$

where μ_0 is the vacuum magnetic susceptibility and $\chi_a = S(\chi_\parallel - \chi_\perp)$, where $\chi_\parallel$ and $\chi_\perp$ are the relative magnetic susceptibilities, parallel and perpendicular to the director of a perfectly aligned nematic liquid crystal.

Discretisation

The symmetrical discretisation of the gradient of a function $g(x)$ has the form

$$\frac{\partial g}{\partial x} \approx \frac{g(x+\ell) - g(x-\ell)}{2\ell}$$

while the asymmetric discretisation has the form:

$$\frac{\partial g}{\partial x} \approx \frac{g(x+\ell) - g(x)}{\ell}$$

or

$$\frac{\partial g}{\partial x} \approx \frac{g(x) - g(x-\ell)}{\ell}.$$

When this is mapped on to a cubic lattice with points (i, j, k),the next neighbours are at a distance $\ell = 1$. The function $g(x)$ is replaced by $n_\mu n_\nu(i, j, k)$ and the asymmetric discretisation is chosen; the symmetric discretisation was found to be unsuitable for the Monte Carlo technique, since it does not involve the value of the function at position x and thus causes the lattice to decouple. In the asymmetric case, each partial derivative has a left and right discretisation; there are therefore eight asymmetrical discretisations for $\nabla n_\mu n_\nu(i, j, k)$[20].

The discretised free energy for a cubic lattice can now be written in the following form:

$$\begin{aligned} f^*_{\text{or}} &= \frac{1}{8}\sum_{r=\pm1}\sum_{s=\pm1}\sum_{t=\pm1}\Bigg[\frac{1}{2}K^*_2\sum_{\lambda\mu\nu=1}^{3}\left(\mathcal{D}^{(r,s,t)}_{\lambda\mu\nu}(i,j,k)\right)^2 \\ &\quad +(K^*_1 - K^*_2)\sum_{\mu=1}^{3}\left(\sum_{\lambda=1}^{3}\mathcal{D}^{(r,s,t)}_{\lambda\lambda\mu}(i,j,k)\right)^2 \\ &\quad +\frac{1}{2}(K^*_3 - K^*_1)\sum_{\mu\nu=1}^{3}\left(\sum_{\lambda=1}^{3}n_\lambda(i,j,k)\mathcal{D}^{(r,s,t)}_{\lambda\mu\nu}(i,j,k)\right)^2\Bigg] \\ &\quad +\left(\frac{\pi}{N+1}B^*(i,j,k)\right)^2\left(\sum_{\nu=1}^{3}n_\nu(i,j,k)\hat{B}_\nu(i,j,k)\right)^2. \end{aligned} \tag{5.5}$$

The asterisks in Equation (5.5) denote dimensionless quantities which are defined later. The elastic part of f^*_{or} is defined as the arithmetic average of the eight asymmetrical discretisations of the derivatives, $\mathcal{D}^{(r,s,t)}_{\lambda\mu\nu}$ with $(r, s, t) \in \{\pm1, \pm1, \pm1\}$. The $\pm$ indicates the right or left discretisation in x-, y- and z-directions respectively, the subscript λ indicates the axis on which the discretisation is performed and $\{\mu\nu\}$ are the normal Cartesian components [20].

A few of the $\mathcal{D}$ functions are shown below:

$$\begin{aligned} \mathcal{D}^{(+1,-1,+1)}_{1\mu\nu}(i,j,k) &:= n_\mu n_\nu(i+1,j,k) - n_\mu n_\nu(i,j,k) \\ \mathcal{D}^{(+1,-1,-1)}_{2\mu\nu}(i,j,k) &:= n_\mu n_\nu(i,j,k) - n_\mu n_\nu(i,j-1,k) \end{aligned}$$

$$
\begin{aligned}
\mathcal{D}_{3\mu\nu}^{(+1,-1,+1)}(i,j,k) &:= n_\mu n_\nu(i,j,k+1) - n_\mu n_\nu(i,j,k) \\
\mathcal{D}_{1\mu\nu}^{(-1,+1,-1)}(i,j,k) &:= n_\mu n_\nu(i,j,k) - n_\mu n_\nu(i-1,j,k) \\
\mathcal{D}_{2\mu\nu}^{(-1,+1,-1)}(i,j,k) &:= n_\mu n_\nu(i,j+1,k) - n_\mu n_\nu(i,j,k) \\
\mathcal{D}_{3\mu\nu}^{(-1,+1,-1)}(i,j,k) &:= n_\mu n_\nu(i,j,k) - n_\mu n_\nu(i,j,k-1)
\end{aligned}
$$

5.2.3 Surface Contributions

For the 3-dimensional system, surface terms play a significant role especially when the bounding surfaces are not flat. Therefore, the surface term can not be ignored and would have to be included in the free energy. Equation (5.2) which is the tensor form of the Frank free energy becomes

$$
\begin{aligned}
f_{el} &= \frac{1}{2}\Big[K_1(\nabla_\lambda n_\lambda)(\nabla_\mu n_\mu) + K_2((\nabla_\lambda n_\mu)^2 - (\nabla_\lambda n_\mu)(\nabla_\mu n_\lambda)) \\
&\quad + (K_3 - K_2)(n_\lambda n_\mu)(\nabla_\lambda n_\nu)(\nabla_\mu n_\nu)] \qquad (5.6)
\end{aligned}
$$

This is algebraically equivalent to Equation (5.1). Again, the director in Equation (5.6) can be written in the form of the dyad **nn**, giving the following form:

$$
\begin{aligned}
f_{el} &= \frac{1}{2}\Big[\frac{1}{2}K_2(\nabla_\lambda n_\mu n_\nu)^2 - K_2(\nabla_\lambda n_\mu n_\nu)(\nabla_\mu n_\lambda n_\nu) \\
&\quad + K_1((\nabla_\lambda n_\lambda n_\nu)(\nabla_\mu n_\mu n_\nu) \\
&\quad + \frac{1}{2}(K_3 - K_1)(n_\lambda n_\mu)(\nabla_\lambda n_\nu n_\kappa)(\nabla_\mu n_\nu n_\kappa)\Big]. \qquad (5.7)
\end{aligned}
$$

Here $\nabla_\lambda n_\mu n_\nu \equiv \nabla_\lambda(n_\mu n_\nu)$ as before. Splitting up the dyad gives back the tensorial form of Equation (5.6). The discretised form of Equation (5.7) can now be written down as follows:

$$
\begin{aligned}
f_{\mathrm{el}}^* &= \frac{1}{8}\sum_{r=\pm1}\sum_{s=\pm1}\sum_{t=\pm1}\Bigg[\frac{1}{2}K_2^*\sum_{\lambda\mu\nu=1}^{3}\Big(\mathcal{D}_{\lambda\mu\nu}^{(r,s,t)}(i,j,k)\Big)^2 \\
&\quad - K_2^*\sum_{\lambda\mu\nu=1}^{3}\Big(\mathcal{D}_{\lambda\mu\nu}^{(r,s,t)}(i,j,k)\mathcal{D}_{\mu\lambda\nu}^{(r,s,t)}(i,j,k)\Big)
\end{aligned}
$$

$$+ \quad K_1^* \sum_{\mu=1}^{3} \left(\sum_{\lambda=1}^{3} \mathcal{D}_{\lambda\lambda\mu}^{(r,s,t)}(i,j,k) \right)^2$$

$$+ \quad \frac{1}{2}(K_3^* - K_1^*) \sum_{\mu\nu=1}^{3} \left(\sum_{\lambda=1}^{3} n_\lambda(i,j,k) \mathcal{D}_{\lambda\mu\nu}^{(r,s,t)}(i,j,k) \right)^2 \Bigg]. \tag{5.8}$$

The dimensionless quantities of Equation (5.5) and Equation (5.8) are defined by the following expressions [20]:

$$K_i = K_i^* K, (i = 1, 2, 3), \qquad F_{or} = \frac{\ell}{2} K F_{or}^*,$$

$$B_\mu = B\hat{B}_\mu, \qquad f_{or} = \frac{K}{2\ell^2} f_{or}^*,$$

$$B = \left(\frac{\pi}{(N_z+1)\ell} \sqrt{\frac{K}{\chi_a}} \right) B^*, \qquad T = \left(k_B^{-1} \frac{\ell}{2} K \right) T^*.$$

Here f is the free energy density and F is total free energy, the free energy density summed up over all lattice points. K is a mean elastic constant, k_B the Boltzmann constant and T the temperature. The lattice point separation is $\ell = 1$ and the thickness of the liquid crystal is $d = (N_z + 1)\ell$ between the two surfaces, where N_z is the number of lattice points along the z direction.

5.3 Simulations

5.3.1 Equilibration Details

Monte Carlo simulations were used to calculate the mean equilibrium orientation field $\langle n_\mu n_\nu(i,j,k) \rangle$. The Metropolis method [5] was used to equilibrate the system at a fixed temperature. Here the temperature is not the thermodynamic temperature, but is part of the numerical technique.

The method begins with a trial rotation by a random angle ψ of the local director $\mathbf{n} \to \tilde{\mathbf{n}}$. The choice of the random angle is uniformly distributed over the interval $[-\psi_m, \psi_m]$, where ψ_m is a fixed parameter, suitably chosen to give a 50% acceptance rate. The energy difference $\Delta F^*(\mathbf{n} \to \tilde{\mathbf{n}})$ between the configuration with the old director $\mathbf{n}$ and the new one $\tilde{\mathbf{n}}$ was calculated. The new director is then accepted

with the probability $p(\mathbf{n} \rightarrow \tilde{\mathbf{n}}) = \min\{1, \exp[-\Delta F^*/T^*]\}$. If the new director was rejected, the old director was retained. A trial rotation of the next director is attempted. Once all directors have been attempted, one Monte Carlo step is made and the process is repeated. After a number of equilibration steps the algorithm calculates the mean equilibrium orientation field $\langle n_\mu n_\nu \rangle$.

5.3.2 Annealing

Due to the fact that the interactions in this model are very short range, defects occur in large lattices when the system is quenched rapidly to a low temperature. The defects tend to get frozen in before they can escape. To remove these defects, annealing techniques mentioned in Section 1.4 were used. The iterative improvement annealing technique was used. The method was seen to give as good results as the simulated annealing technique [36], yet it completed its task in a shorter simulation time. Each simulation run started at a high reduced temperature $T^* = 1.0$ which was then allowed to equilibrate for N_{equil} steps. The temperature was then reduced by 5% and allowed to equilibrate again. This process of temperature reduction and equilibration is repeated for N_{temp} annealing steps. Typical runs would take $N_{\text{equil}} = 10^4 - 10^5$ equilibration steps and $N_{\text{temp}} = 100 - 150$ temperature annealing steps. Figure 5.2 shows the progress of the order parameter and energy as a function of MC sweeps for a typical iterative annealing run.

5.4 Results

Lattice systems of 2-dimensions and 3-dimensions were modelled using Monte Carlo simulation. The 2-dimensional systems had fixed boundaries in the y-direction and periodic boundaries in the x-direction. The fixed boundaries consisted of surfaces with triangular and sinusoidal gratings. The lattice size for the 2-D model consisted of 64×64 directors. The 3-dimensional systems had fixed boundaries in the z-direction and periodic in the others. The fixed boundaries used were either flat,

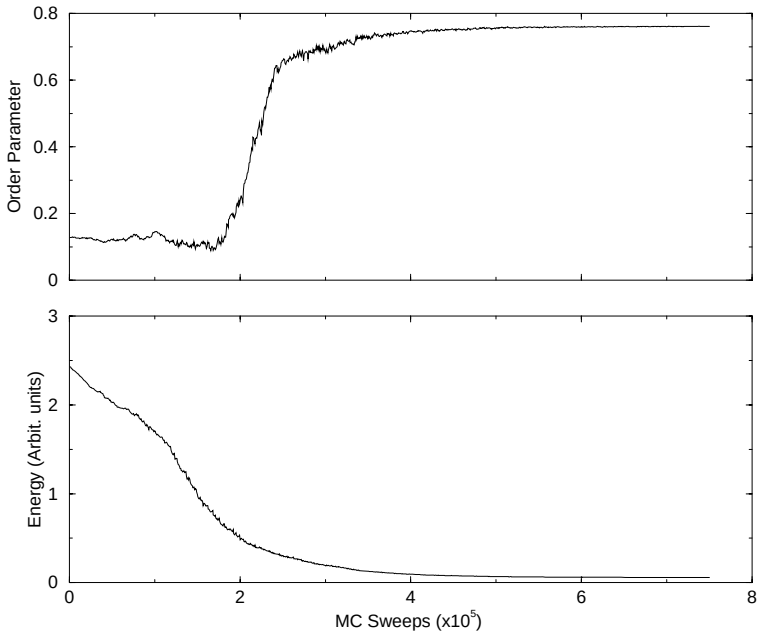

Figure 5.2: Order Parameter and Energy as a function of MC sweeps

triangular or bigrated, i.e. the surface follows a sinusoidal pattern in the x- and y-directions. The flat surfaces system was used as a test for the model and the technique in three dimensions. The 3-dimensional systems consisted of lattices of $24 \times 24 \times 24$ directors. Annealing techniques [36] were used to minimise the energy and equilibrate the systems.

5.4.1 Triangular Grating

Simulation runs were done for two-dimensional systems with an ideal single triangular grating surface. This type of grating is also known as *sawtoothed*. The free surface was kept flat. Figure 5.3 shows two equilibrated configurations with different orientations at the free surface. The first has an orientation that is normal to the free surface, this system is highly ordered and the total energy of the system is low. The second has an orientation that is planar to the free surface. This system is at a higher energy and slightly disordered around the points of the triangles. Both systems have homeotropic anchoring on the grated surface. It is therefore concluded

that the normal orientation - being the lowest in energy - is the preferred orientation for such a system. The height to half-base ratio of these triangular gratings is 1:1. No bistable states were observed for this case.

Figure 5.3: Snapshots of director profiles for two different anchoring angles at the flat surface with a height to half-base ratio of 1:1 of the triangular grating.

When the height of the triangular gratings were reduced by a half to a height to half-base ratio of 1:2, bistability was observed. Figure 5.4 shows the bistable nature of a triangular grating where the free surface orientation is normal. The two systems are optically distinguishable - being mirror images of each other - and degenerate in energy. In comparison, Newton and Spiller [101] found bistability for the triangular grating at a triangular height to half-base ratio of 1:0.8 for the same type of system. The two stable states that Newton and Spiller obtained were from two different initial configurations and lead to two different states from the ones shown in Figure 5.4. The system they obtained from the initial $h-$ state had a director field comparable to the ones presented in Figure 5.4. Their $v-$ produced a state that was similar to the low energy state presented in Figure 5.3.

Figure 5.4: Snapshots of director profiles of two systems with the same anchoring angles at the flat surface with a height to half-base ratio of 1:2 of the triangular grating.

5.4.2 Real Gratings

Newton and Spiller [100] have done Monte Carlo simulations using the Gruhn and Hess model with real surfaces obtained from scanning electron micrograph profiles. Newton and Spiller have found three stable states - see Section 2.4 for details - which were not degenerate in energy.

Using the iterative annealing technique on the same surface profile, we found only one stable state. This state corresponds to Newton and Spillers lowest energy configuration, the $v-$ state [101]. The real surface profile is shown in Figure 5.5. It is possible that their other states are a by-product of a biased initial configuration. It is possible that a lower grating amplitude would produce bistability with degeneracy in energy as with the triangular grating.

5.4.3 Frederiks Transition

Consider a nematic cell with given boundary conditions, such that a uniform director field results. When a magnetic or electric field is applied, a conflict arises between the orienting effect of the boundaries and the orienting effect of the applied field.

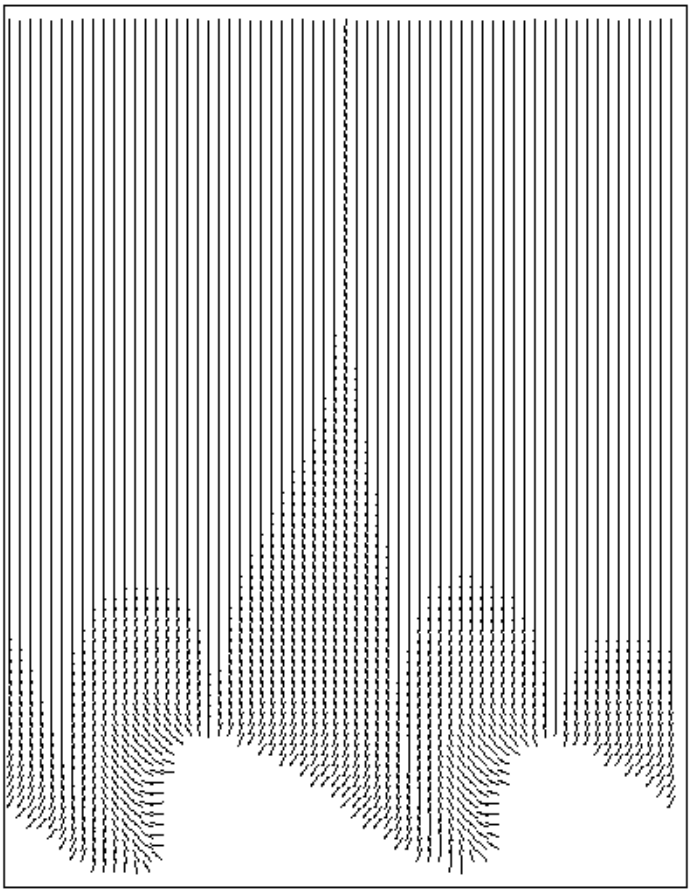

Figure 5.5: Snapshot of the director profile for a system with a real surface profile.

This causes a distortion of the original field to occur. In the case where the external field is perpendicular to the original director, the distortion normally sets in only if the strength of the applied field exceeds a certain well-defined threshold value. This type of transition is call a Frederiks transition [1].

Analytical Solutions

In the case of an applied magnetic field, de Gennes [2] showed that the threshold field $B_{c,i}$ corresponds to

$$B_{c,i} = \frac{\pi}{d}\left(\frac{K_i}{\chi_a}\right) \tag{5.9}$$

where d is the thickness of the nematic layer, χ_a the magnetic susceptibility anisotropy and the constants $K_i (i = 1, 2, 3)$ are the Frank elastic constants. Vertogen and de Jeu [1] showed that the relationship between the maximum tilt angle θ_m and the applied magnetic field is of the following form

$$\frac{B}{B_c} = \frac{2}{\pi}\int_0^{\frac{\pi}{2}} d\psi \left(\frac{1 + \kappa \sin^2\theta_m \sin^2\psi}{1 - \sin^2\theta_m \sin^2\psi}\right)^{\frac{1}{2}}, \tag{5.10}$$

where $\kappa = 0$ for the twist geometry, $\kappa = (K_3 - K_1)/K_1$ for the splay geometry and $\kappa = (K_1 - K_3)/K_3$ for the bend geometry. This type of integral is known as a complete elliptical integral of the first kind.

Simulation Results

Simulations were done on a system with flat fixed boundaries. The runs were done for the splay geometry, where the anchoring at the surfaces is planar and the applied field is normal to the surface. Even though the Frederiks threshold for the splay geometry depends only on K_1, the director field for $B > B_c$ varies with K_3/K_1 as seen in Equation (5.10).

In Figure (5.6) the maximum angle θ_m between the director and the easy axis is shown for field strength between $B/B_c = 0.5$ and $B/B_c = 2.0$ for various ratios of K_3/K_1. The simulation results are compared with the analytical solution of

Equation (5.10). The results show total agreement between the simulation results and the analytical solutions. The same is also true for the bend geometry where the director field varies with K_1/K_3 (not shown here). These results are in agreement with the Hobdell and Windle [126] results. They used a lattice model based on the discretized free energy to study Frederiks transition.

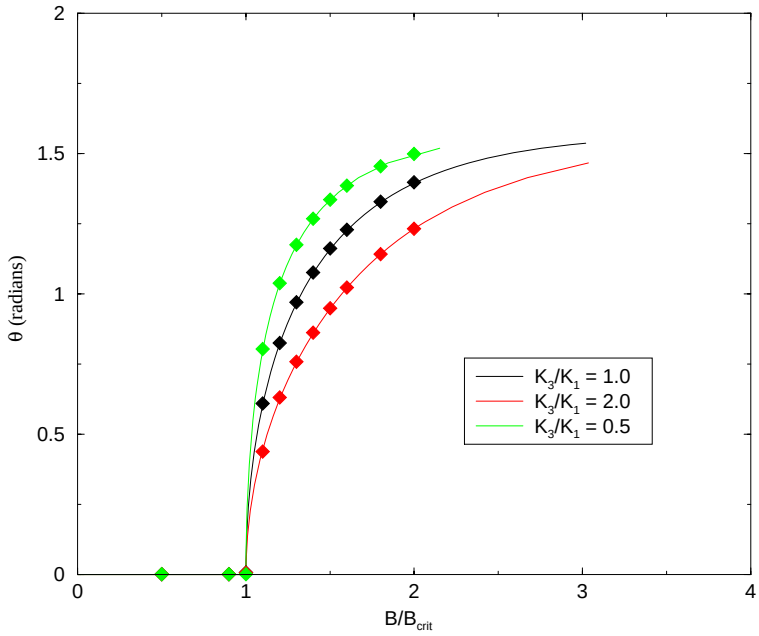

Figure 5.6: Maximum tilt angle θ_m for the splay geometry. The points are simulation results and the curves show the analytical solutions.

5.4.4 Bigrating

The bigrated system consists of two surfaces. The first is flat and the second follows a sinusoidal pattern in both the x and the y directions - a bigrating. This surface is defined as $z = a\sin(2\pi x/L_1) + b\sin(2\pi y/L_2)$, where a and b are the amplitudes and L_1 and L_2 are the wavelengths of the grating in the x and the y directions respectively. This type of surface can be experimentally created using photolithographic gratings with sinusoidal profiles obtained by interferometric exposure of the photoresist [125]. The profile of such a surface is depicted in Figure 5.7. The directors

are constrained tangentially to the surface with a particular azimuthal angle ϕ. The tangent vector as a function of ϕ for the directors on the surface is defined as

$$\hat{\mathbf{t}} = \frac{\cos\phi\,\hat{\mathbf{x}} + \sin\phi\,\hat{\mathbf{y}} + (k_1 a\cos\phi\cos k_1 x + k_2 b\sin\phi\cos k_2 y)\hat{\mathbf{z}}}{[1 + (k_1 a\cos\phi\cos k_1 x + k_2 b\sin\phi\cos k_2 y)^2]^{\frac{1}{2}}} \tag{5.11}$$

where $k_1 = 2\pi/L_1$ and $k_2 = 2\pi/L_2$ are the wavenumbers of the sinusoidal surface [127]. This vector follows the undulation of the surface.

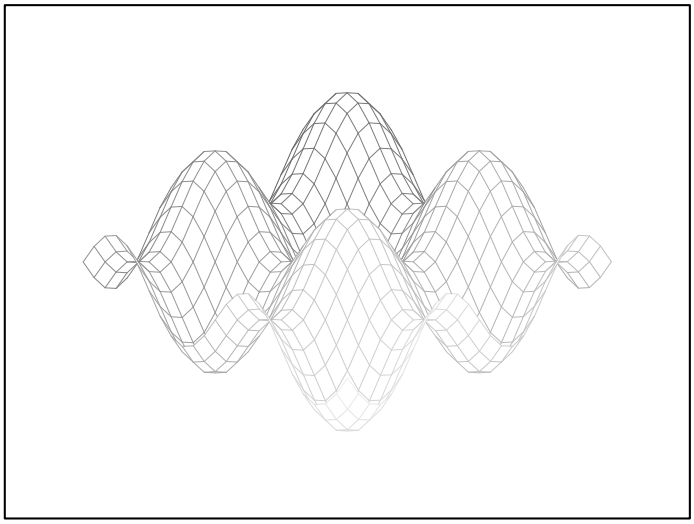

Figure 5.7: Surface profile of the bidimensional grating.

Simulation runs were done for a set of values of the azimuthal angle ϕ to determine the preferred orientation. The values chosen for the wave amplitudes were $a = 10$ and $b = 10$, while the values for the wave numbers were $k_1 = 2\pi/n_x$ and $k_2 = 2\pi/n_y$ where $n_x = n_y = 24$ are the number of lattice points along the x- and y-directions. The preferred orientation would have the lowest energy among the set of orientations and would be considered a stable state. Each run was allowed to equilibrate using the iterative annealing method. Once equilibrated the total energy of the system was calculated. Figure 5.8 shows the dependence of energy on the azimuthal angle ϕ, the orientation of the tangential vector at the bigrated surface. The energy is lowest when the tangential vector is along either of the two diagonals

(i.e. $\phi = \pi/4$ and $\phi = 3\pi/4$). This shows that the two diagonal orientations are the most stable states and that leads to the conclusion that a bigrating does cause bistability.

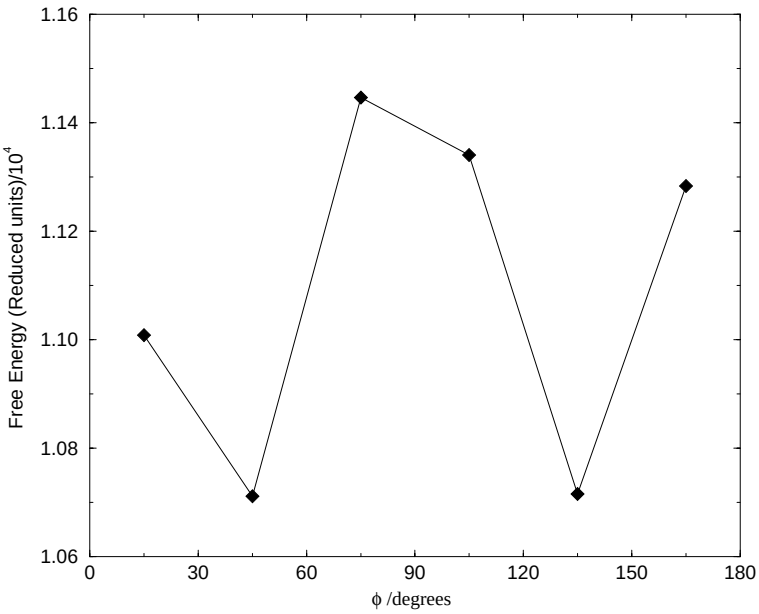

Figure 5.8: Energy as a function of the angle of orientation of the director at the bigrated surface.

Figure 5.9 shows an equilibrated configuration for the bigrating system looking at the system from the side. This shows the large oscillations in the surface. It also shows that the director field is planar above the undulated surface and that the distortions dissipate rapidly with distance away from the surface. Figure 5.10 shows two equilibrated configurations for the bigrating system looking at the system from the top. The snapshot on the right shows one of the two diagonally preferred alignments with an azimuthal anchoring angle of $3\pi/4$. The other preferred orientation is obtained when this system is rotated by $\pi/2$ clockwise around the z-axis. This figure also shows the degree of alignment as each layer - starting from the bottom all the way to the top - each director is perfectly aligned parallel to the ones anchored at the surface. The snapshot on the left shows a less preferred orientation, here the azimuthal anchoring angle is $\pi/12$. The directors of each layer are not parallel to

the ones below them causing a higher energy level

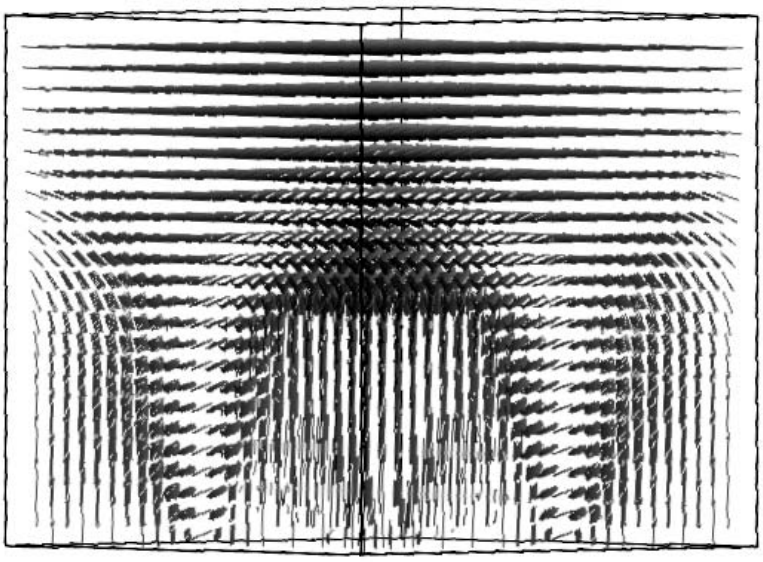

Figure 5.9: Snapshot of the bigrated system looking at it from the side. The system has a fixed azimuthal angle of $\phi = \pi/4$.

5.5 Summary

To test bistability using the Gruhn and Hess [20] model in two dimensions, triangular grating surfaces were used. The lowest energy configurations were obtained and bistability was observed. This is in agreement with Newton and Spiller [100, 101]. The model of Gruhn and Hess was extended to three dimensions and a magnetic field was applied to a system with flat surfaces. A Frederiks transition occurred at the critical field strength. The results presented here were in agreement with the Hobdell and Windle [126] results for the splay geometry and are in perfect agreement with analytical solutions. This shows that the model can be used to model the switching

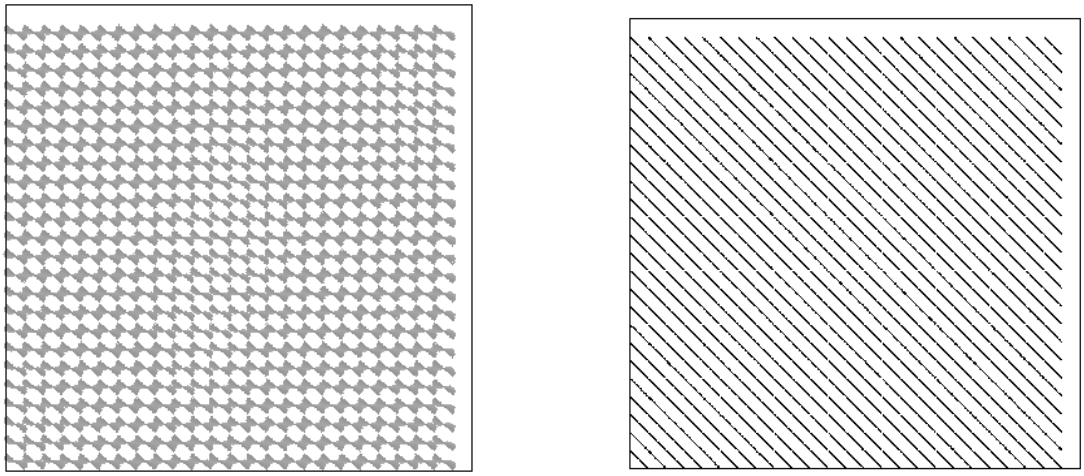

Figure 5.10: Snapshots of the bigrated system looking at them from the top. The system on the left has an azimuthal angle of $\phi = \pi/12$ and the one on the right has an azimuthal angle of $\phi = 3\pi/4$.

of liquid crystal devices. Finally, bistability was observed in a three dimensional system with a bigrated surface. The two stable states are degenerate in energy and have significantly different director orientations which are optically distinguishable. This is in agreement with experimental findings [125]. This kind of behaviour has great importance to liquid crystal displays (LCD). Current technologies used in LCDs are based on a single stable state which requires a constant applied voltage to maintain any other (switched) state. A bistable LCD would only require a short voltage pulse to switch from one state to the other and vice-versa. This would reduce the energy requirements to operate LCDs. Switching or flexoelectric effects resulting from applying an electric field were not addressed in this thesis, these may prove to be a fruitful area for further research.

Chapter 6

Conclusion

In this thesis, several aspects of the behaviour of liquid crystals near interfaces were investigated using computer simulation. This started with a study using long flexible molecules, of the form C7GBC7, using constant-NPT molecular dynamics. The bulk phase behaviour of the model at zero-pressure was investigated. It was observed that the model formed a smectic phase below a temperature of $T = 385$K in agreement with experimental findings for molecules with roughly similar shape. The structure and the degree of ordering of the smectic phase was investigated in detail. It was observed that it formed weak smectic ordering. A smectic-vapour film was set up and a study of its structure was carried out using constant-NVT ensemble MD. The director at the centre of the smectic film maintained its orientation normal to the interface. A surface melting of the smectic occurred at the interfaces. Extensive simulation studies of a mixture of C7GBC7 and a short, single-tailed molecule of the form C7GB were carried out. The bulk phase behaviour of this model was studied at zero-pressure. An ordered phase was observed below the temperature $T = 350$K. A liquid-vapour film of the mixture was set up and a detailed study of its structure was carried out using constant-NVT ensemble MD. Here the director rotated to become parallel to the interface. The film was observed to form smectic domains in its centre, while the interfacial region was seen to disorder. Substantial disordered regions were also observed in between the smectic domains. A small

amount of segregation of the two species between ordered and disordered domains was observed. The nematic phase of this model was found to be unstable. Hence, a study of the nematic-vapour interface using this model was not possible. However, the model should not be discarded entirely, other possible avenues of investigation still exist. These could be in the form of using shorter tails, having dissimilar chain lengths or changing the energy anisotropy parameter to one that would increase the stability range of the nematic phase.

Another liquid crystal interface that has hardly been studied through simulation, is the isotropic-nematic interface. Here, an extensive investigation of the properties and structure of this interface was carried out using computer simulation. The model consisted of long spherocylinders of length-to-width of 20 and 50. The isotropic-nematic bulk coexistence of the spherocylinders was studied using Gibbs ensemble Monte Carlo. An isotropic-nematic interface was set up at a suitable coexisting density and constant-NVT MD simulations were used. Two director orientations at the interface were investigated for $L/D = 20$, these were at an orientation parallel to the interface and one normal to the interface. A planar orientation of the director was found to be the preferred orientation, this was the orientation of the director at the interface for the $L/D = 50$ system. Density, order parameter and biaxial order parameter profiles were calculated. The order parameter and density profiles were independently fitted to a hyperbolic tangent function. It was observed that the profiles fitted well to the function, and from the fits, the interfacial widths and positions were obtained. A shift in the positions of the interfaces between the two profiles was also observed. A significant biaxiality effect was observed for the long ($L/D = 50$) spherocylinders. The results are in good agreement with experimental findings and with theoretical predictions using similar models.

The third liquid crystal interface studied is the liquid-solid interface or more precisely, the effects of different surface topographies on a nematic liquid crystal. A detailed study was carried out using a simple lattice model of the director field, to investigate the effect of two different surface topographies in creating bistable

devices. Monte Carlo simulations were used to model nematic liquid crystal in contact with triangular gratings in two-dimensions and bigrated surfaces in three dimensions. Bistability was observed in both cases in agreement with other studies using simulation and with experimental findings. Studies of the Frederiks transition were also carried out and were found to be in agreement with analytical solutions and other simulation studies. The benefit of bistability to device switching is enormous and hence, is of great importance to model actual switching and the dynamics of switching. As most liquid crystal devices use electric fields to switch between states rather than magnetic fields, the effects of flexoelectricity are also of great importance and are worth further investigation.

Bibliography

[1] G. Vertogen and W.H. de Jeu. *Thermotropic Liquid Crystals, Fundamentals.* Springer-Verlag, Berlin, 1988.

[2] P.G. deGennes and J. Prost. *The Physics of Liquid Crystals.* Clarendon Press, Oxford, 1993.

[3] P.J. Collings and J.S. Patel. Introduction to the science and technology of liquid crystals. In P.J. Collings and J.S. Patel, editors, *Handbook of Liquid Crystal Research*, chapter 1, page 1. Oxford university press, 1997.

[4] F. C. Frank. On the theory of liquid crystals. *Discuss. Faraday Soc.*, 25:19, 1958.

[5] M.P. Allen and D.J. Tildesley. *Computer Simulation of Liquids.* Clarendon Press, Oxford, 1986.

[6] J. G. Gay and B. J. Berne. Modification of the overlap potential to mimic a linear site-site potentialll. *J. Chem. Phys.*, 74:3316, 1981.

[7] P. A. Lebwohl and G. Lasher. Nematic liquid crystal order - A Monte Carlo calculation. *Phys. Rev. A*, 6:426, 1972.

[8] R.A. Pelcovits. Theory and computation. In P.J. Collings and J.S. Patel, editors, *Handbook of Liquid Crystal Research*, chapter 3, page 71. Oxford university press, 1997.

[9] J. P. Hansen and L. Verlet. Phase transitions of the Lennard-Jones system. *Phys. Rev.*, 184:151, 1969.

[10] J. Kushick and B. J. Berne. Computer simulations of anisotropic molecular fluids. *J. Chem. Phys.*, 64:1362, 1976.

[11] G. R. Luckhurst, R. A. Stephens, and R. W. Phippen. Computer-simulation studies of anisotropic systems: XIX. Mesophases formed by the Gay-Berne model mesogen. *Liq. Cryst.*, 8:451–464, 1990.

[12] Michael P. Allen, Glenn T. Evans, Daan Frenkel, and Bela Mulder. Hard convex body fluids. *Adv. Chem. Phys.*, 86:1–166, 1993.

[13] T. Kihara. The second virial coefficient of non-spherical molecules. *J. Phys. Soc. Japan*, 6:289–296, 1951.

[14] R.C. Armstrong. kinetic theory and rheology of dilute solutions of flexible macromolecules. i. steady state behavior. *J. Chem. Phys.*, 60:724, 1973.

[15] G. S. Grest and K. Kremer. Molecular-dynamics simulation for polymers in the presence of a heat bath. *Phys. Rev. A*, 33:3628, 1986.

[16] P. van der Ploeg and H.J.C. Berendsen. Molecular-dynamics of a bilayer-membrane. *Molec. Phys.*, 49:233, 1983.

[17] S. Leggetter and D.J. Tildesley. The computer simulation of adsorbed hydrocarbons. *Molec. Phys.*, 68:519, 1989.

[18] J. P. Hansen. Molecular dynamics simulations of coulomb systems in two and three dimensions. In G. Ciccotti and W. G. Hoover, editors, *Molecular Dynamics Simulations of Statistical Mechanical Systems*, pages 89–129. North-Holland, Amsterdam, 1986.

[19] J.-P. Ryckaert and A. Bellemans. Molecular dynamics of liquid *n*-Butane near its boiling point. *Chem. Phys. Lett.*, 30:123, 1975.

[20] T. Gruhn and S. Hess. Monte Carlo simulation of the director field of a nematic liquid crystal with three elastic coefficients. *Z. Naturforsch.*, 51a:1, 1996.

[21] H. Goldstein. *Classical Mechanics*. Addison Wesley, Reading, Massachusetts, second edition, 1980.

[22] M.A. Warren, M.P. Allen, M.R. Wilson, A. Sauron, W. Smith, and G. Germano. GBMEGA: A domain decomposition parallel molecular dynamics program to simulate Gay-Berne and later soft spherocylinders.

[23] M.R. Wilson. GBMOL: A replicated data molecular dynamics program to simulate combinations of Gay-Berne and Lennard-Jones sites, 1996.

[24] J.-P. Ryckaert, G. Ciccotti, and H. J. C. Berendsen. Numerical integration of the cartesian equations of motion of a system with constraints: molecular dynamics of n-alkanes. *J. Comput. Phys.*, 23:327, 1977.

[25] H. C. Andersen et al. New molecular dynamics methods for various ensembles. Report of CECAM Workshop, CECAM, Orsay, France, 1984.

[26] W. G. Hoover, A. J. C. Ladd, and B. Moran. High-strain-rate plastic-flow studied via non-equilibrium molecular-dynamics. *Phys. Rev. Lett.*, 48:1818, 1982.

[27] D. J. Evans. Computer experiment for non-linear thermodynamics of couette-flow. *J. Chem. Phys.*, 78:3297, 1983.

[28] Michael P. Allen and Dominic J. Tildesley. *Computer simulation of liquids*. Clarendon Press, Oxford, paperback edition, 1989. ISBN 0–19–855645–4, 385pp.

[29] H. C. Andersen. Molecular dynamics simulations at constant pressure and/or temperature. *J. Chem. Phys.*, 72:2384–2393, 1980.

[30] D. Frenkel and B. Smit. *Understanding molecular simulation : from algorithms to applications*. Academic Press, San Diego, 1996. ISBN 0–12–267370–0.

[31] M.R. Wilson. Parallel molecular dynamics techniques for the simulation of anisotropic systems. In C. Zannoni and P. Pasini, editors, *Advances in the Computer Simulations of Liquid Crystals*, volume ?? of NATO *ASI Series C*, pages ???–???, Dordrecht, to be published. Kluwer Academic Publishers. Proceedings of the NATO Advanced Study Institute 'Computer Simulations of Liquid Crystals', Erice, Italy, June 11 - 22, 1998.

[32] M.A. Warren. *The Computer Simulation of Liquid Crystals*. PhD thesis, University of Bristol, 1997.

[33] A. Z. Panagiotopoulos. Direct determination of phase coexistence properties of fluids by Monte Carlo simulation in a new ensemble. *Molec. Phys.*, 61:813–826, 1987.

[34] S. Kirkpatrick. Optimization by simulated annealing: Quantitive studies. *J. Stat. Phys.*, 34(5/6):975, 1984.

[35] S. Kirkpatrick, C.D. Gelatt Jr., and M.P. Vecchi. Optimization by simulated annealing. *Science*, 220(4598):671, 1983.

[36] W. H. Press, B. P. Flannery, S. A. Teukolsky, and W. T. Vetterling. *Numerical Recipes in Fortran*. Cambridge University Press, Cambridge, 2nd edition, 1992.

[37] S. Dietrich. Structures in fluids induced by interfaces. *J. Phys. Cond. Mat.*, 8(47):9127–9141, 1996.

[38] F.N. Braun, T.J. Sluckin, E. Velasco, and L. Mederos. Oblique anchoring at a free nematic surface. *Phys. Rev. E*, 53(1):706, 1996.

[39] Margarida Telo da Gama. Liquid crystal interfaces. In M. Baus, L. F. Rull, and J. P. Ryckaert, editors, *Observation, Prediction and Simulation of Phase Transitions in Complex Fluids*, volume 460 of NATO *ASI Series C*, pages 243–292. Kluwer Academic Publishers, Dordrecht, 1995. Proceedings of the NATO Advanced Study Institute and Enrico Fermi Course LXXIX on 'Observation and Prediction of Phase Transitions in Complex Fluids', Varenna, Italy, July 25–August 8, 1994. ISBN 0–7923–3439–6.

[40] T. J. Sluckin and A. Poniewierski. Orientational wetting transitions and related phenomena in nematics. In C. A. Croxton, editor, *Fluid Interfacial Phenomena*, chapter 5, pages 215–259. Wiley, 1986.

[41] E.H. Hauge. The wetting transition. In E.G.D. Cohen, editor, *Fundamental problems in statistical mechanics*, volume VI, page 65, Trondheim,Norway, June 1985. North-Holland.

[42] D. E. Sullivan and M. M. Telo da Gama. Wetting transitions and multilayer adsorption at fluid interfaces. In C. A. Croxton, editor, *Fluid Interfacial Phenomena*, page 45. Wiley, 1986.

[43] M.A. Bouchiat and D. Langevin-Cruchon. Molecular order at the free surface of a nematic liquid crystal from light reflectivity measurements. *Phys. Lett. A*, 34(6):331, 1971.

[44] D. Langevin. Analyse spectrale de la lumière diffusée par la surface libre d'un cristal liquide nématique. Mesure de la tension superficielle et des coefficients de viscosité. *J. Phys., Paris*, 33:249, 1972.

[45] P. Chiarelli, S. Faetti, and L. Fronzoni. Experimental measurement of the director orientation at the free surface of a nematic liquid crystal. *Lettere Al Nuovo Cimento*, 36(3):60, 1983.

[46] M.G.J. Gannon and T.E. Faber. The surface tension of nematic liquid crystals. *Phil. Mag. A*, 37(1):117–135, 1978.

[47] P. Chiarelli, S. Faetti, and L. Fronzoni. Structural transition at the free surface of the nematic liquid crystals MBBA and EBBA. *J. Phys., Paris*, 44:1061–1067, 1983.

[48] J.D. Parsons. A molecular theory of surface tension in nematic liquid crystals. *J. Phys., Paris*, 37:1187, 1976.

[49] H. Kasten and G. Strobl. Nematic wetting at the free surface of 4-cyano-4′-*n*-alkyl-biphenyls. *J. Chem. Phys.*, 103(15):6768, 1995.

[50] M. A. Osipov and S. Hess. Density functional approach to the theory of interfacial properties of nematic liquid crystals. *J. Chem. Phys.*, 99:4181, 1993.

[51] M. M. Telo da Gama. The interfacial properties of a model of a nematic liquid-crystal I the nematic-isotropic and the nematic-vapor interfaces. *Molec. Phys.*, 52:585, 1984.

[52] J.H. Thurtell, M.M. Telo da Gama, and K.E. Gubbins. The liquid-vapour interface of simple models of nematic liquid crystals. *Molec. Phys.*, 54(2):321–332, 1985.

[53] H. Kimura and H. Nakano. Statistical theory of surface tension and molecular orientations at the free surface in nematic liquid crystals. *J. Phys. Soc. Japan*, 54(5):1730–1736, 1985.

[54] B. Tjipto-Margo and D.E. Sullivan. Molecular-interactions and interface properties of nematic liquid-crystals. *J. Chem. Phys.*, 88:6620, 1988.

[55] B. Tjipto-Margo, A. K. Sen, L. Mederos, and D.E. Sullivan. The liquid-vapour interface of nematic liquid crystals. *Molec. Phys.*, 67:601, 1989.

[56] E. Martín Del Río, M.M. Telo da Gama, E. de Miguel, and L.F. Rull. Surface induced alignment at model nematic interfaces. *Phys. Rev. E*, 52(5):5028, 1995.

[57] E. Martín Del Río, M. M. Telo da Gama, E. de Miguel, and L. F. Rull. Wetting and interfacial order at nematic free surfaces. *Europhys. Lett.*, 35:189, 1996.

[58] C. D. Holcomb, P. Clancy, and J. A. Zollweg. A critical study of the simulation of the liquid-vapour interface of a Lennard-Jones fluid. *Molec. Phys.*, 78:437–459, 1993.

[59] Enrique de Miguel, Elvira Martín del Río, Julian T. Brown, and Michael P. Allen. Effect of the attractive interactions on the phase behaviour of the Gay-Berne liquid crystal model. *J. Chem. Phys.*, 105:4234–4249, 1996.

[60] Julian T. Brown, Michael P. Allen, Enrique de Miguel, and Elvira Martín del Río. Effects of elongation on the phase behaviour of the Gay-Berne fluid. *Phys. Rev. E*, 57:6685–6699, 1998.

[61] E. de Miguel, L. F. Rull, M. K. Chalam, and K. E. Gubbins. Liquid vapour coexistence of the Gay-Berne fluid by Gibbs ensemble simulation. *Molec. Phys.*, 71:1223, 1990.

[62] A. M. Somoza and P. Tarazona. Density functional approximation for hard-body liquid-crystals. *J. Chem. Phys.*, 91:571, 1989.

[63] E. Martín Del Río, E. de Miguel, and L.F. Rull. Computer simulation of the liquid-vapour interface in liquid crystals. *Physica A*, 213:138–147, 1995.

[64] Elvira Martín del Río and Enrique de Miguel. Computer simulation study of the free surfaces of a liquid crystal model. *Phys. Rev. E*, 55:2916–2924, 1997.

[65] A. P. J. Emerson, S. Faetti, and C. Zannoni. Monte Carlo simulation of the nematic-vapour interface for a Gay-Berne liquid crystal. *Chem. Phys. Lett.*, 271:241, 1997.

[66] S. J. Mills, C. M. Care, M. P. Neal, and D. J. Cleaver. Computer simulation of an unconfined liquid crystal film. *Phys. Rev. E*, 58:3284, 1998.

[67] G. Durand. Order electricity in liquid crystals. *Physica A*, 163:94–100, 1990.

[68] D. Langevin and M.A. Bouchiat. Molecular order and surface tension for the nematic-isotropic interface of MBBA, deduced from light reflectivity and light scattering measurements. *Mol. Cryst. Liq. Cryst.*, 22:317, 1973.

[69] S. Faetti and V. Palleschi. Nematic-isotropic interface of some members of the homologous series of 4-cyano-4′-(n-alkyl)biphenyl liquid crystals. *Phys. Rev. A*, 30(6):3241, 1984.

[70] W. Chen, T. Sato, and A. Teramoto. Measurement of the interfacial tension between coexisting isotropic and nematic phases of lyotropic polymer liquid crystal. *Macromolecules*, 29:4283, 1996.

[71] L. Onsager. The effects of shape on the interaction of colloidal particles. *Ann. N. Y. Acad. Sci.*, 51:627, 1949.

[72] P.G. de Gennes. Short range order effects in the isotropic phase of nematics and cholesterics. *Mol. Cryst. Liq. Cryst.*, 12:193, 1971.

[73] M. Doi and N. Kuzuu. Structure of the interface between the nematic phase and the isotropic phase in the rodlike molecules. *J. Appl. Polym. Sci., Appl. Polym. Symp.*, 41:65, 1985.

[74] H. Kimura and H. Nakano. Statistical theory of surface tension and molecular orientations in nematic liquid crystals.ii. the nematic-isotropic interface. *J. Phys. Soc. Japan*, 55(12):4186, 1986.

[75] W.E. McMullen. Molecular theory of the isotropic-nematic interface: Hard spherocylinders. *Phys. Rev. A*, 38(12):6384, 1988.

[76] W.E. McMullen. Interfacial polar ordering and anomalous tilt angles at isotropic-nematic interfaces. *Phys. Rev. A*, 40(5):2649, 1989.

[77] B.G. Moore and W.E. McMullen. Isotropic-nematic interface of hard spherocylinders:Beyond the square-gradient approximation. *Phys. Rev. A*, 42(10):6042, 1990.

[78] Z.Y. Chen and J. Noolandi. Numerical solution of the Onsager problem for an isotropic-nematic interface. *Phys. Rev. A*, 45:2389, 1992.

[79] Z.Y. Chen. Biaxial effect at an isotropic-nematic interface. *Phys. Rev. E*, 47(5):3765, 1993.

[80] S. Cui, O. Akcakir, and Z.Y. Chen. Isotropic-nematic interface of liquid-crystalline polymers. *Phys. Rev. E*, 51(5):4548, 1995.

[81] D.L. Koch and O.G. Harlen. Interfacial tension at the boundary between nematic and isotropic phases of a hard rod solution. *Macromolecules*, 32:219–226, 1999.

[82] R. Hołyst and A. Poniewierski. Director orientation at the nematic-phase–isotropic-phase interface for the model of hard spherocylinders. *Phys. Rev. A*, 38:1527, 1988.

[83] M.A. Bates and C. Zannoni. A molecular dynamics simulation study of the nematic-isotropic interface of a Gay-Berne liquid crystal. *Chem. Phys. Lett.*, 280:40, 1997.

[84] M.P. Allen. Molecular simulation and theory of the isotropic-nematic interface. *In Press*, 1999.

[85] M.A. Bates. Planar anchoring at the smectic A-isotropic interface. A molecular dynamics simulation study. *Chem. Phys. Lett.*, 288:209, 1998.

[86] B. Jérôme. Interfacial structural transitions in nematic liquid crystals. *J. Phys. Cond. Mat.*, 6:A269–A273, 1994.

[87] B. Jérôme. Surface alignment. In D. Demus, J. Goodby, G.W. Gray, H.-W. Spiess, and V. Vill, editors, *Handbook of Liquid Crystals*, volume 1, chapter 10, page 534. Wiley-VCH, 1998.

[88] B. Jérôme. Surface effects and anchoring in liquid crystals. *Rep. Prog. Phys.*, 54:391–451, 1991.

[89] Y.R. Shen. Surface properties probed by second-harmonic and sum-frequency generation. *Nature*, 337(9):519, Febuary 1979.

[90] W. Chen, M.B. Feller, and Y.R. Shen. Investigation of anisotropic molecular orientational distributions of liquid-crystal monolayers by optical second-harmonic generation. *Phys. Rev. Lett.*, 63(24):2665, 1989.

[91] M.B. Feller, W. Chen, and Y.R. Shen. Investigation of surface-induced alignment of liquid-crystal molecules by optical second-harmonic generation. *Phys. Rev. A*, 43(12):6778, 1991.

[92] D.W. Berreman. Solid surface shape and the alignment of an adjacent nematic liquid crystal. *Phys. Rev. Lett.*, 28(26):1683, 1972.

[93] D.W. Berreman. Alignment of liquid crystals by grooved surfaces. *Mol. Cryst. Liq. Cryst.*, 23:215–231, 1973.

[94] U. Wolff, W. Greubel, and H. Krüger. The homogeneous alignment of liquid crystal layers. *Mol. Cryst. Liq. Cryst.*, 23:187–196, 1973.

[95] M. K. Chalam, K. E. Gubbins, E. de Miguel, and L. F. Rull. A molecular simulation of a liquid crystal model: bulk and confined fluid. *Molec. Simul.*, 7:357–385, 1991.

[96] Z. Zhang, A. Chakrabarti, O. G. Mouritsen, and M. J. Zuckermann. Substrate-induced bulk alignment of liquid crystals. *Phys. Rev. E*, 53:2461–2465, 1996.

[97] J. Stelzer, P. Galatola, G. Barbero, and L. Longa. Molecular dynamics simulations of surface-induced ordering in a nematic liquid crystal. *Phys. Rev. E*, 55(1):477, 1997.

[98] G. D. Wall and D. J. Cleaver. Computer simulation studies of confined liquid crystal films. *Phys. Rev. E*, 56:4306–4316, 1997.

[99] Michael P. Allen. Molecular simulation and theory of liquid crystal surface anchoring. *Molec. Phys.*, 96:1391–1397, 1999.

[100] C.J. Newton and T.P. Spiller. Bistable nematic liquid crystal device modelling. *Unpublished*, March 1997.

[101] T.P. Spiller and C.J. Newton. Private communication. Unpublished, 1998.

[102] M.R. Wilson. Molecular dynamics simulations of flexible liquid crystal molecules using a Gay-Berne/Lennard-Jones model. *J. Chem. Phys.*, 107:8654, 1997.

[103] C. McBride, M.R. Wilson, and J.A.K Howard. Molecular dynamics simulations of liquid crystal phases using atomistic potentials. *Molec. Phys.*, 93(6):955–964, 1998.

[104] E. de Miguel, L. F. Rull, M. K. Chalam, and K. E. Gubbins. Liquid crystal phase diagram of the Gay-Berne fluid. *Molec. Phys.*, 74:405–424, 1991.

[105] G. La Penna, D. Catalano, and C.A. Veracini. A rigid core-flexible chain model for mesogenic molecules in molecular dynamics simulations of liquid crystals. *J. Chem. Phys.*, 105(16):7097, 1996.

[106] Alexey V. Lyulin, Muataz S. Al-Barwani, Michael P. Allen, Mark R. Wilson, Igor Neelov, and Nicholas K. Allsopp. Molecular dynamics simulation of main chain liquid crystalline polymers. *Macromolecules*, 31:4626–4634, 1998.

[107] C. McBride and M.R. Wilson. Molecular dynamics simulations of a flexible liquid crystal. *Molec. Phys.*, 97(4):511–522, 1999.

[108] D. Demus. One hundred years of liquid crystal chemistry: thermotropic liquid crystals with conventional and unconventional molecular structure. *Liq. Cryst.*, 5(1):75–110, 1989.

[109] D. Demus. Chemical structure and mesogenic properties. In D. Demus, J. Goodby, G.W. Gray, H.-W. Spiess, and V. Vill, editors, *Handbook of Liquid Crystals*, volume 1, chapter VI, page 133. Wiley-VCH, 1998.

[110] J. Billard and L. Mamlok. Mesophases de derives du cyclohexane. *Mol. Cryst. Liq. Cryst.*, 41:217–222, 1978.

[111] H. Schubert, H.-J. Lorenz, R. Hoffmann, and F. Franke. Neue kristallin-flüssige p-Terphenylderivate. *Z. Chem.*, 6:337, 1966.

[112] Douglas J. Cleaver, Christopher M. Care, Michael P. Allen, and Maureen P. Neal. Extension and generalization of the Gay-Berne potential. *Phys. Rev. E*, 54:559–567, 1996.

[113] E. de Miguel, L. F. Rull, and K. E. Gubbins. Dynamics of the Gay-Berne fluid. *Phys. Rev. A*, 45:3813–3822, 1992.

[114] J.P. Ryckaert. Special geometrical constraints in the molecular dynamics of chain molecules. *Molec. Phys.*, 55:549, 1985.

[115] E. Martín del Río, Enrique de Miguel, and L. Rull. Computer-simulation of the liquid-vapor interface in liquid- crystals. *Physica A*, 213:138–147, 1995.

[116] R.A Bemrose, C.M. Care, D.J. Cleaver, and M.P. Neal. A molecular dynamics of a bi-disperse liquid crystal mixture using a generalized Gay-Berne potential. *Molec. Phys.*, 90(4):625–635, 1997.

[117] M.R. Wilson and J. Ilnytskyi. Domain decomposition version of GBMOL. Work in Progress.

[118] S. C. McGrother, D. C. Williamson, and G. Jackson. A re-examination of the phase diagram of hard spherocylinders. *J. Chem. Phys.*, 104:6755, 1996.

[119] P. Bolhuis and D. Frenkel. Tracing the phase boundaries of hard spherocylinders. *J. Chem. Phys.*, 106:666, 1997.

[120] Michael P. Allen, Mark A. Warren, Mark. R. Wilson, Alain Sauron, and William Smith. Molecular dynamics calculation of elastic constants in Gay-Berne nematic liquid crystals. *J. Chem. Phys.*, 105:2850–2858, 1996.

[121] Michael P. Allen. Simulation and phase diagrams. In K. Binder and G. Ciccotti, editors, *Monte Carlo and molecular dynamics of condensed matter systems*, volume 49, chapter 10, pages 255–284. Italian Physical Society, Bologna, 1996. Proceedings of the Euroconference on 'Computer simulation in condensed matter physics and chemistry', Como, Italy, July 3–28, 1995, ISBN 88-7794-078-6.

[122] M. Monkade, M. Boix, and G. Durand. Order electricity and oblique nematic orientation on rough solid surfaces. *Europhys. Lett.*, 5(8):697–702, 1988.

[123] G. Barbero, G. Skačej, A.L. Alexe-Ionescu, and S. Žumer. Nematic ordering in a cell with modulated surface anchoring: Effects of flexoelectricity. *Phys. Rev. E*, 60(1):628, 1999.

[124] G. Barbero, T. Beica, A.L. Alexe-Ionescu, and R. Moldovan. Anchoring energy and easy direction of non uniform surfaces. *J. de Physique II*, 2:2011–2024, 1992.

[125] R. Barberi, I. Dozov, M. Giocondo, M. Iovane, Ph. Martinot-Lagarde, D. Stonescu, S. Tonchev, and L.V. Tsonev. Azimuthal anchoring of nematic on undulated substrate: Elasticity versus memory. *Eur. Phys. J. B*, 6:93–91, 1998.

[126] J. Hobdell and A. Windle. A numerical technique for predicting microstructure in liquid crystalline polymers. *Liq. Cryst.*, 23(2):157–173, 1997.

[127] T.P. Spiller. Liquid crystal sandwiches. Unpublished, 1997.